Gesellschaft für Anlagen- und Reaktorsicherheit (GRS) mbH

Radionuclide transport and retention in natural rock formations

Ruprechtov site

GRS - 218

Gesellschaft für Anlagen- und Reaktorsicherheit (GRS) mbH

Radionuclide transport and retention in natural rock formations

Ruprechtov site

Ulrich Noseck
Thomas Brasser

May 2006

Remark:

This report was prepared under contract No. 02 E 9551 with the German Bundesministerium für Wirtschaft und Technologie (BMWi).

The work was conducted by the Gesellschft für Anlagen- und Reaktorsicherheit (GRS) mbH.

The authors are responsible for the content of this report.

GRS - 218
ISBN 3-931995-88-7

Deskriptoren:
Aktiver Abfall, Ausbreitung, Endlagerung, Geochemie, Geosphäre, Grundwasser, Huminstoff, Langzeitsicherheit, Nuklidtransport, Sorption, Tschechien, Uran, Wasserchemie

Acknowledgments

Type and extent of the results from investigations at Czech Ruprechtov site which are compiled in this report have only been enabled by close co-operation with the following partners (in alphabetical order of institution). Several contributions of these partners are included in the report and noted at the corresponding points.

Kazimierz Rozanski, Marek Dulinski
AGH - University of Technology
Faculty of Physics and Nuclear Techniques
al. Mickiewicza 30
30-059 Kraków, Polen
eMail: rozanski@novell.ftj.agh.edu.pl / dulinski@novell.ftj.agh.edu.pl

Shaun Reeder
British Geological Survey
Keyworth, Nottingham
NG12 5GG, Vereinigtes Königreich
eMail: s.reeder@bgs.ac.uk

Bernd Grambow, Abdelouas Abdesselam, Yves Andres
Ecole des Mines de Nantes
Laboraitoire SUBATECH
4, rue Alfred Kastler
44307 Nantes Cedex 3, Frankreich
eMail: grambow@subatech.in2p3.fr / abdeloua@subatech.in2p3.fr

Johannes Fachinger
Forschungszentrum Jülich - ISR
52425 Jülich
eMail: j.fachinger@fz.juelich.de

Melissa Denecke, Horst Geckeis, Wolgang Hauser
Forschungszentrum Karlsruhe
Institut für Nukleare Entsorgung (INE)
76021 Karlsruhe
eMail: denecke@ine.fzk.de / geckeis@ine.fzk.de / hauser@ine.fzk.de

Hans-Jürgen Förster
Universität Potsdam
Institut für Geowissenschaften
14476 Golm
eMail: for@geo.uni-potsdam.de

Petr Rajlich
Jihočeské muzeum v Českých Budějovicích
Dukelská 1
370 51 České Budějovice, Tschechische Republik
eMail: rajlich@muzeumcb.cz

Ales Laciok, Mirek Hercik, Vaclava Havlova
Nuclear Research Institute (NRI) Řež plz
25068 Řež, Tschechische Republik
eMail: lac@ujv.cz / her@ujv.cz / hvl@ujv.cz

Walter Pohl, Dieter Zachmann, Dagmar Schönwiese
Technische Universität Braunschweig
Institut für Umweltgeologie
Pockelsstraße 3
38106 Braunschweig
eMail: walter.pohl@tu-bs.de / d.zachmann@tu-bs.de / d.schoenwiese@tu-bs.de

Juhani Suksi
University Helsinki
Department of Chemistry
A. I. Virtasenaukio 1
00014 Helsinki
eMail: juhani.suksi@helsinki.fi

Janusz Janeczek
Uniwersytet Śląskii
Bankowa 12
40-007 Katowice, Polen
eMail: janeczek@us.edu.pl

Contents

1 Introduction

Deep geological disposal is based on a multi-barrier concept in which clay materials often play an important role as geological barriers. Detailed investigations of suitable geological analogues may lead to a better understanding of the complex interrelations between transport and sorption of radionuclides in argillaceous media under natural conditions, and especially on very long-term scales relevant for Performance assessment (PA).

The Ruprechtov site was chosen because its geological and geochemical conditions are similar to sedimentary sequences which cover often potential host rocks for underground waste repositories. It is situated in the north-western part of the Czech Republic in a Tertiary basin of the Eger (Ohře) rift composed of clay and organic material (coal, lignite), with places of high uranium concentrations. Within a bilateral project this site has been investigated by GRS, Germany and NRI, Czech Republic in order to identify the main mobilisation/immobilisation processes for PA-relevant elements, namely uranium.

The work presented here is a continuation of the previous project phase the results of which have been documented in /NOS 02/. In this last project phase the site investigation was limited to a small area of about 200 m^3. Three exploration boreholes and two boreholes for detailed investigation were available at that time. The main intention of the new project phase was to enlarge the investigation area, in order to better understand the structure and the hydrogeochemical conditions of the overall system.

On the one hand this includes the characterisation of the hydrogeological conditions in order to understand the regional groundwater flow and potential uranium transport processes on a larger spatial scale. Therefore the spatial extension of uranium-rich layers, water-bearing horizons and lithological units as well as groundwater ages and flow directions need to be determined. On that basis a conceptual model for the groundwater flow at Ruprechtov site can be developed.

On the other hand it includes the characterization of the Erzgebirge granites and the interface granite-kaolin-clay/ignite. The aim is to reach a better knowledge about uranium release from granite and enrichment processes in the argillaceous sediments.

In this context a better characterization of the immobile uranium phases, i.e. redox state, mineral phase and sorbed fraction is performed. Therefore surface specific methods like electron micro-probe, SEM-EDS spectroscopy or µ-XRF and µ-XAFS as well as bulk analysis like chemical U(IV)/U(VI) separation and radiometric methods have been applied. Specific sorption/desorption experiments are performed in order to estimate the role of sorption.

Additionally, investigations are carried out concerning the role of colloids and of microbial processes, which might impact the uranium mobility in the system. Humic colloids can play a role in uranium transport at Ruprechtov site, since lignite-rich sediments with sedimentary organic carbon (SOC) concentrations up to 50 % are observed in direct vicinity of the water bearing horizons. This situation is similar to Gorleben site, where lignite-rich layers in the quaternary sediments occur. At Gorleben site the release of humic substances from lignite material causes dissolved organic carbon (DOC) concentrations up to 200 mg/l, mainly composed of humic acids and fulvic acids.

This report mainly summarises the results from the present project phase and integrates all available results. In chapter 2 the site is described briefly with its general features. Chapter 3 comprises a description of today`s geological features of Ruprechtov site and information about the geological development as well as location of boreholes and wells, results from drill core description and geophysical logging. In chapter 4 the conceptual hydrogeological model is presented, which is mainly based on results from isotope-geochemical characterization and pumping tests measured in various wells. Chapter 5 contains the results from geochemical characterisation of sediments and groundwater with emphasis on uranium behaviour. This chapter includes the description of sorption/desorption experiments and characterisation of colloids and microbial effects. In chapter 6 scenarios for uranium enrichment at the site are proposed on the basis of all integrated information. Finally chapter 7 summarises all findings with emphasis on the relation to performance assessment.

2 Site description

The investigation area Ruprechtov is situated in NW part of Czech Republic, app. 8 km N of Karlovy Vary (Carlsbad) and 20 km S of the borderline between Federal Republic of Germany and Czech Republic close to Oberwiesenthal, resp. Jachymov (Fig. 2.1).

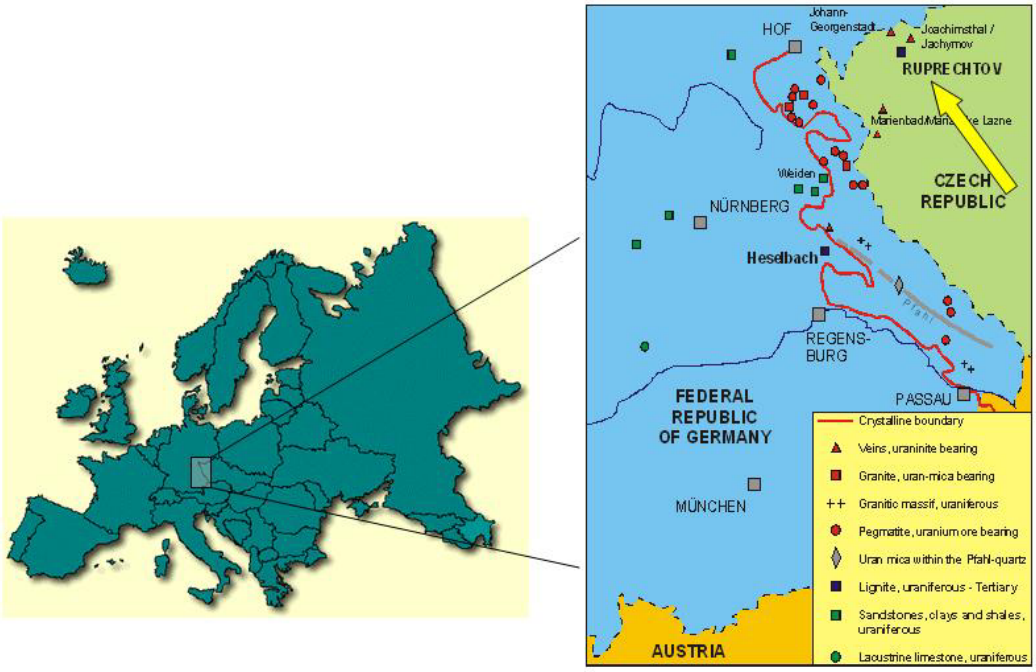

Fig. 2.1: Location of Ruprechtov site in NW Czech Republic

Closest town is Ostrov nad Ohří (German: Schlackenwerth), app. 6 km ENE (Fig. 2.2, Fig. 2.3). The investigation area itself is characterized by relatively tabular morphology (app. 470 m asl.). The close-by village of Ruprechtov reaches a topographical height of up to 520 m, Hroznětín is located slightly lower at app. 450 m asl.

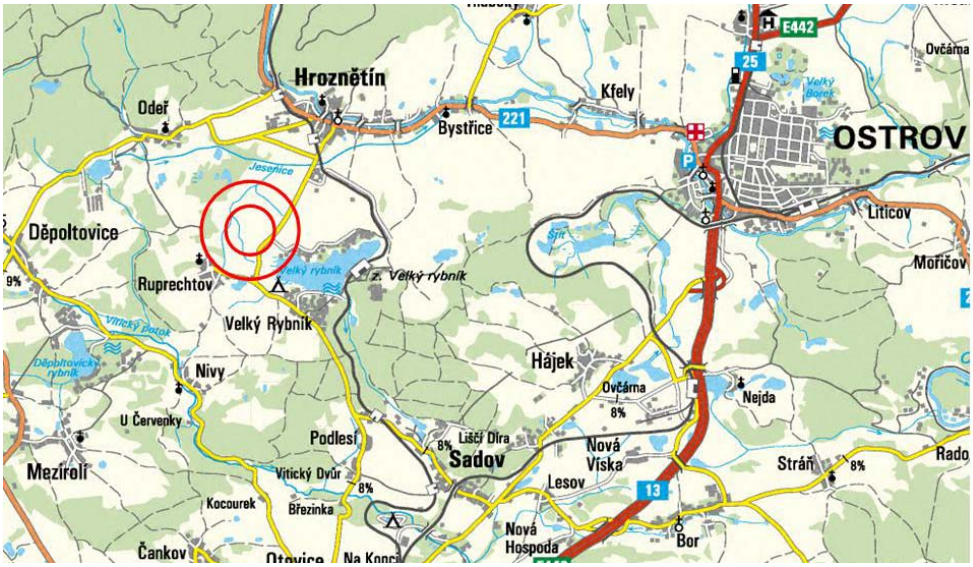

Fig. 2.2: Cut-out from road map 1:100,000 with location of investigation area (red circles) WSW of Ostrov; actual horizontal picture size: app. 12.5 km

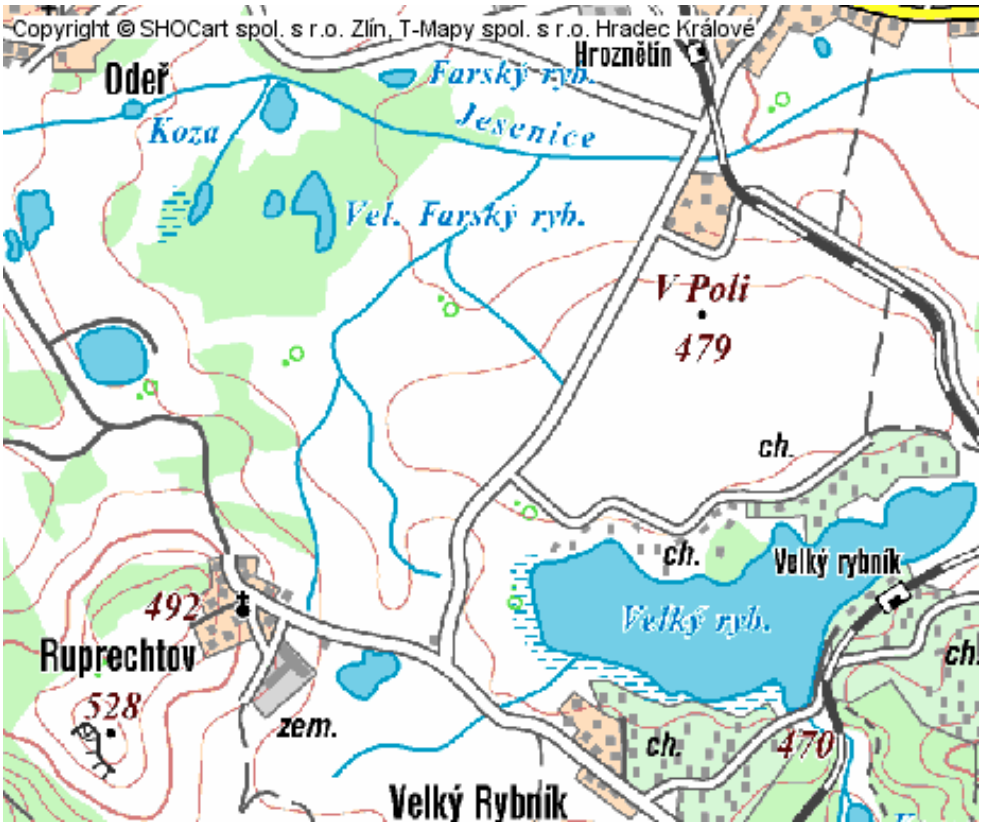

Fig. 2.3: Cut-out from topographical map 1:50,000 with investigation area NE of the village of Ruprechtov and WNW of Velký rybnic; actual horizontal picture size: app. 2.5 km

Geologically, Ruprechtov site is located in the Hroznětín part of Sokolov basin which is part of the Ohre rift, a SW-NE trending Graben structure parallel to the Krušné hory mts. (see chapter 3 for details). This Graben structure is very well seen on Fig. 2.5 where dark green colours indicate the graben margins as well as granitic rock.

The areal view of investigation area (Fig. 2.6) gives an impression of topography of the site which is also represented in a 3D-visualization (Fig. 2.7)

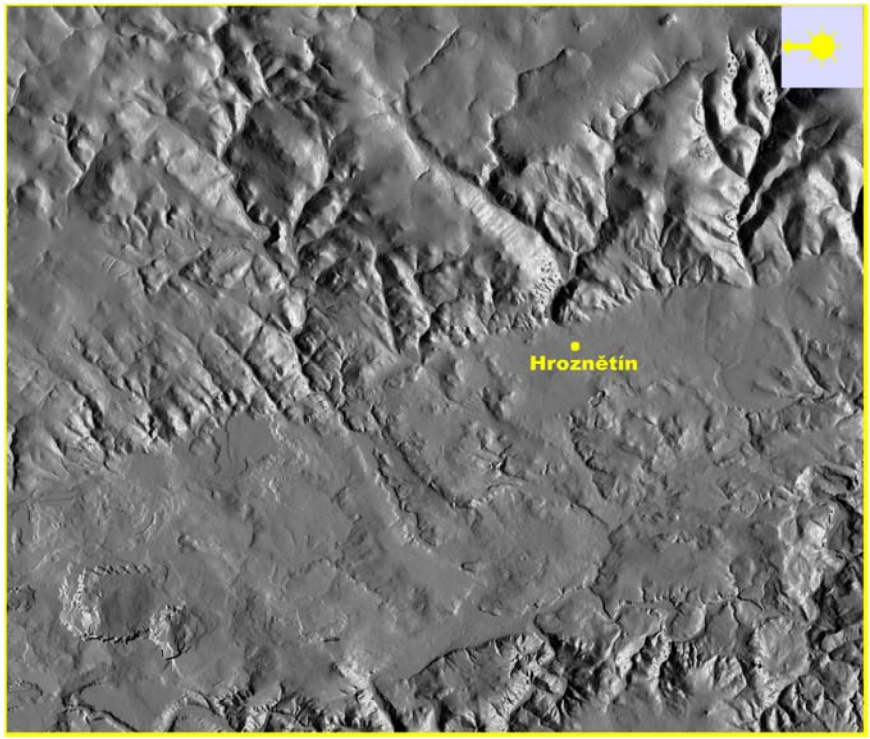

Fig. 2.4: Morphology of the area around Hroznětín village. The Graben-structure of Sokolov basin (from lower-left to middle-right) is clearly marked by sharp faults. In the upper half part of Erzgebirge mountains can be seen

Fig. 2.5: Satellite view of Hrosnětín part of Sokolov basin with location of investigation area (yellow circles) beween Krušné hory mts. in the North and the city of Karlovy Vary in the South (created with Google-Earth). The Graben structure is well seen by its sharp margins (dark green colours).

Fig. 2.6: S-N aereal view of investigation area; in the foreground village and pond Velký rybnik, backdrop the Krušné hory mts.; in front of ore mountains the two villages of Hrosnětín (right) and Oděř (left). Ruprechtov village is tapping directly at left-middle image border

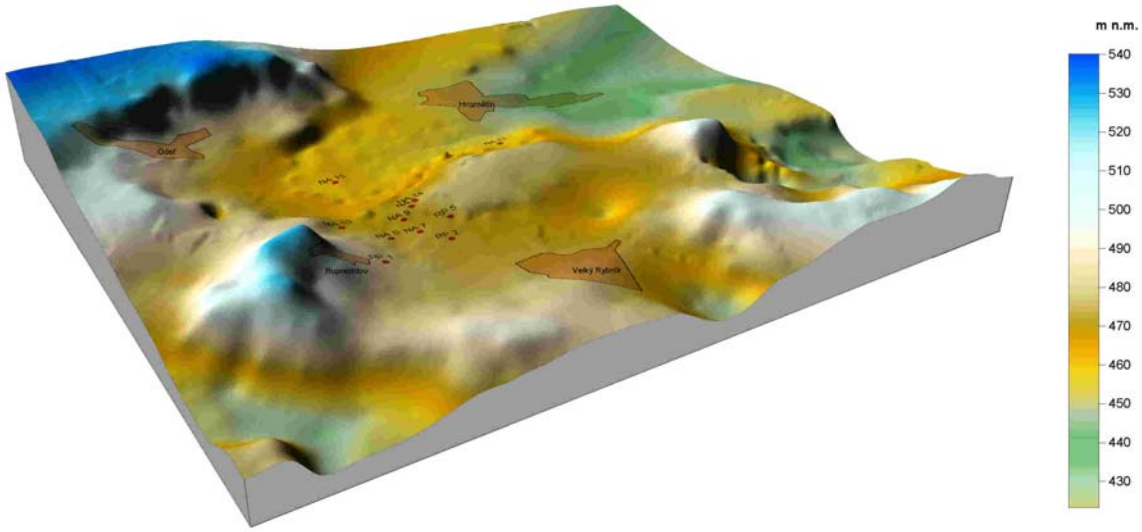

Fig. 2.7: 3D-visualization of morphology of investigation area (view from SW to NE); the cone at Ruprechtov village (SW edge) is formed by a basaltic dike, the steep incline at left image border represents a foothill of Krušné hory mts.

3 Geology

3.1 Geology of the Ohre Rift Region

A rather actual overview of the general geological situation of the Ohre-rift region is published by /ULR 02/. The following descriptions are focussed on the investigation area and are mainly based on this publication which also refers to numerous citations (not indicated in this text) on specific topics.

3.1.1 Introduction

An extensive rift system was formed in western and central Europe due to the collision of the African/Eurasian plates in Early Cenozoic (Fig. 3.1). It shows intermittently volcanic activity lasting till the present, and is marked by a system of more or less ramified graben structures representing a major tectonic feature within the Neoeurope. This system partly follows important Variscan lithospheric boundaries and extends over wide areas of Europe (Spain, France, Germany, Czech Republic). The easternmost segment of the European Cenozoic rift system is represented by the Ohre (Eger) Graben in the Bohemian Massif (Fig. 3.1).

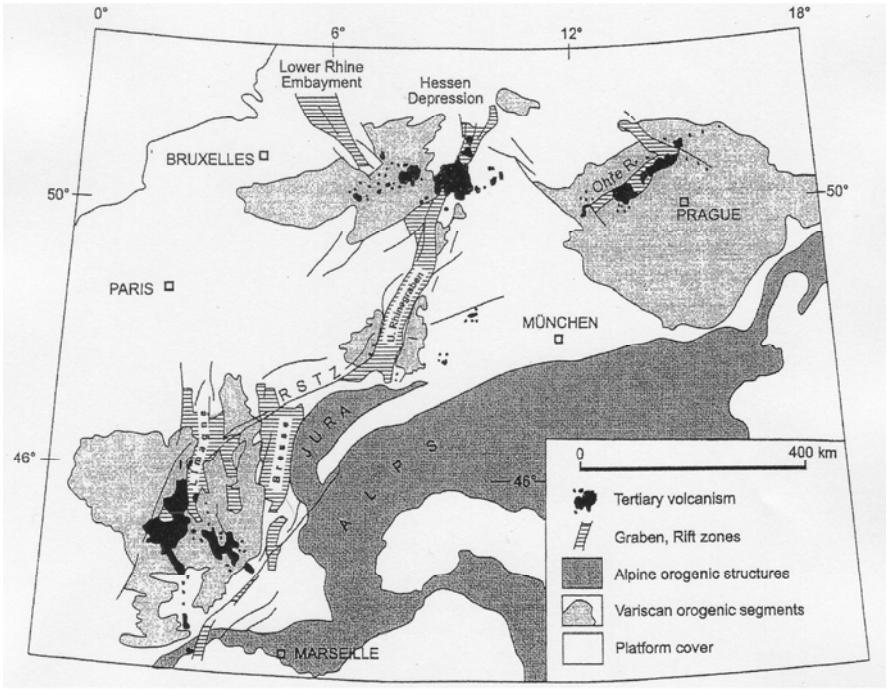

Fig. 3.1: A scheme of the European Cenozoic rift system with marked areas of intensive volcanic activity (adapted from /PRO 95/)

Volcanic activity in the European Cenozoic rift system is concentrated into intrusive complexes and complexes with preserved surface volcanic products (e.g., Auvergne area, Kaiserstuhl, Vogelsberg, Eifel, Doupovske hory Mts., Ceske Stredohori Mts.) in the grabens as well as in shoulder blocks, preceded by pre-rift intrusions since the Cretaceous. Some grabens are almost free of volcanic products (Upper Rhine Graben). Volcanic activity continues till the present in some segments of the rift system. In addition, geophysical measurements show high heat flow, elevated seismicity, thinned crust and anomalous upper mantle structure, possibly related to magmatic activity.

Volcanic activity is explained as related to lithospheric flexuring caused by displacement of large units of lithosphere represented by Alpine nappes resulting in mantle upwelling followed by adiabatic decompression, partial melting of the upper mantle and injection of mantle-derived magmas. A principally different approach is represented by the concept of the presence of several smaller mantle plumes in central and western Europe or even the existence of a single hot spot 2,000 km in diameter.

3.1.2 Characteristics of the Ohre Rift

The term ‘Ohre Rift’ (OR) is applied to the region formed in the NW part of the Bohemian Massif (BM) showing increased volcanic activity culminating in the Middle Oligocene to Lower Miocene (app. 32-24 My) and prominent subsidence during the Early Oligocene to Late Miocene crustal extension (Fig. 3.2). The region features a morphologically asymmetrical graben with a well-defined fault scarp in the NW and a morphologically indistinct limitation in the SE. It parallels other rift structures of the European Cenozoic rift system in the timing of magmatic activity and the presence of two geochemically distinct series of volcanic products attributed to pre-rift and rift stages of development.

Within the stable-lithosphere conditions of the BM, the OR is anomalous not only in its volcanological and geomorphological phenomena but also in its elevated heat flow, hydrothermal activity and CO_2 emanations.

The OR graben (also *Eger Graben)* trends NE-SW for a distance of ca. 190 km. To the NW and SE, the limits of the OR graben are markedly defined by systems of faults, which have been known since the late 19th century and show vertical post-Cretaceous displacement of several hundred metres. During the Tertiary, episodes of normal dip-

slip movements on NE-SW-striking fault segments dipping to the graben alternated with strike-slip movements on the same faults and on faults striking roughly E-W.

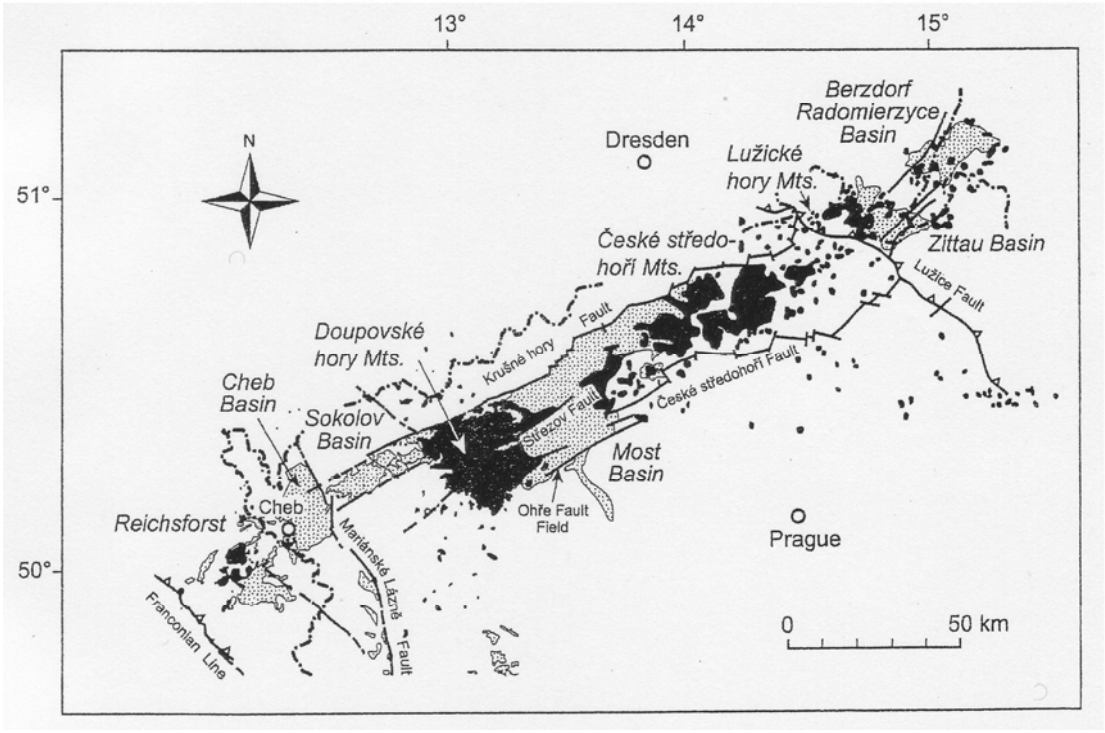

Fig. 3.2: A scheme of the region of fhe Ohre Rift showing the marginal faults of the OR graben, principal volcanic centres (black) and the present extent of tertiary sediments (dotted areas) (adapted from /CHR 01/)

The most prominent volcanic regions lying within the Ohre rift graben are the Doupovske hory mts. (huge explosive volcano and shield volcano), the Ceske stredohori mts. (effusions filling rift valley and composite volcano) and their NE continuation - the Luzicke hory mts. (mostly exhumed subvolcanic bodies).

Four major areas of tertiary sediments are preserved in the Ohre rift (from NE to SW): the Zittau and Berzdorf basins, the Most Basin, the Sokolov Basin and the Cheb Basin. Of these, only the Most and Sokolov basins are located within the limits of the Ohre rift graben proper. The basins are separated from one another by volcanic domains and by fault systems which cross-cut the Ohre rift graben axis at high angles. The prominent, NE-trending fault systems, which confine the Most and Sokolov basins, as essentially erosional relicts in the present-day topography, are relatively young compared to the Oligocene to Lower Miocene age of the basin fill.

Different models on the structure of the Ohre rift and its graben structure have been formulated, among which the most important come from a) Hibsch (1930), b) Kopecky (1978), c) Malkovsky (1977, 1980, 1985), and d) from coal geologists working in the tertiary basins in the Krušné hory piedmont area (Hurnik 1982, Hurnik and Havlena 1984). These four models are briefly reviewed and cited in /ULR 02/.

3.1.3 Cenozoic volcanic products of the Ohre Rift region

The young intraplate volcanism of the Bohemian Massif forms an integral part of the Central European Volcanic Province (CEVP). The existence of an age-related differentiated volcanic series in the Neoidic Subprovince (Late Cretaceous to Cenozoic) of the Bohemian Massif has been established in association with the continued volcanic activity in the Bohemian Massif (79-0.26 My). Two phases were recognised, producing two principal rock series:

A Pre-rift series of ultramafic ultra-alkaline volcanism consisting of a unimodal series of olivine melilitolite-polzenite-olivine melilitite/olivine nephelinite (79-49 My, Upper Cretaceous to Paleogene), which occurs exclusively in blocks flanking the later Ohre Rift. It may represent the precursor of subsequent rifting, or could be a manifestation of an independent mantle plume.

B Prevailing alkaline volcanism (42-0.26 My, Eocene to Pleistocene with a maximum at 32-20 My, Oligocene to Miocene), formed by two coexisting inexpressive bimodal series - weakly alkaline series (olivine nephelinite/basanite - trachybasaltlalkali olivine basalt - trachyte) and strongly alkaline series (nephelinite/tephrite = phonolite). The distribution of products of this series in the NW part of the Bohemian Massif is controlled by the course of the Ohre rift and the Labe Tectono-Volcanic Zone. The main episode (42-16 My) is characterised in the Doupovské hory mts. area by mostly unimodal (foidite) rock series.

3.1.4 Doupovské hory Mts.

The largest preserved volcanic complex belonging to the Ohre rift - the Doupovské hory (DH) mts. - covers an area of approx. 30-40 km in diameter. This area has not been affected by erosion as much as the České středohoří volcanic complex so the superficial volcanic products (lavas of olivine-poor nephelinite/tephrite - trachybasalt

association and pyroclastics) are better preserved. The maximum inferred present-day thickness of the products reaches 500 m. Not a long time ago, this complex has been believed to represent a deeply eroded stratovolcano with the central caldera developed near the former town of Doupov. Two age-related volcanic formations were recognised in the Doupovské hory:

a) The volcanic activity started with Plinian explosions from the central crater vent producing air-fall tuffs and pyroclastic flows (ignimbrites). The tuffs were partly resedimented in probable lake environment at the distal parts of the complex. K-Ar data measured on altered dark mica (phlogopite-vermiculite mixed-layered structure) from tuffs of the Detan locality resulted in 37.7 My. These tuffs are overlain by tephritic flow (Vrbicka) newly dated at 32.6 ± 1.5 My. Several other smaller vents identified in the northern part of the complex (Telcov - Martinov - Lestkov area) also produced pyroclastics, but of Strombolian- and Hawaian-type eruptions.

b) The younger volcanic sequence is predominantly effusive, sometimes with only thin subordinate air-fall tuff layers developed. The effusion of different types of the olivine-free lavas (foidites and tephrites substantially prevail over olivine foidites and basanites) cover the largest area of the complex. The lavas are often of vesicular structure and brecciated (aa facies). Dating of massive rocks of lava flows overlying the older explosive sequences yielded different ages - glassy "leucitite" lying on dark mica-bearing tuff at Dverce - 25.1 Ma, "leucite tephrite" at Vojkovice near Karlovy Vary - 22.5 Ma.

Dynamics of the volcanic activity is documented by presence of lahar accumulations which originated on the slopes of the volcano by possible volcanic tremor and moved downslope using the radial-arranged valleys. The volcanic activity of the Doupovské hory (33-22 My) can be attributed to the main volcanic episode of the Ohre rift.

3.1.5 Tertiary basins in the Ohre Rift region

Sedimentation in the rift area started with the Late Eocene Stare Sedlo Formation of fluviolacustrine origin. These sand-dominated deposits are dated by the thermophilic evergreen vegetation dominated by the extinct Hamamelidaceae, Fagaceae and Lauraceae. Sites rich in diagnostic plant fossils are confined to the Sokolov and Cheb basins and to the DH. Sedimentation of sands; clays, limestones, coal seams and diatomites took place in small basins and depressions. Such sediments are locally rich

in fossil plants and animals. A cross section through central part of the Sokolov basin with its typical stratigraphy is presented in Fig. 3.3. Not all of the geological units shown are represented in Hroznětín part of the basin with Ruprechtov site. Especially the No's 1 and 2 are not found at that site today, No. 4 is represented by a small lignitic horizon and No. 5 is also coming across just as a thin layer.

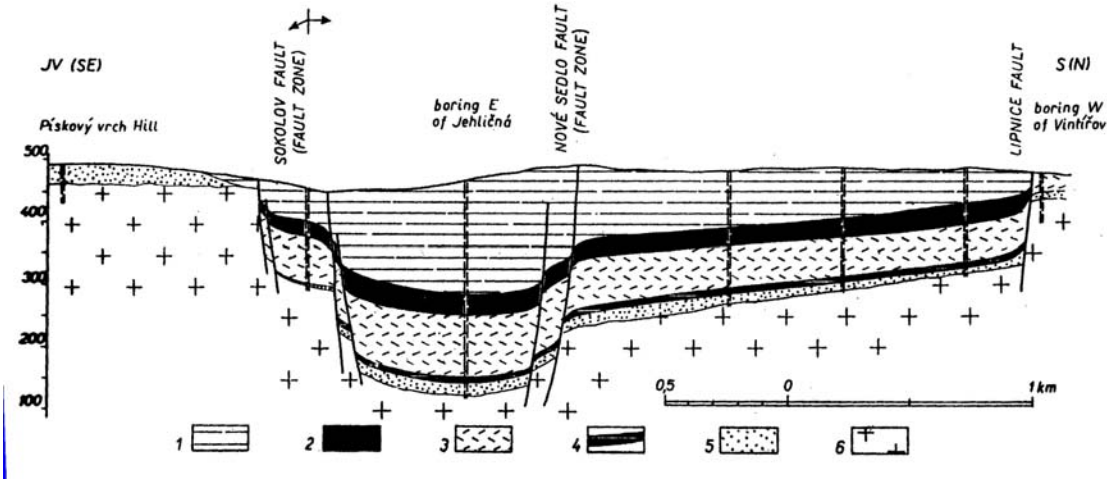

Fig. 3.3: Cross section through the central part of the Sokolov Basin (from /SVO 66/). Legend: 1: Cypros claystone / 2: Main Seam Formation / 3: Volcanogenic Series / 4: Josef-seam Formation / 5: Staré Sedlo basal clastics / 6: Granite

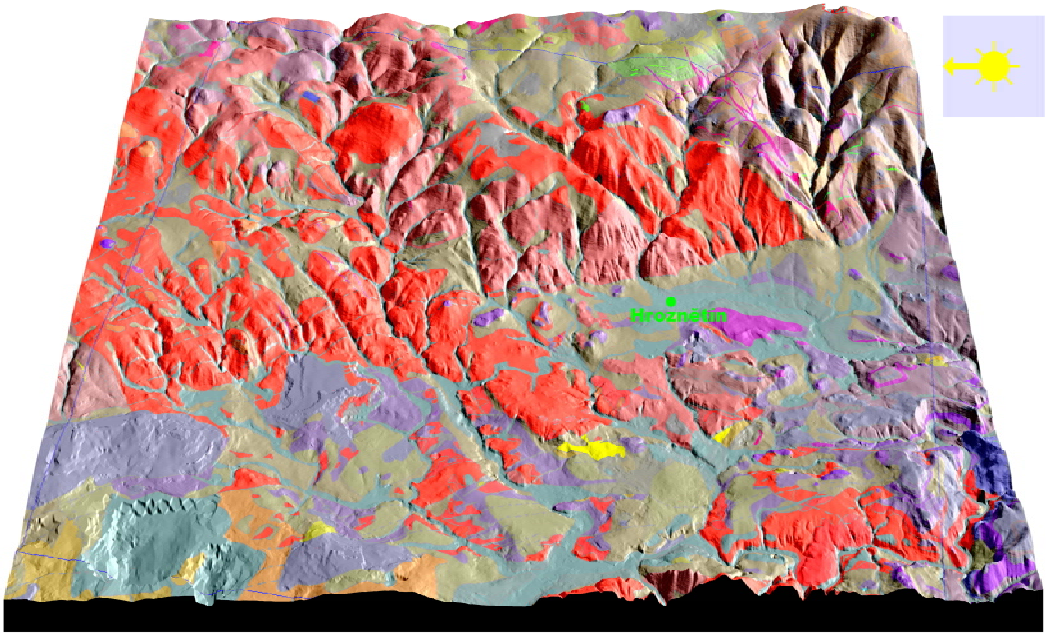

Fig. 3.4: Relief map of parts of Erzgebirge and Sokolov basin with notation of main geological units: red = granitic rock; purple = volcanic rock; other = Tertiary sediments

3.1.6 Issues of mineral and thermal waters in the Ohre Rift region

The piedmont zone of the Krušné hory mts. is well known by many mineral and thermal waters occurrences. Even though mineral waters are spread all over this region, the most distinguished are two areas: the Teplice Spa and Usti nad Labem-Decin thermal water region in the NE and the "Spa triangle" of Karlovy Vary *(Carlsbad),* Marianske Lazne *(Marienbad)* and Frantiskovy Lazne *(Franzensbad)* in the SW. In both these areas mineral waters are of different origin and character.

West Bohemian mineral waters are frequently designated as the Carlsbad type, characterised by prevailing sodium, sulphate, chloride and bicarbonate contents, rnostly accompanied by CO_2. From this "basic" Carlsbad type, a wide gamut of mineral waters has originated depending on their local hydrogeologic position and different influences acting both in space and time. Differences in hydrogeologic conditions result in extraordinary variability in their chemical and physical properties, chemical composition, TDS and CO_2 contents and their temperature ranging within a broad interval from cold to thermal waters up to 73°C in the Karlovy Vary Spa,.

Sedimentary fill of the Cheb and Sokolov basins and the crystalline complexes in their basement represent two different hydrogeologic environments, dissimilar in their properties: chemical composition of recipient rocks, geometry and anatomy of hydrogeologic bodies, distribution, magnitude and variability of permeability and other hydraulic properties, groundwater flow characteristics and possibilities of groundwater storage. Mineral water occurrences can therefore be found in entirely different hydrogeologic environments. For example, host rock of the thermal waters of the Karlovy Vary Spa is granite, cold mineral waters of the Marianske Lazne, Spa occur in different types of crystalline rocks (granites, amphibolites, gneisses) and those of the Frantiskovy Lazne Spa in Neogene deposits of the Cheb Basin. Originally, these mineral waters were encountered on the surface in springs and in relatively shallow water wells with TDS up to 6 g/L.

Carbon dioxide is generally considered to be of deep-seated origin, as a post-volcanic product of the former Tertiary and Quaternary volcanic activity in the region. On the other hand, with the exception of bicarbonates, no general agreement has been reached concerning the origin of other main mineral water constituents (chlorides, sulphates and partly also sodium). Some of the authors consider the origin of main constituents as a result of interactions in respective rock-water-CO_2 systems, others

assume origin connected with volcanic activities. Salt-water content having originated from lakes or seas in different geologic eras was considered in the 1960's. /DVO 98/ presumed that the Carlsbad type is a mixture of recently recharged waters with relict brines from Tertiary closed lakes that occurred under semi-arid conditions. These brines descended into intensively fractured rocks or were preserved as synsedimentary or post-sedirnentary waters in Tertiary deposits. Bicarbonates and other constituents are products of rock-water interaction, sometimes under a supporting effect of CO_2. This approach can well explain the extraordinary variability of. physical and chemical properties of West Bohemian mineral waters in dependence on the depth of groundwater flow (temperature), different CO_2 content, degree of leaching of aquifer system and chemical composition of recipient rocks.

3.1.7 Uranium mineralisation in Neogene coal-bearing sediments

The area of Tertiary sub- Krušné sedimentation includes alltogether three separate limnic basins; The Chomutov-Most Teplice basin, the Sokolov basin and the Cheb basin. These basins are either partly rimmed or underlain by granitic or basaltic rocks.

The sedimentation within these basins begins with mostly sandy sediments during the Lowex and Middle Oligocene filling shallow depressions. After denudation and volcanic activity, major Tertiary sedimentation occurred at the beginning of the Miocene. Individual basins partly differ from one another in their lithological development, stratigraphic sequence and total thickness.

From the viewpoint of economic uranium concentrations, the largest Chomutov-Most Teplice basin is the least promising because uranium is almost non-existent there. This is believed to be due to the absence of granitic rocks in their basement.

Regarding the Cheb basin, some uranium mineralisation was found to occur mostly in the westernmost part close to the Smrciny (Fichtelgebirge) granite massif. Small ore accumulations of no economic importance are confined to the basal Tertiary sediments of pelitic-psammitic facies with organic matter.

Following former exploration results, the Sokolov basin appears to be the most promising for the occurrence of uranium mineralisation. Its basement is composed of the Cesky les crystalline complex in the west and kaolinised granite of the Karlovy Vary pluton in the east. The Staré-Sedlo formation fills shallow depressions in the basement

relief. It is followed by the productive formation which consists of the Josef coal seam, a volcanogenic series and the major coal seam. The cypress formation is composed of bituminous shales.

Fourteen uranium deposits and occurrences were explored in the eastern part of the Sokolov basin, at five localities mining took place.

On a regional scale, the uranium mineralisation is usually confined to parts of the basin close to the outcrops of granitic basement or to places where the basement is composed of granite. There is a strong correlation between uranium accumulation and the relief of the granitic basement. The ore layers occur in depressions which may be of either erosional or structural origin. The geological structure of the deposits is characterised by considerable variation in thickness and faces composition of sediments which formed in shallow basins under extensive volcanic and tectonic activities. Transgressions of the basin sediments onto neighbouring complexes appear to be favorable for the development of ore bodies. This kind of contact seems to be more suitable for longer supply of uranium-bearing solutions or detrital material enriched by uranium into accumulation space.

As the uranium mineralisation is confined mostly to sediments high in organic matter, the shape and position of ore bodies is roughly conformable to the form and position of coal seams or coal and tuffite layers.

The extent and morphology of ore bodies are basically simple and similar for most localities. The bodies are of flat, isometric or lobate elongated form, sometimes separated by thin, sterile layers. their dimensions vary from about several up to 100,000 m², their thickness from a few tens of cm up to 5 m.

The mineralisation of the sub-Krusne hory basins can be characterised as exclusively uranium-bearing, even though some localities show higher concentrations of beryllium, germanium and gallium. The mineralisation can be classified as disseminated, confined to the matrix of psammite-psephite sediments or to coal.

The following uranium minerals were identified: autunite, torbernite, earthy uraninite, coffinite, brannerite; uranium phosphates. Among the other ore minerals, pyrite, melnikovite, marcasite, arsenopyrite, galena, ilmenite, sphalerite and psilomelane are the most common.

The uranium deposits of the sub-Krušné hory tertiary basins are described in literature mostly (e.g. /KOM 94/) as of sedimentary (hydrogenic) origin, the granitoids of the Karlovy Vary and Smrciny plutons being the primary source of the uranium. A detailed scenario for uranium accumulation at Ruprechtov site, including new results from this project, will be introduced and discussed in chapter 6.

3.2 Geology of Investigation area

The regional geology of the Ruprechtov area (Hroznětín part of Sokolov basin), a lithogical overview, the history of uranium exploration and uranium mining as well as the site selection procedure for Ruprechtov as a Natural Analogue have been described in detail in /NOS 02/. Fig. 3.5 illustrates the overall geological situation in Sokolov basin which also can be identified by a satellite image of the same area (Fig. 3.6). The very local geology is shown in Fig. 3.7 which is based on mapping in the scale of 1:10 000. It becomes clear that the widespread pyroclastics are underlain and surrounded (in the S) by granitic rocks which are supposed to be the primary uranium source as discussed in the following chapters.

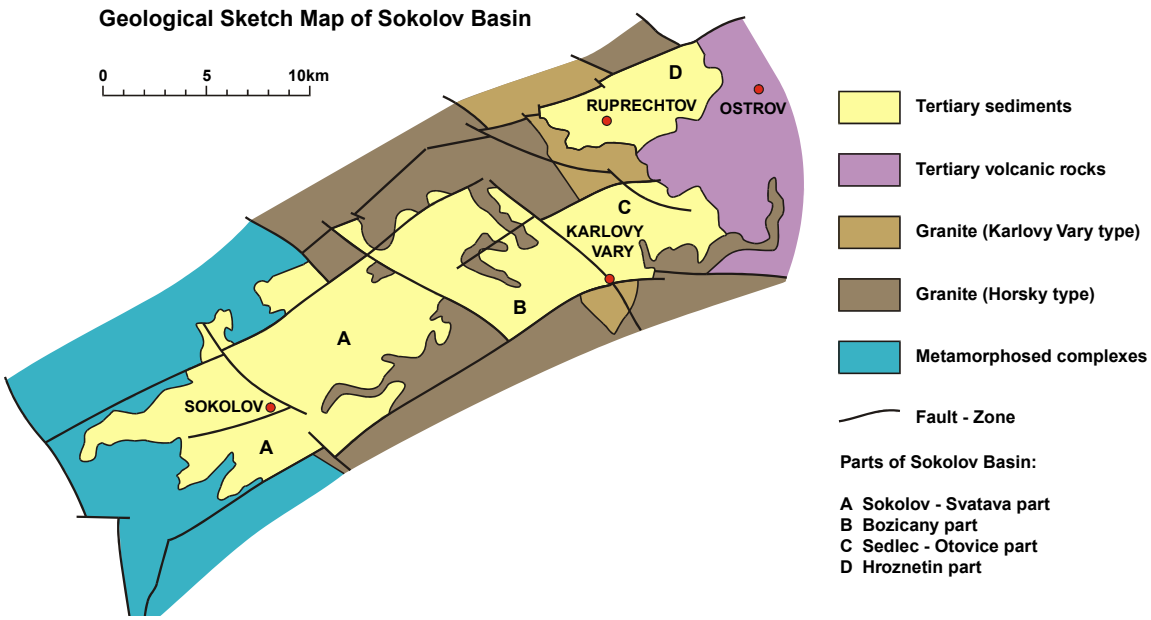

Fig. 3.5: Geological sketch map of Sokolov Basin; the Hroznětín part with Ruprechtov site (NE) is marked by letter “D”

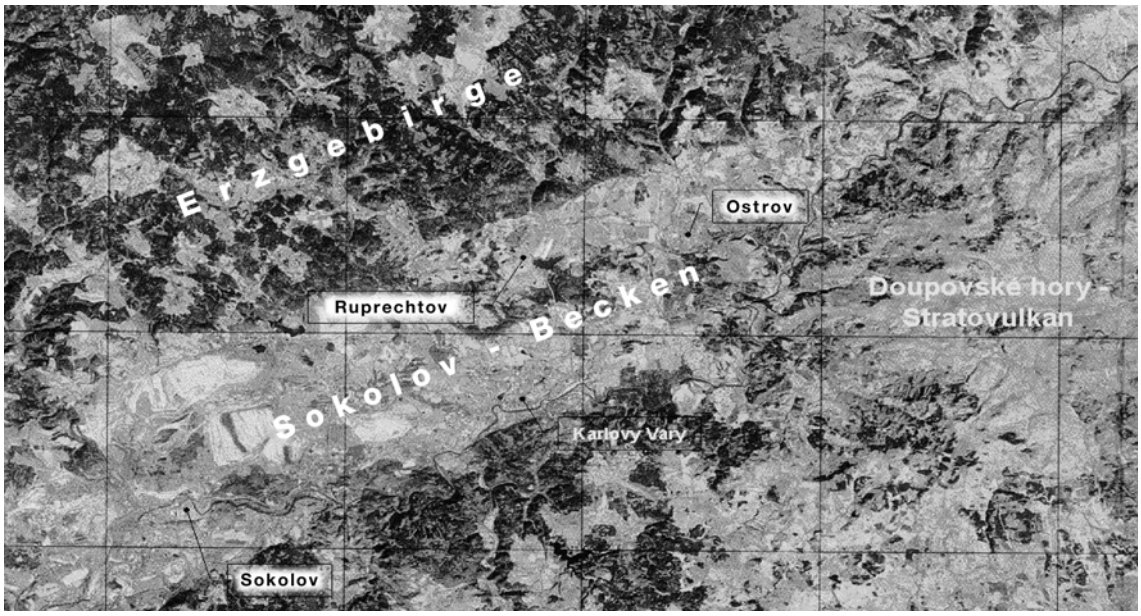

Fig. 3.6: Satellite view of Sokolov basin with location of Ruprechtov investigation area

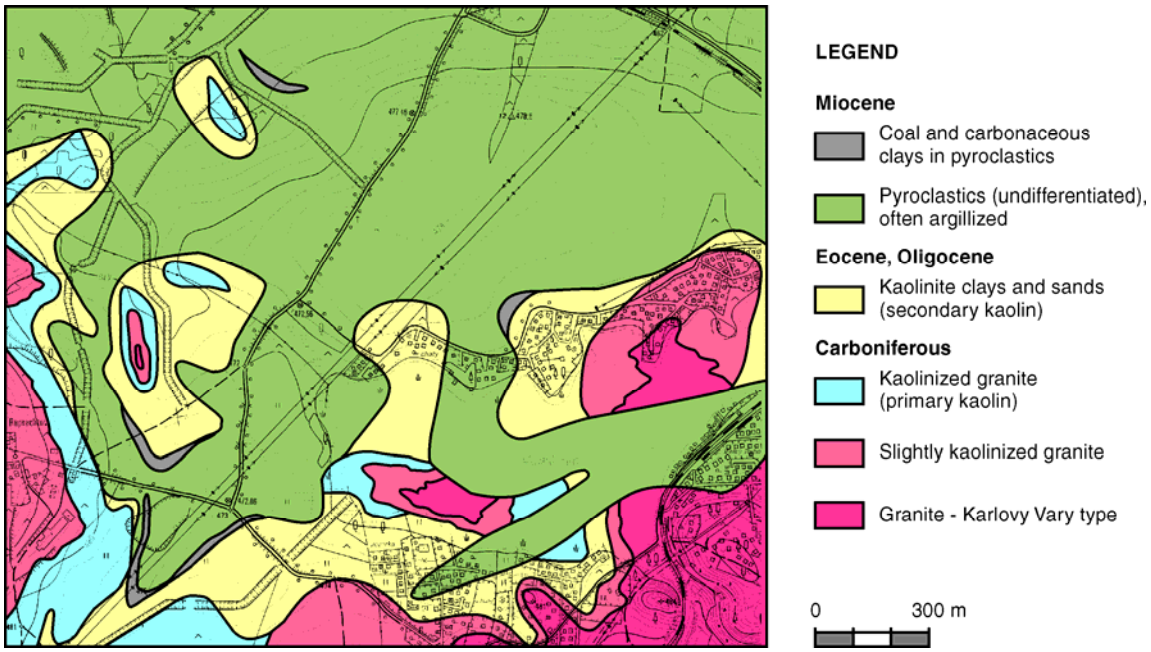

Fig. 3.7: Detailled geological map of investigation area based on geological mapping 1:10 000; in the lower right section of this figure pond and village of Velký rybnik are located; Ruprechtov village is tapping directly at lower left image border. Actual scale: see legend

Tab. 3.1: Geological sequence in Hroznětín part of Sokolov basin (after /BRA 98/)

Geological formation	General lithology	Site specifics	Age (My)
Quaternary	humous arable soil, loam		Quaternary (app. 0.01 – 1.8)
Cypris-formation	kaolinic clay with sandy interlayers	*not sedimentated*	
Volcano-dedritic formation	pyroclastics (tuff, volcanic agglomerates), subaquatic volcanic sediments, brown-coal seams	clayey lignites, no distinct coal seams	Miocene (app. 5.3 – 23.8)
Staré-Sedlo-formation	fine- to coarse-grained sandstone with kaolinic cement, kaolinitic clay	*not developed completely* secondary kaolin	Upper Eocene to Lower Oligocene (app. 37 – 28.5)
Underlying strata (undifferentiated)	granite (partly kaolinised)		Carboniferous (app. 295 - 360)

In summary, the main geological units of the Ruprechtov site, as considered in the following chapters, are (from top) – see also Tab. 3.1:

- Pyroclastic sediments (mostly argillized [bentonitized])
- Clay/lignite-sand layer (main horizon with uranium accumulation)
- Kaolin (weathering product of granite)
- Granite (also outcropping)

In the near surrounding also basaltic dykes occur and are outcropping (e.g. at Ruprechtov village, Hajek site).

Different sources and regulations (e.g. DIN, considered in GeoDin software) cause application of different colours in maps and profiles plotted in this report. The main differences are compiled in the following Tab. 3.2.

Tab. 3.2: Colour of geological units in maps, profiles and GeoDin-profiles (boreholes)

Unit	Maps + Profiles	GeoDin-Profiles
Soil, Quaternary	not plotted	
Pyroclastic sediments		
Clay/lignite-sand		sand
Kaolin	secondary primary	kaolinised granite
Granite		

Note: Due to unequivocal definition of the Staré Sedlo Formation an overlapping of the terms “secondary kaolin” (maps + profiles) and “sand” (GeoDin-Profiles) is possible

3.3 Drilling campaigns

After choosing the uranium accumulation supposed to exist at Ruprechtov site as investigation area in late 1996 several drilling campaigns have been realised in order to investigate the uranium anomaly with respect to its features as a Natural Analogue, the first ones (1996 and 1997) with the main objective to verify the existence of such anomaly so that site specific scientific investigations could start in summer 1999. All drilling campaigns are summerised in Tab. 3.3 with notation of drilling number, date and main objectives of the destined campaign.

Tab. 3.3: Drilling campaigns at Ruprechtov site

Campaign	Drill No.	Date	Main Objectives
I	NA1-NA2	Dec 1996	1st verification of U-anomaly, general stratigraphy, lithology and rock chemistry of the site
II	NA3	Dec 1997	Additional sediment analyses
III	NA4-NA5	Jun/Jul 1999	Specific sampling of sediments and ground-waters (gauge wells), detailed analyses
IV	NA6-NA9	May/Jun 2002	Horizontal & vertical expansion of investigation area incl. outcropping/underlying granite as U-source, specific samplings, hydraulics, in-situ measurements
V	NA10-NA15	Nov/Dec 2003	Expansion of investigation area, proof of model assumptions, proof of preceeding analyses, kaolin-sampling, in-situ measurements

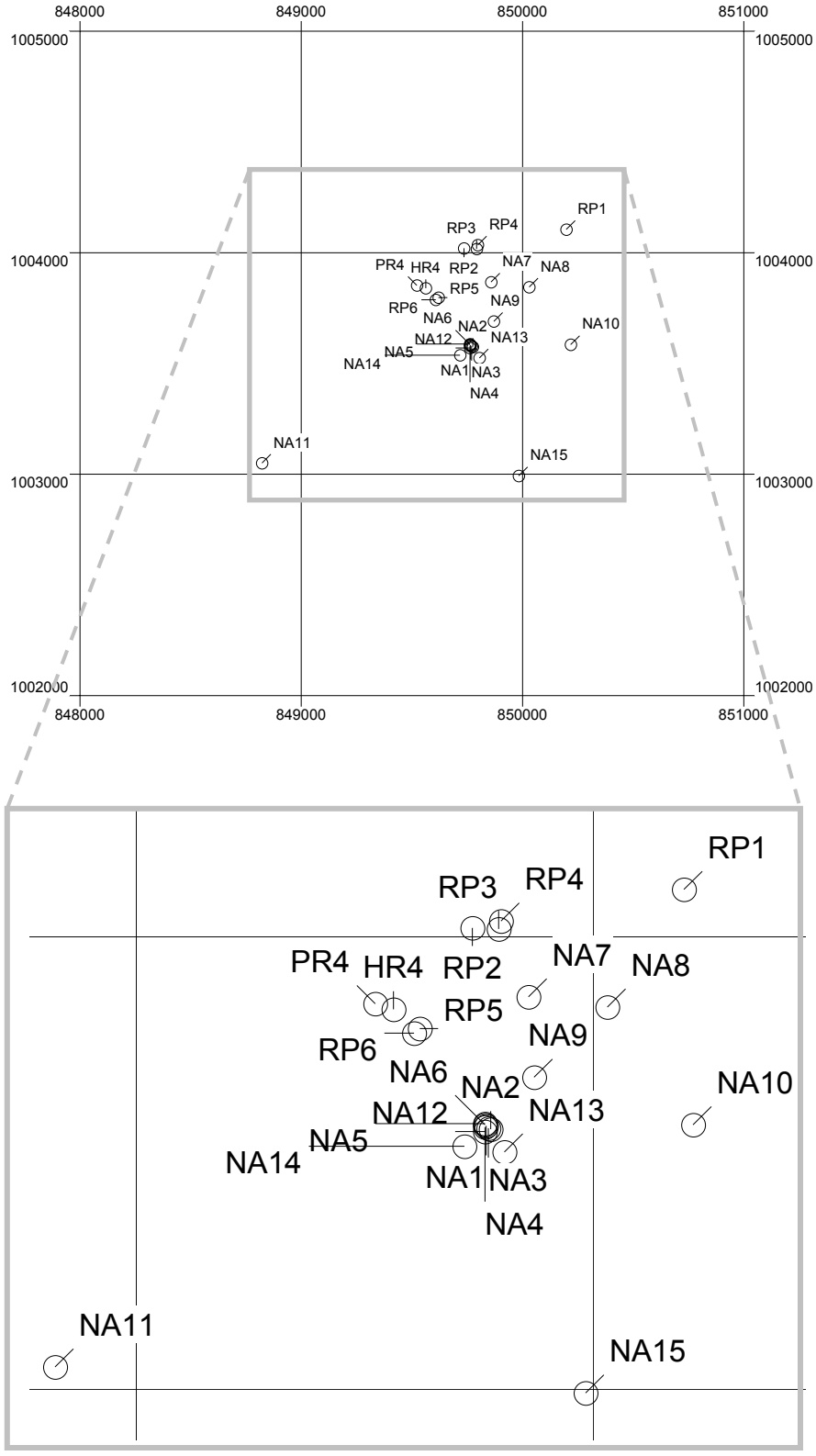

Fig. 3.8: Plot of investigation drillholes used for the project. Due to Czech coordinate system North (N) in this Geodin-figure is at the bottom of the figure

The position of all drillings (NA1- NA15) and additionally also several drillings which have been made available by a local mining company (titled: “RP”, “PR” and “HR”) are plotted in Fig. 3.8 and Fig. 3.9, the coordinates are tabulated in Tab. 3.4.

Tab. 3.4: Coordinates of drillings

	X	Y	Z (terrain) [m a.s.l]	Z (top of casing) [m a.s.l]
NA1	1.003.583,10	849.765,80	471,81	no casing
NA2	1.003.573,90	849.775,10	471,65	no casing
NA3	1.003.578,40	849.770,65	471,70	no casing
NA 4	1.003.579,55	849.762,30	471,70	472,41
NA 5	1.003.587,60	849.761,35	471,78	472,72
NA 6	1.003.585,72	849.763,58	471,73	472,68
NA 7	1.003.867,20	849.856,26	472,10	473,02
NA 8	1.003.845,24	850.029,18	471,44	472,41
NA 9	1.003.689,14	849.870,56	470,75	471,59
NA 10	1.003.585,45	850.217,03	470,77	471,94
NA 11	1.003.049,83	848.821,66	458,28	459,08
NA 12	1.003.568,80	849.762,64	471,52	472,53
NA 13	1.003.526,19	849.804,48	470,49	471,45
NA 14	1.003.537,57	849.717,15	471,65	472,68
NA 15	1.002.992,71	849.983,25	461,15	462,05
RP 1	1.004.104,54	850.196,78	479,08	480,32
RP 2	1.004.020,19	849.735,73	471,42	472,49
RP 3	1.004.017,84	849.792,23	472,24	473,42
RP 4	1.004.035,18	849.797,65	472,03	473,10
RP 5	1.003.798,38	849.620,38	472,14	472,67
RP 6	1.003.786,33	849.608,66	472,37	472,96
HR 4	1.003.839,08	849.561,42	472,29	472,62
PR 4	1.003.851,27	849.522,19	472,86	473,23

Simplified as well as detailed geological profiles of all drillings are documented in the annex.

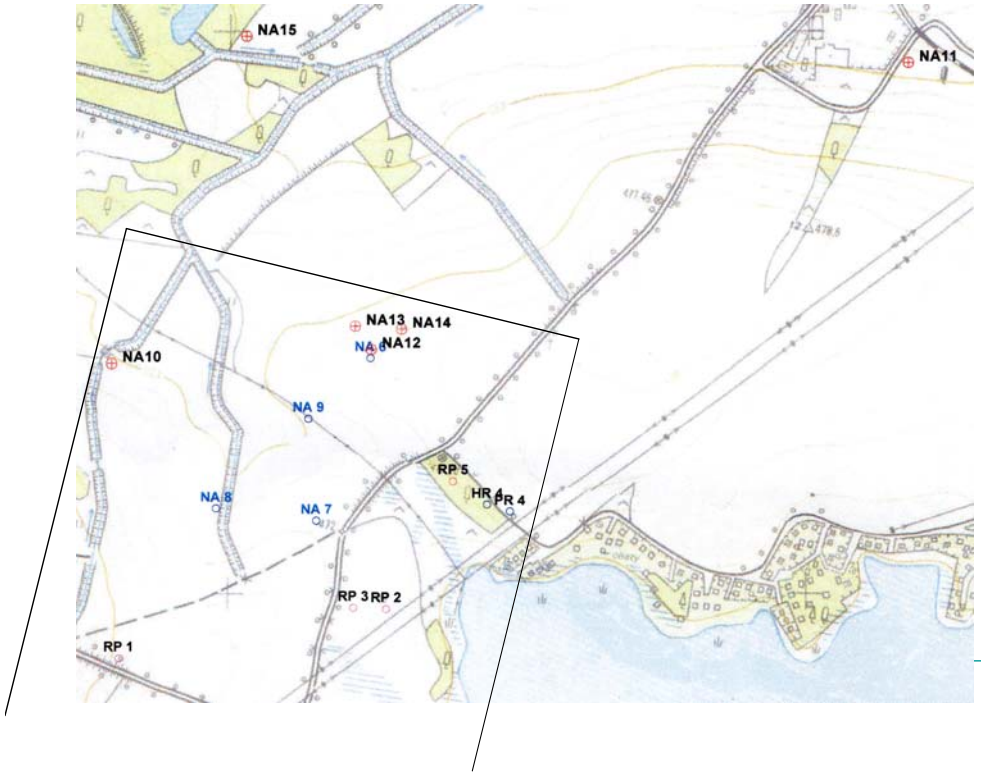

Fig. 3.9: Plot of borehole locations on topographical map 1:10 000

Beside general informations on geology / stratigraphy of the site and construction of groundwater gauges a further main objective of most drillholes has been to gain sediment samples for detailled lab investigations. Since the first two campaigns just have been performed for verification of an uranium anomaly, no special measures had been taken for sampling and storage of core samples. Starting with specific investigations in 1999, the redox-sensitivity of minerals needed safekeeping of samples. An overview of referring measures is given in Tab. 3.5 (see also Fig. 3.10).

Tab. 3.5: Development of drilling procedures at Ruprechtov site

Campaign	Measures	Advantages	Disadvantages	Remarks
III NA4-NA5	Drilling without drilling fluid; drilling/sampling of specified section with use of inner liner; sealing of abutting liner faces by wax with low melting point	Very effective sealing against air contamination	No inspection and description of core material; difficult preparation of aliquots	Not easy to handle (deletion of liner by tenacious clay sediments)
IV NA6-NA9	"normal" core drilling and extraction by core tube without drilling fluid; immediate inspection / description of core material and direct sealing in PVC-tubes	Inspection of core quality, immediate information on stratigraphy; effective protection of core material against reactions with air; easy and quick preparation of aliquots	Rupturing of cores during hauling the core tube; filling of core spaces by drilling mud with slight contamination of outer core	Altogether faultily core quality
V NA10-NA15	Like campaign IV, but slight usage of drilling fluid (formation water)	Significantly improved core quality; less core contamination than in campaign IV		

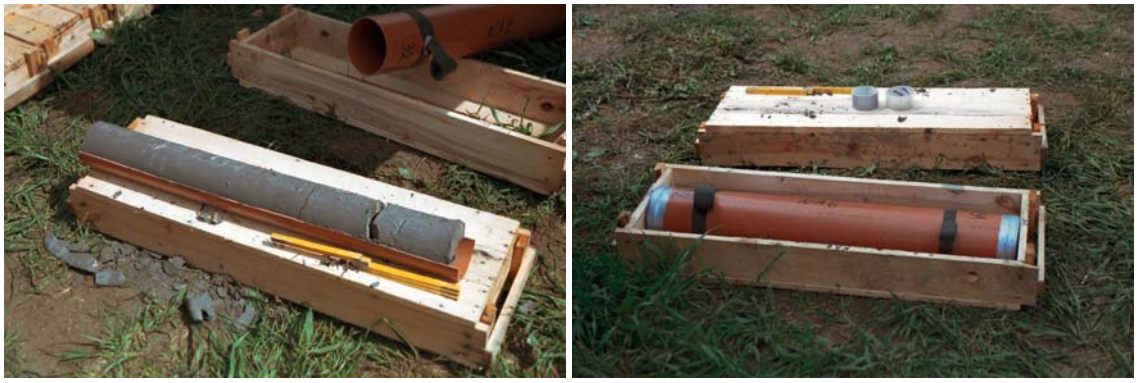

Fig. 3.10: Most effective way of preserving redox-sensitive minerals for lab investigations: a) prompt decription of the core in the field (left) and immediate sealing in PVC-tube with nitrogen-filling (right)

3.4 Sedimentology at Ruprechtov site

Drillings NA1 to NA5 have been described in detail in former reports /BRA 98/, /NOS 02/. The following summary of results from new boreholes NA6 to NA15 is based mainly on an expertise by P. Bosák (Institute of Geology, Academy of Sciences,

Prague) who has been involved in the project for sedimentological surveying. The subsequent results are based exclusively on this survey and do not consider detailed chemical, mineralogical and radiometric investigations so that conclusions on uranium origin could vary from statements later in this report.

In contrast to some older geological documentations, especially final reports of geological exploration at various stages, the actual observations made during the Natural Analogue project, suggested that the identification of suitable correlation horizons or surfaces would be difficult. The most suitable horizons for correlation could be: (1) base of the weathering profile in the Karlovy Vary pluton, (2) top of the primary kaolin, and (3) top of secondary kaolin/base of the Volcanoclastic Formation. Seam horizons in the Volcanoclastic Formation are developed irregularly in horizontal as well as vertical direction and do not persist over distances so that they don't present hydraulic connections and can't be correlated directly. First three horizons represent geological boundaries; two of them are boundaries of clearly definable lithostratigraphic units but are very uneven. The first boundary can be determined only on the basis of technological tests and poses the accepted boundary between weathered and unweathered granitoid. The use of wireline logging for the definition of correlation horizons/boundaries or sequences is not fully possible due to the high facies variability of the basin fill in all directions.

The study of previous results including those of drilling indicated problems with an unequivocal definition of the Staré Sedlo Formation. A new lithostratigraphic unit – secondary kaolin – was introduced. This unit includes redeposited primary kaolin with coarse detrital admixture, locally with some proportion of volcanoclastic material, formed after the end of deposition of the Staré Sedlo Formation and before the onset of deposition of the Volcanoclastic Formation. It is mostly represented by colluvial, colluvio-fluvial and alluvial sediments. It has been hitherto ranked within the Staré Sedlo Formation. The Staré Sedlo Formation itself has not been documented in the new boreholes directly but might have also an counterpart in a sandy horizon found in several boreholes underneath the lowest clay-lignite seam, inducing the term "clay/lignite-sand" used for the horizon with uranium anomalies.

The study of previous results also suggested the problem of the paleotopography origin before the deposition of the Volcanoclastic Formation and the role of tectonic movements as relief-forming agents. /BOS 05/ intepreted the relatively steep paleoslopes in primary kaolin (up to 35°) with shaping by faults before the onset of

deposition of the Volcanoclastic Formation. Details will be discussed in chapter 6. Kaolinisation - in his interpretation - is seen as a result of intensive weathering, not of hydrothermal alteration. The main stage of kaolinisation took place before, and simultaneously with, the deposition of the Staré Sedlo Formation and provided sources of silica for its silicification. It cannot be excluded that kaolinisation continued even after partial destruction of the Staré Sedlo Formation in a setting of rejuvenation of relief dynamics due to the reactivation of tectonic processes.

The analysis of new drill cores revealed high facies and lithological variability in horizontal and vertical directions, which complicates (or even precludes) correlations within the Volcanoclastic Formation even over short distances of metres to tens of metres. This fact is explained by the prevailing character of deposition of the Volcanoclastic Formation: deposition from mudflows and debris flows (lahars) combined with the deposition on an alluvial plain dominated by floodplain-lacustrine habitats. Accumulation of volcanoclastic material was areally uneven.

High facies variability in all directions suggests that stable conditions favourable for the deposition of thick coal seams were not established. Coal deposition took place in mire-lacustrine setting. The area of organic matter accumulation was subjected to floodings of irregular periodicity, depositing fine sediments of crevasse-splay and flood facies and – in upper horizons – also mudflows and debris flows interrupting continuous plant matter accumulation. Numerous pyrite concretions and grains may evidence a markedly reducing environment of deposition and very early diagenesis (syndiagenesis) of sediments with dispersed coal matter and of coal seams and coal interbeds.

/BOS 05/ concludes that the interpretation of sedimentological results indicates a syngenetic model of accumulation of radioactive elements with a low probability of their later redistribution/mobilization rather than epigenetic infiltration enrichment and that a hydrothermal origin can be rejected. Major portion of the uranium mineralisation seems to have been sorbed by organic-rich sediments or iron compounds from surface waters. This is also suggested by the presence of kaolinised remains of rocks of the Karlovy Vary pluton (kaolinised feldspars) and heavy mineral assemblages typical for the Karlovy Vary pluton and the Krušné hory Crystalline Complex in almost all mineralised horizons. Weathering fluids enriched in soluble uranium complexes and compounds could have derived from destructed weathering profiles on granitic rocks

and from the erosion of unweathered granitic rocks from paleohighs inside the depocentre as well as from more remote sources (Krušné hory Mts.).

In chapter 6 results of sedimentological as well as recent lab investigations within the project will be used to develop a most likely scenario for uranium mobilisation, transport and retention which doesn't match with all previous views and interpretations but seems to explain the site specific knowledge more comprehensively.

3.5 Geological profiles across investigation area

Based on geological description of boreholes and processing with the software programm GeoDin (v. 3.0) several profile lines across the investigation area could be constructed (Fig. 3.11 to Fig. 3.16), which, in combination with existings maps, reports, assumptions etc., are summarised in the schematic geological profile of investigation area (Fig. 3.17) which again forms the basis for all considerations concerning uranium mobilisation, -transport and -retardation processes described in following chapters.

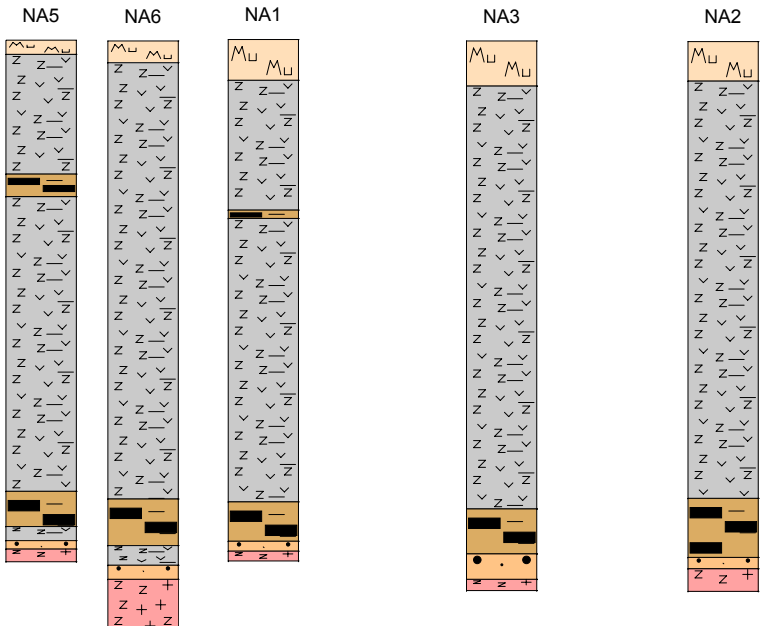

Legend: **light orange (top)**: soil, Quaternary / **grey**: volcanoclastics / **brown/black**: clay-lignite horizon / **dark orange**: sandy horizon / **red**: kaolin, kaolinised granite or granite (for details see annex)

Fig. 3.11: Geological profile representing drillings NA5, NA6, NA1, NA3 and NA2 (for location of drillings see Fig. 3.8 and Fig. 3.9)

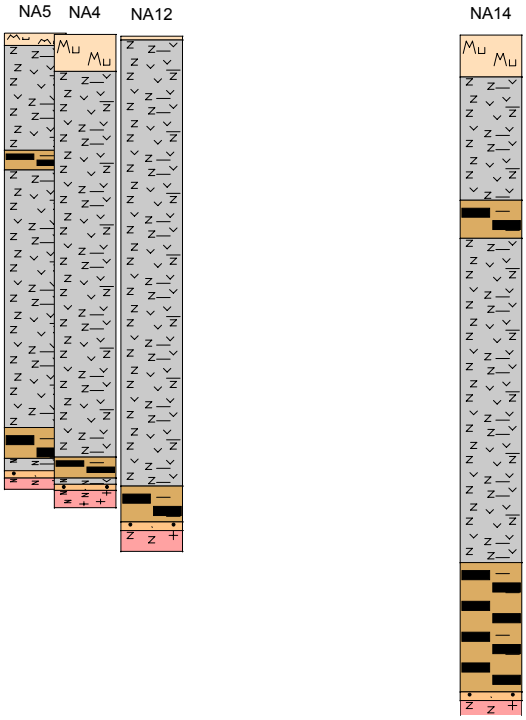

Fig. 3.12: Geological profile representing drillings NA5, NA4, NA12 and NA14 (for location of drillings see Fig. 3.8 and Fig. 3.9) – Legend: see Fig. 3.11

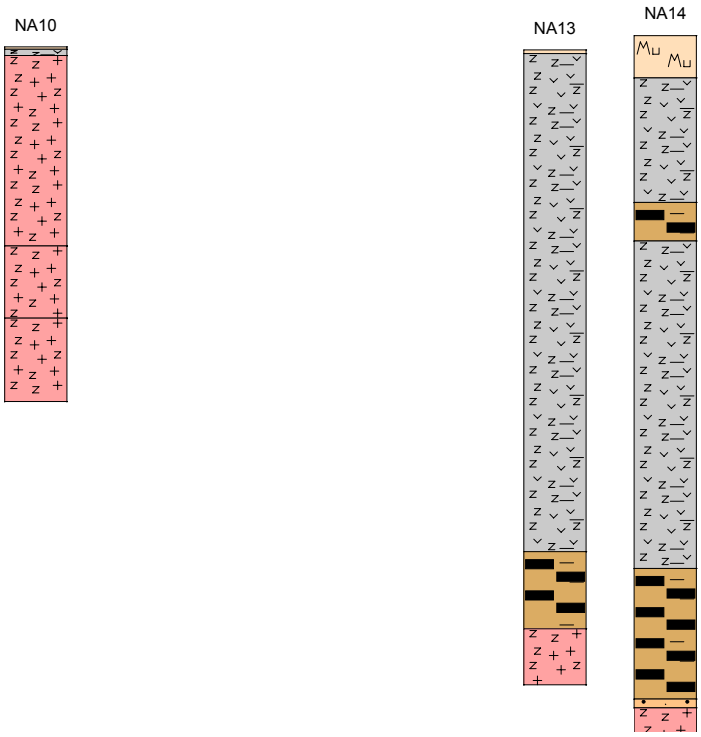

Fig. 3.13: Geological profile representing drillings NA10, NA13 and NA14 (for location of drillings see Fig. 3.8 and Fig. 3.9) – Legend: see Fig. 3.11

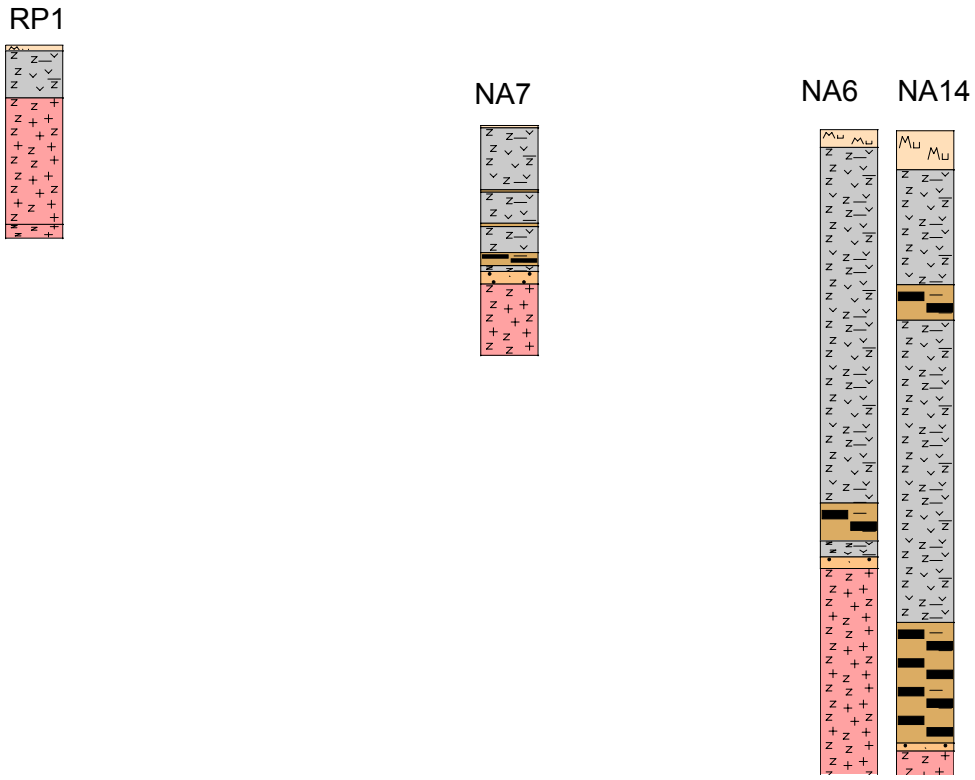

Fig. 3.14: Geological profile representing drillings RP1, NA7, NA6 and NA14 (for location of drillings see Fig. 3.8 and Fig. 3.9) – Legend: see Fig. 3.11

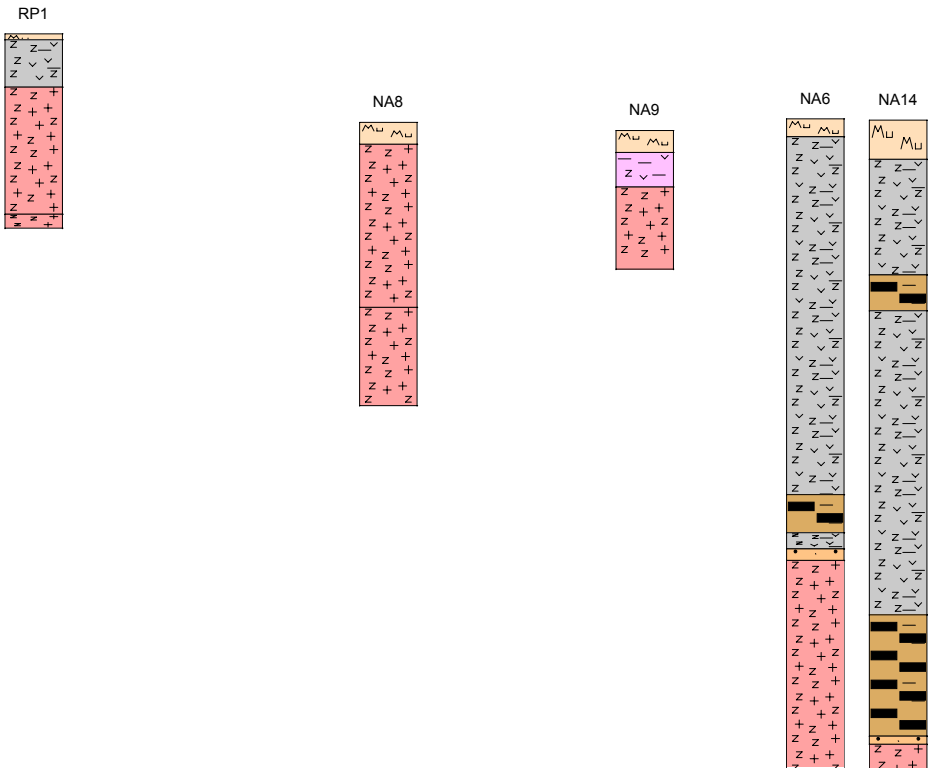

Fig. 3.15: Geological profile representing drillings RP1, NA8, NA9, NA6 and NA14 (for location of drillings see Fig. 3.8 and Fig. 3.9) – Legend: see Fig. 3.11

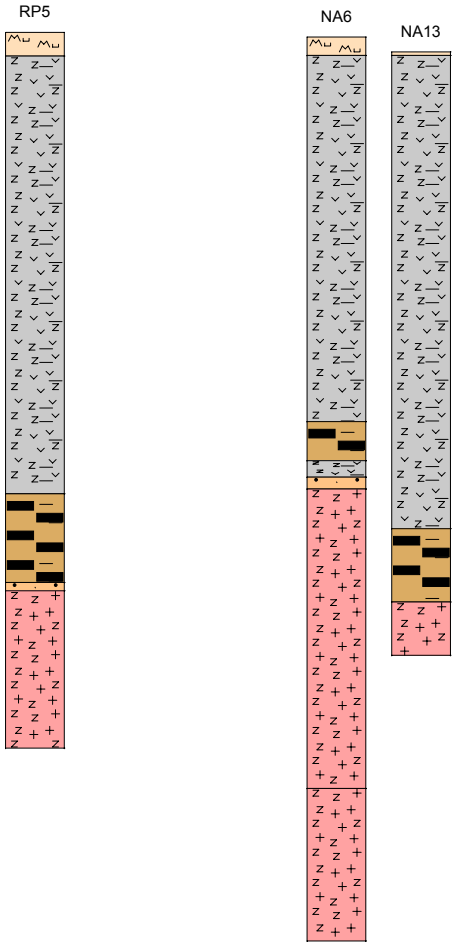

Fig. 3.16: Geological profile representing drillings RP5, NA6 and NA13 (for location of drillings see Fig. 3.8 and Fig. 3.9) – Legend: see Fig. 3.11

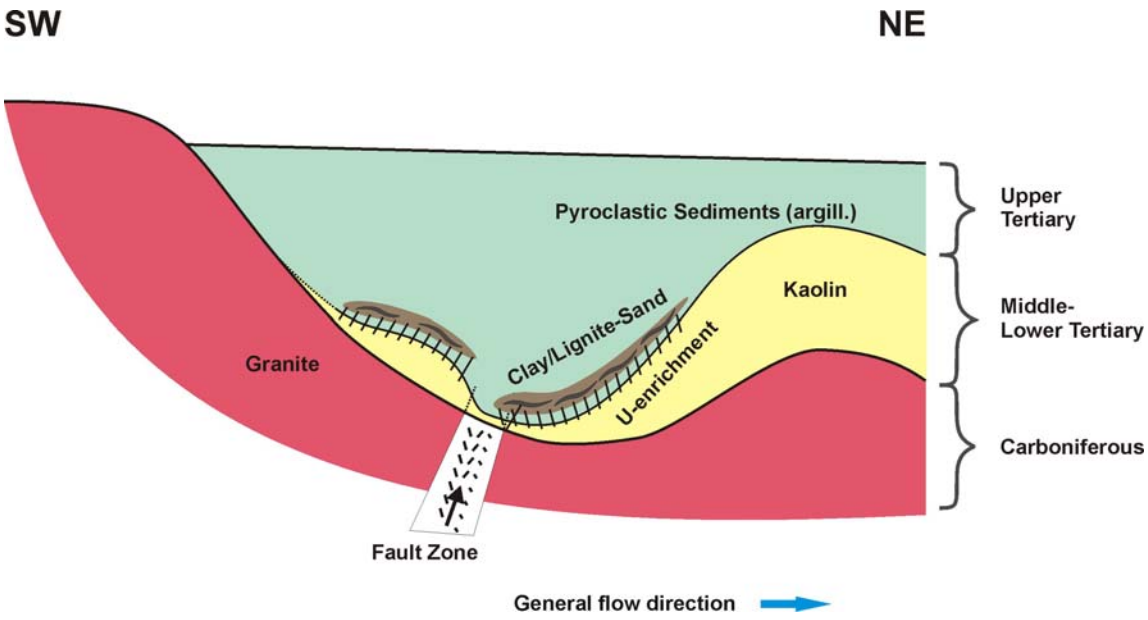

Fig. 3.17: Schematic geological profile of investigation area based on Fig. 3.11 - Fig. 3.16

3.6 Geological development of Ruprechtov site

The following sequence of sketches (Fig. 3.18) summarises firstly the new ideas of the development of the Ruprechtov site as shown in Fig. 3.17. It's aim is to represent single important steps that led to the current geometry of rock units and to the development of the uranium mineralisation style. Therefore it is not drawn to scale. Details including the uranium history are discussed in chapter 6 (scenarios).

The single stages schematically cover the following development:

a) The "old" pre Tertiary landscape is dominated by granitic rock which is charcterised by an uneven surface with hills and valleys caused mainly by the old structure of granite body but also some older faults. Sediment deposits occur in the valleys and also some detrital uranium minerals are deposited (which is contradicting to a pre Tertiary kaolinisation, as discussed later in detail). The landscape is covered by vegetation – grass, trees and swamps dominate the valleys and form the base material for later lignitic horizons.

b) Due to violent volcanic outbursts the area is covered by ash falls. The estimated primary thickness of the ash sequences is app. 200 m.

c) Groundwater, strongly enriched in CO_2, either from gas trapped in the ashes and/or pouring out from fault zones alters the rocks. Kaoline is formed in the place of granites and granite derived slope and valley deposits and is accompanied by mobilisation of uranium. K and Fe is also leached from granites and deposited in bentonites. A Bentonitisation and sideritisation takes place in the volcanic ashes. This alteration enhances the mobilisation of Ti and P that is introduced into forming kaolines. Mobilised uranium will already be sorbed on / close to forming lignites.

d) The onset of tectonic phase (app. 16-15 my) is marked by the intrusions of basalts in the form of dykes and laccolithes. This lead to contact metamorphism of surrounding rocks, except kaolines and could trigger locally hydrothermal flow which scavenges the uranium from deeper parts of granites. Uranium is sorbed on the lignites in places of thin and/or absent underlying kaoline.

e) A very young (Pliocene?) phase affects slope deposits of the main Krušné hory fault. Important erosion removes larger parts of volcanic strata. The whole area is tilted in the normal faulting as a consequence of the crustal stretching. The deepest part of the basin (140 m) is therefore close to main Krušné hory fault.

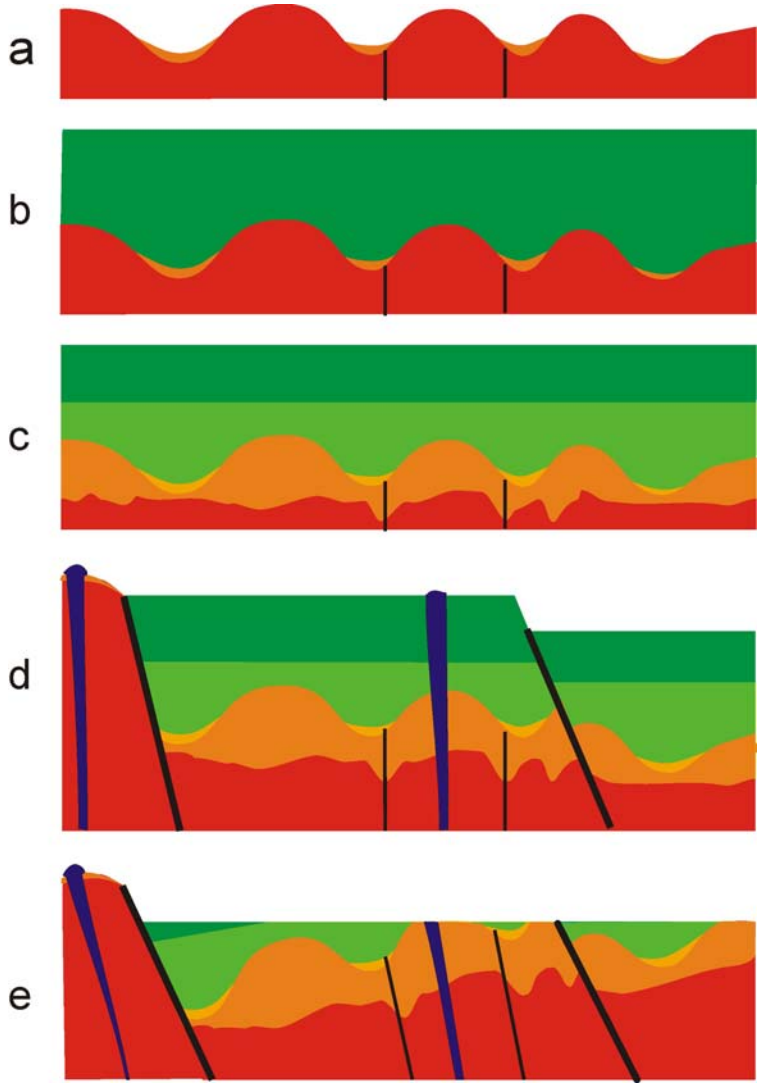

Fig. 3.18: Sketch sequence of geological development of Ruprechtov site (for explanations see text) – not to scale

3.7 Summary

The Sokolov Basin is one of altogether three tertiary basins in a complicated graben system, developed in SE foreland of the Krušné Hory Mts. (Erzgebirge). This structure is also interpreted as a rift valley in the sense of plate tectonics. The origin of the

graben system is connected with the Alpian-Carpathian orogeny. The underlying rocks are predominantly formed by kaolinised granites of Carboniferous age.

The classical concept divided the sedimentary filling of the basin into the following formations (from top to bottom):

- Cypris Formation
- Main Coal Seam Formation
- Volcanodetritic Formation
- Coal Seam Josef Formation
- Staré Sedlo Formation

In contrast, modern stratigraphy distinguishes just between:

- Cypris Formation
- Volcanodetritic Formation with coal seams
- Staré Sedlo Formation

Staré Sedlo Formation

Sedimentation of this Formation started in Upper Eocene and continued to Lower? Oligocene. Predominant rock type is fine- to coarse-grained sandstone with kaolinitic cement, locally with admixture of gravel. Kaolinite clay is also present. In some places, sandstone is silicificated to the form of quarzite. The Thickness of sediments ranges between 0-10 m, exceptionally up to 40 m. At Ruprechtov site a rather thin sandy horizon at the base of Tertiary might be interpreted as a substitute of the Staré Sedlo Formation.

Volcanodetritic Formation with coal seams

This Formation is divided from the Staré Sedlo Formation by a distinct hiatus. Sedimentation started in Lower Miocene. The Formation is developed under strong tectonic and volcanic activity. In the western part of Sokolov Basin sedimentation starts by the lignite coal seam Josef. The maximum thickness of this seam is up to 40 m. The sedimentation continued with a complex of pyroclastics, predominantly tuffs and volcanic agglomerates. These rocks are often argillized to bentonite. Subaquatic volcanic sediments are also present. Only in the western part of the basin, two distinct lignite seams are present in the upper most part of Formation. The total thickness of

the formation varies in the range 10-350 m. Sediments of Volcanodetritic Formation at Ruprechtov are represented mainly by altered tuffs. Instead of a distinct coal seam only some clayey-lignitic layers are found, mainly near the base of Tertiary and for the purposes of the current project mostly susumed with subjacent sandy layer to the so-called “clay/lignite-sand” horizon.

Cypris Formation

Sedimentation of this Formation started after significant deepening of the basin, but without a distinct hiatus. The Cypris Formation is predominantly built by monotonous kaolinite clays with some sandy intercalations and locally with intercalations of redeposited volcanodetritic material. Total thickness of the Formation varies from 0 to 180 m. At Ruprechtov today no more sediments of this formation are found.

Hroznětín part of Sokolov Basin

The Hroznětín part is the most north-eastern part of Sokolov Basin. Due to its position and especially its vicinity to Doupovské Hory mts. stratovolcano, this part developed differently. The most important differences are as follows:

- The Stare Sedlo Formation is not developed continuously and its thickness is just up to 5 m. Lithologically it is built up by kaolinite clay and sand („secondary kaolin"). No quarzites are present.

- Distinct coal seams are not developed. There are present only a few meters thick representatives in the form of clayey lignite or carbonaceous clay in the pyroclastics. Uraniun mineralisation is bound to these sediments and its surrounding in some parts.

- The Cypris Formation is in total not present, because of emersion of this part of basin in the time of its sedimentation.

4 Hydrogeology

From old boreholes and hydrogeological models developed in the past it is known that the general flow field in the tertiary basin is directed from SW to NE. However the models consider the pyroclastic sediments as one homogeneous layer with averaged water conducting properties. It was also assumed that the kaolin horizon, reaching thicknesses of several ten of meters, acts as a hydraulic barrier between the underlying granite and the water bearing system in the pyroclastic sediments, i.e. granite and Tertiary are independent hydraulic systems.

Current laboratory and on-site (pumping tests, Fig. 4.1) measurements of hydraulic conductivities at selected drill cores made clear that only distinct water bearing layers with kf-values of 10^{-5} to 10^{-7} m/s and a thickness of about 1-2 meter exist, mainly in the surrounding of the clay/lignite-sand layer, whereas the pyroclastic sediments (sensu strictu) are very low permeable with typical kf-values of 10^{-10} to 10^{-11} m/s. An overview of the pumping test, performed in several boreholes is given in Tab. 4.1.

Fig. 4.1: Photograph of pumping test at borehole NA8

Tab. 4.1: Results of hydrogeological pumping test

Tested well	Geol. Unit	Aquifer Depth [m]	Aquifer Thickness [m]	Analysis Method	Hydraulic Parameter		
					T [m^2/s]	K [m/s]	S
NA 4	tertiary sediments	34.0	3.0	Theis	4.55E-06	1.52E-06	7.06E-05
NA 5	tertiary sediments	19.5	1.7	Theis	9.30E-08	5.47E-08	3.97E-05
NA 6	tertiary sediments	33.8	3.2	Theis Recovery	1.80E-06	5.62E-07	5.80E-05
NA 7A	tertiary sediments	16.3	2.9	Slug Test	5.45E-07	1.88E-07	
NA 7B	tertiary sediments	10.5	0.5	Cooper-Jacob	2.20E-05	4.40E-05	1.56E-07
NA 8	granite	8.5	16.0	Average	3.20E-05	2.00E-06	1.13E-06
NA 9	tertiary sediments	4.5	1.5	Theis	4.90E-06	3.26E-06	5.32E-03
NA 10	granite	19	9.5	Theis	2.72E-07	2.86E-08	1.06E-03
NA 11	tertiary sediments	33.3	1.0	Theis	6.50E-06	6.50E-06	9.19E-03
NA 12	tertiary sediments	35.2	3.3	Theis Recovery	1.25E-06	3.80E-07	5.83E-05
NA 13	tertiary sediments	39.2	10.0	Theis Recovery	2.30E-08	2.30E-09	4.50E-04
NA 14	granite	67.6	14.6	Theis	4.01E-07	2.75E-08	1.60E-03
NA 15	tertiary sediments	29.8	2.4	Theis	2.85E-07	1.19E-07	3.05E-04
RP 1	granite	5	15.0	Theis	5.05E-06	3.37E-07	8.20E-04
RP 2	tertiary sediments	33.8	0.7	Average	1.94E-06	2.78E-06	4.53E-03
RP 3	tertiary sediments	27.0	1.0	Theis Recovery	2.25E-05	2.25E-05	
RP 5	tertiary sediments granite	30	28.0	Theis	1.42E-06	5.08E-08	4.94E-04

Another important feature of the site is a strong morphology of the interface kaolin / pyroclastic sediments and significant differences in kaolin thickness. As illustrated in Fig. 4.2 the interface shows a structure with hills and valleys, where highest kaolin thickness corresponds to evaluations and lowest thickness of only few meters coincides with valleys. Therefore, areas with very low kaolin thickness might represent a connection between the groundwater systems in granite and Tertiary.

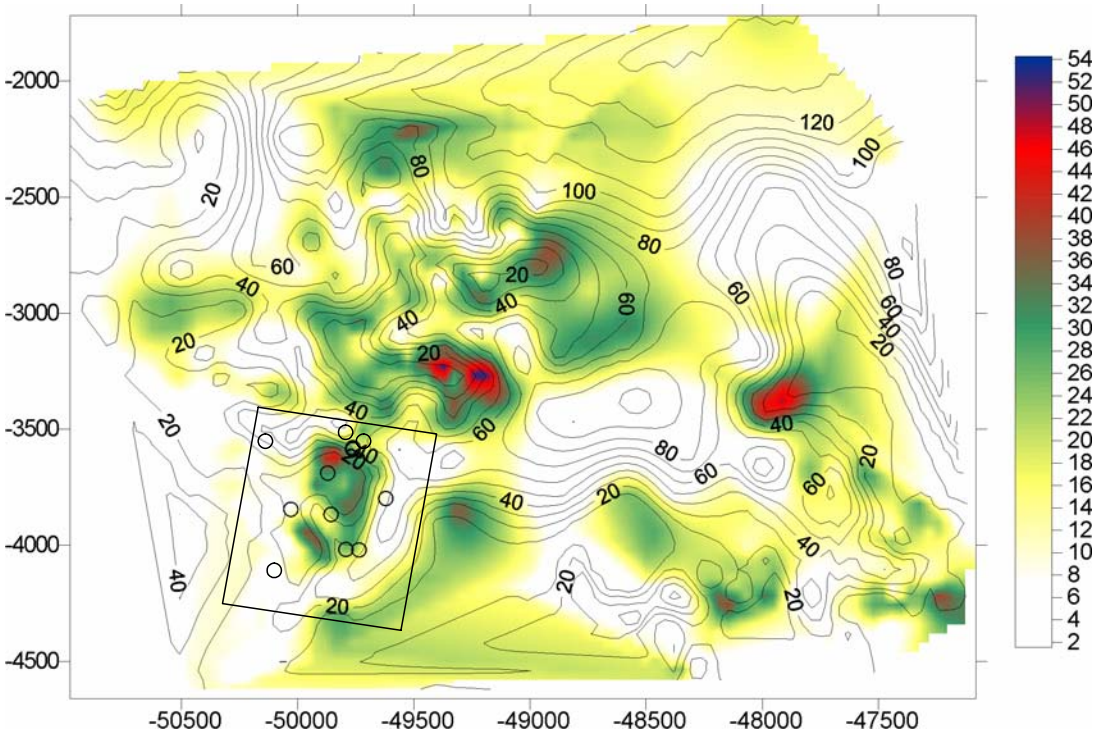

Fig. 4.2: Morphology of the interface pyroclastics/kaolin (isolines [m]) and kaolin thickness in meters (denoted by the colour bar). The black rectangle (lower-left) indicates the investigation area with boreholes

4.1 Boreholes for hydrogeological investigation

In order to understand U-migration and mobilisation/immobilisation processes as well as the behaviour of organic matter a more detailed knowledge of the hydrogeological flow regime of the site is essential. Altogether twelve wells from recent drilling campaigns have been lined to sample and characterise undisturbed groundwater from aquiferous horizons (NA4-NA15). Additionally six more boreholes, which were drilled by a company, who intends to mine kaolin at the site, became available. A restriction of these boreholes is that filter horizons cover long distances and therefore water samples might present mixtures from different water bearing horizons.

The depth of the filter horizons of all boreholes are listed in Tab. 4.2.

Tab. 4.2: Depth of filter horizons for wells from Ruprechtov site

Well	Depth of filter-horizon [m]	Well	Depth of filter-horizon [m]
granite		Clay/lignite-sand horizon	
NA8	8.5-24	**NA4**	34.5-36.5
RP1	10-20	**NA6**	33.4-37.4
NA10	19.5-27.5	**NA11**	33.2-39
NA14	67.6-77.6	**NA12**	36.5-39.3
HR4	46,5-95	**NA13**	42-48
Near-surface layers		**NA15**	28.8-31.6
NA5	19.3-21.3	**RP2**	25-43
NA7	15.5-19.5	**RP3**	25-48
NA9	4.4-10	**RP5**	30-58
		PR4	5-32

Altogether five boreholes for granitic water are available. Three of them were drilled into outcropping granite in south east and east of the area (RP1, NA8, NA10) and two of them touch the underlying granite (NA14, HR4). Most of the boreholes are filtered in the uranium bearing clay/lignite-sand horizon. Due to the strong morphology of the kaolin and consequently of the tertiary structure the depth of the clay-lignite/sand layer varies between 20 to 60 m in the investigation area. The location of each borehole is shown in Fig. 4.3 and Fig. 4.4.

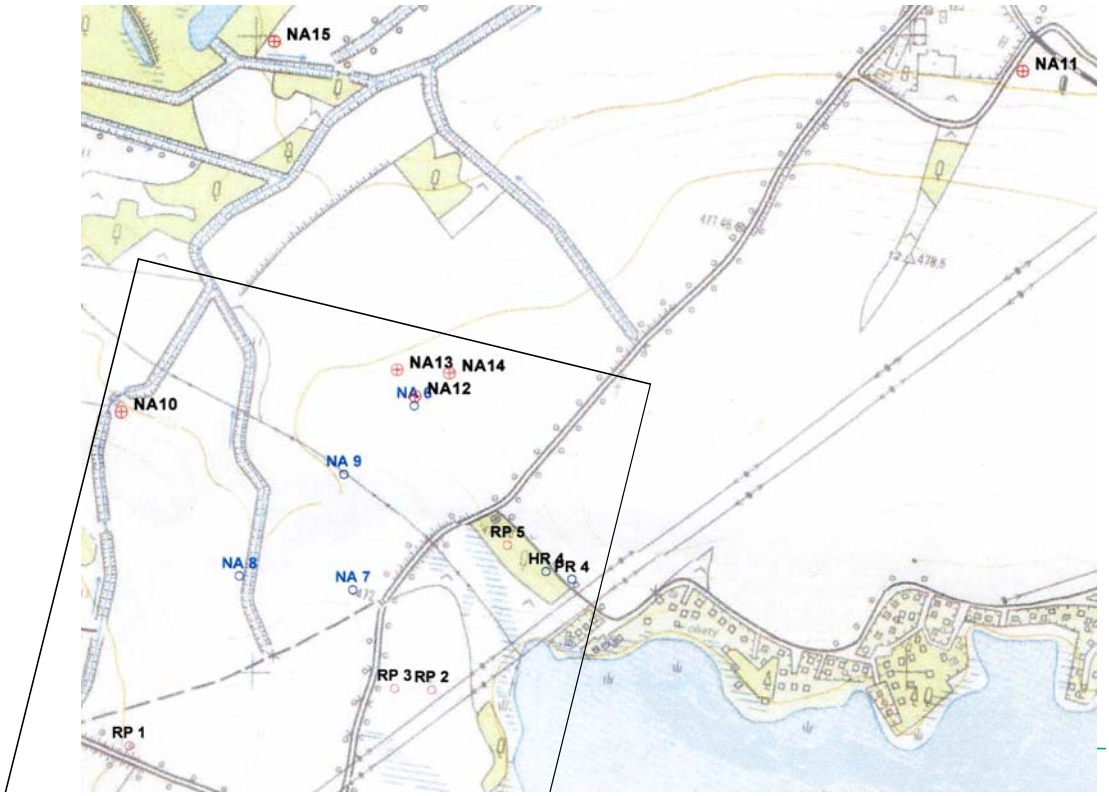

Fig. 4.3: Location of selected boreholes at Ruprechtov site

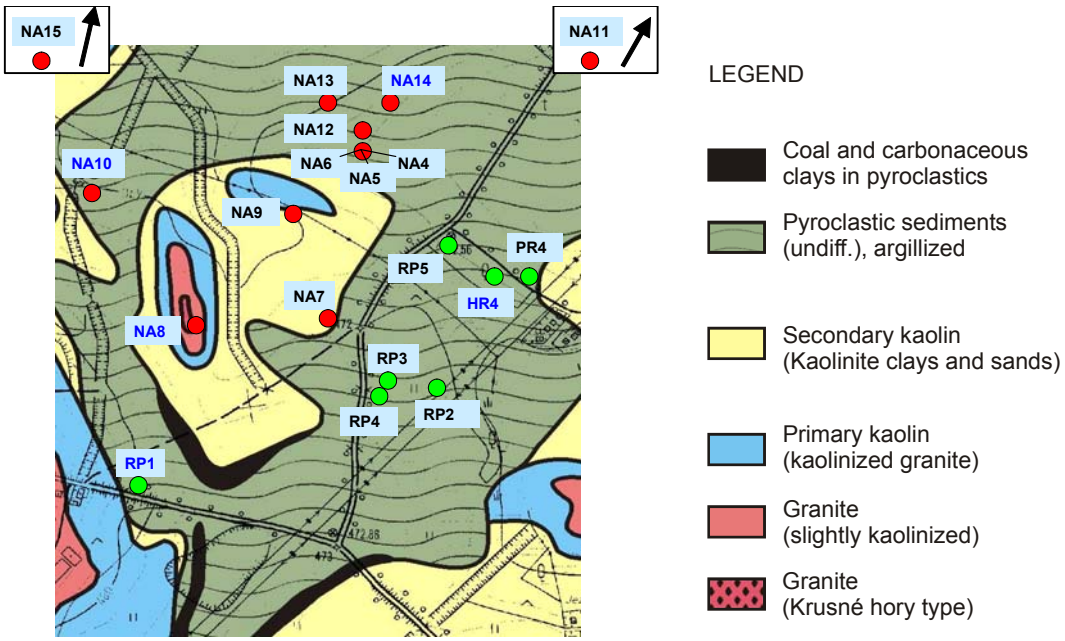

Fig. 4.4: Detailed view of borehole locations at Ruprechtov site correlated to geologic map**.** Boreholes in granite are indicated by blue font. Red dots: boreholes drilled within the scope of the project; green dots: boreholes drilled by a Czech company but were available for additional information

4.2 Isotope data for hydrogeological investigation

Natural isotope analyses of distinct groundwater have been performed to characterise the hydrogeological flow regime in more detail. Analyses were carried out by *K. Rozanski et al.* and at the Czech Nuclear Research Institute (NRI). In representative near surface waters $^{2}H/^{1}H$ and $^{18}O/^{16}O$ - isotope ratios have been analysed to identify typical local infiltration waters /NOS 02/. In the deeper groundwaters $^{2}H/^{1}H$ and $^{18}O/^{16}O$ - isotope as well as ^{3}H, ^{14}C concentrations and $^{13}C/^{12}C$ isotope ratios in DIC have been determined from each well.

$^{2}H/^{1}H$ and $^{18}O/^{16}O$ isotope ratios, the concentrations of the stable isotopes and the $^{13}C/^{12}C$-isotope ratio are given as per mille deviation $\delta^{2}H$, $\delta^{18}O$, or $\delta^{13}C$ of the respective isotope ratio R in the sample from the isotope ratio of international standards (SMOW, PDB resp.). The analytical uncertainties of the analyses are 0.1 ‰ for $\delta^{18}O$ and $\delta^{13}C$, and 1.0 ‰ for $\delta^{2}H$. The concentration of tritium is given as ratio of ^{3}H to ^{1}H. A ratio of $^{3}H/^{1}H = 10^{-18}$ is one tritium unit (TU). The analytical uncertainty of the analysis is 0.5 TU. The concentration of ^{14}C is given in percent modern carbon (pmc).

A complete list with concentrations of the natural isotopes in the wells is given in Tab. 4.3. In the following, the results together with all other available information from Ruprechtov site are used to interpret the complex hydrogeological flow regime at the site.

Tab. 4.3: Stable isotope and tritium data as well as carbon isotope data in DIC

Sample	Sampl. date	$\delta^{18}O$ (‰)	$\delta^{2}H$ (‰)	^{3}H [TU]	$\delta^{13}C$ (‰) DIC	^{14}C [pMC]	DIC [mg/l]
NA4	04-11-99	-9.71	-68.2	0.0			71
	07-11-00	-9.81	-66.9	0.0	-10.4	3.2 ± 0.5	71
	25-01-03	-9.83	-68.9	0.0	-11.7	3.2 ± 0.3	
NA5	04-11-99	-8.93	-62.6	0.0			90
	07-11-00	-8.98	-62.2	0.9	-10.6	4.3 ± 0.5	88
	25-01-03	-9.03	-60.9	0.0	-11.2	6.4 ± 0.3	
NA6	25-01-03	-9.34	-64.8	0.7			
	16-05-03	-9.26	-65.5	0.2	-12.4	13.1 ± 0.5	42
	25-05-04	-9.23	-68.4	0.8			60
NA7A	16-05-03	-8.96	-61.5	0.2			57
NA7B	16-05-03	-9.00	-61.1	0.0	-26.6	39.4	58
NA8	16-05-03	-9.22	-62.9	1.1	-21.9	71.9 ± 0.3	9
NA9	16-05-03	-8.95	-60.8	0.0	-20.5	72.1 ± 0.3	37
NA10	25-05-04	-8.89	-65,2	1.6	-16.2	54.61	34
NA11	25-05-04	-8.99	-65.8	1.5	-9.6	7.84	82
NA12	25-05-04	-8.87	-63.2	0.3	-16.0	26.45	67
NA13	25-05-04	-9.28	-67.4	1.5	-12.3		69
NA14	25-05-04	-9.36	-67.5	0.6	-12.8	9.79	69
NA15	25-05-04	-9.88	-70.9	0.2	-13.7	11.83	39
RP1	16-05-03	-9.52	-66.9	0.2	-16.8	21.0 ± 0.5	32
RP2	16-05-03	-9.81	-69.0	1.1	-13.2	16.8 ± 0.5	69
RP3	04-09-03	-9.60	-68.2	1.0		13.3	60
RP5	16-05-03	-9.73	-68.2	0.0	-11.7	6.4 ± 0.5	61
PR4	25-05-04	-9.25		9.7			
HR4	25-05-04	-9.43		1.2			
	04-09-03				-16.1	29.9	

4.3 Results

4.3.1 Stable isotopes and tritium

The results of the stable isotope analyses are shown in Fig. 4.5. In general the isotope contents follow the world meteoric water line (WMWL). However, the values measured in 2004 (NA6, NA11-NA14) show a slight shift away from the WMWL. The only borehole which has been analysed earlier is NA6. The measured value from May 2003 is shown in light blue colour. This indicates that the shift occurred only in δ^2H-values in direction of lower values. Therefore, the following discussion is mainly focussed on δ^{18}O values.

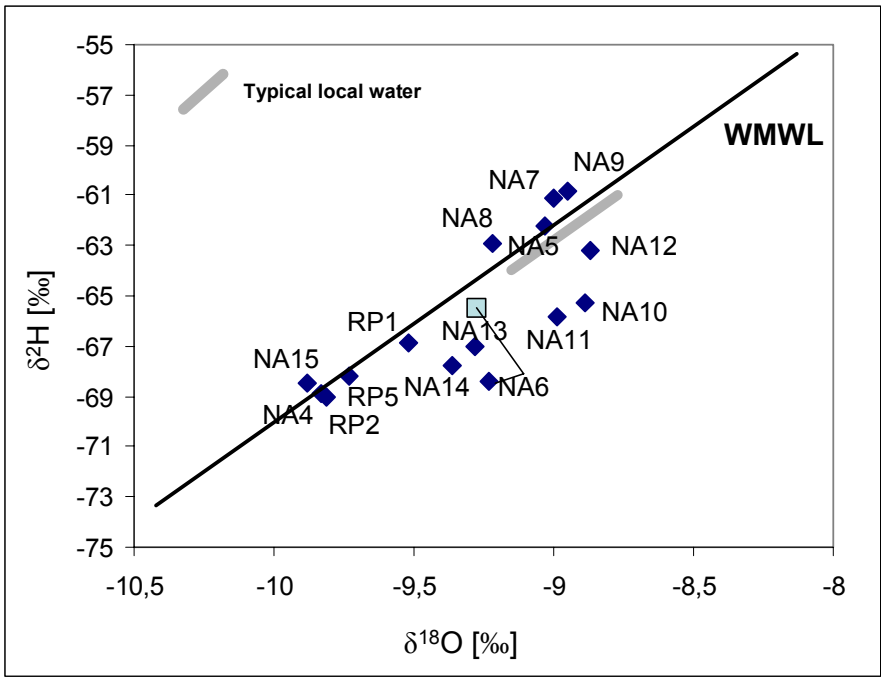

Fig. 4.5: Stable isotopes δ^{18}O vs δ^2H. The bold grey line denotes isotope signature of typical infiltration water from the area

The data range of recent local waters is marked by the bold grey line. In Fig. 4.6 the data are mapped in correlation to the geological map. In general, the waters can be divided into two groups, isotopically more heavier groundwater in the NW of the investigation area (marked in blue colour) and isotopically light groundwater in the SE (marked in grey colour). The waters in the NW can be subdivided into a group with δ^{18}O values between -8.9 and -9.0 and a group with δ^{18}O values between -9.2 and -9.4 .

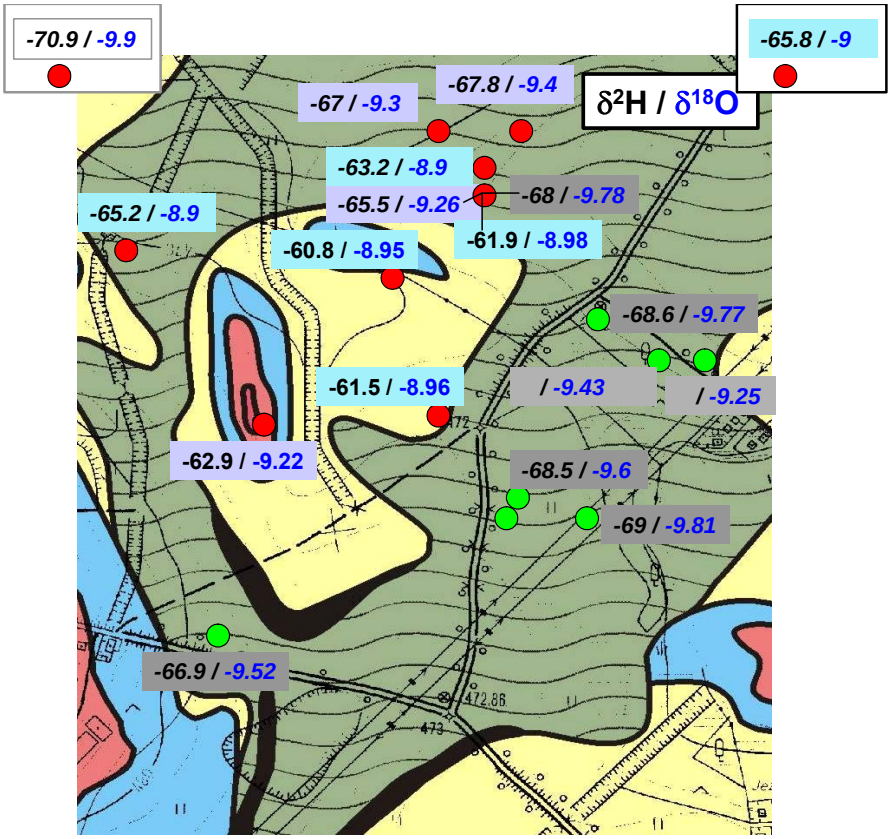

Fig. 4.6: Distribution of stable isotopes in different boreholes at Ruprechtov site

Before interpreting the data it should be mentioned that the water levels observed in our boreholes confirm the flow direction assumed in older models. Fig. 4.7 shows the distribution of water levels measured in April 2004. In general they confirm a hydraulic gradient from SW to NE.

The boreholes with granite waters are marked in blue, all others in grey colour. The three western wells NA10, NA8 and RP1 represent water from near-surface granite. Their isotope signatures are significantly different. Whereas NA8 and NA10 reflect signatures of recent local waters, water from RP1 is isotopically lighter, indicating an infiltration level elevated by about 200-300 m. Trace amounts of tritium present in wells NA10 and NA8 confirm presence of younger water. This is a strong indication for two different infiltration areas, one in the outcropping granite in the west and one in the elevated area in the south-west.

All waters from near-surface layers, NA9, NA7 and NA5 (15 to 20 m depth) show isotope ratios similar to NA8 and NA10, indicating hydraulic connection to the infiltration area in the west. ^{14}C content of 72 pmc and $\delta^{13}C$ content of -21 ‰ in NA8

(later shown in Fig. 4.15) indicate mixture with some older water formed almost without contact with $CaCO_3$. This result is supported by very low DIC concentrations of 9 mg/l (cf. section 4.3.2).

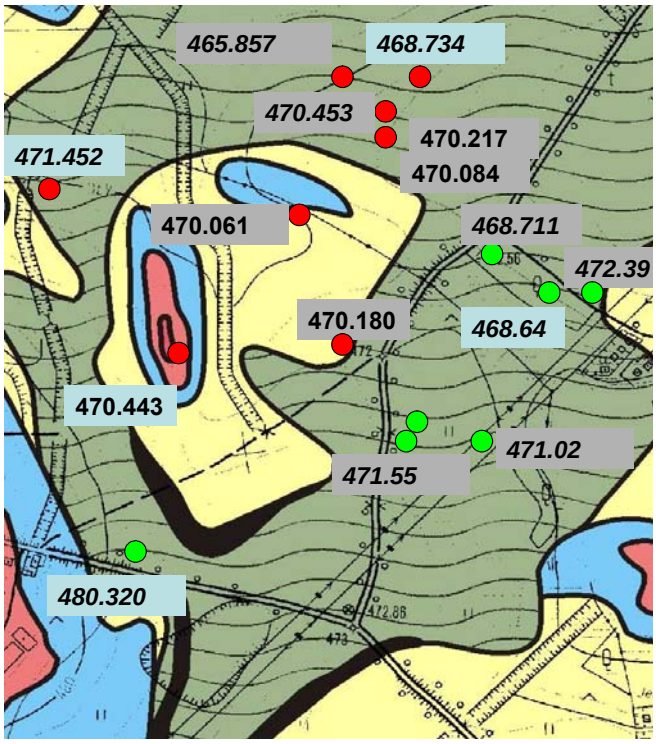

Fig. 4.7: Water levels measured in April 2004

The isotope signatures in wells from the northern part of the model area show some variations. NA12 signature is similar to NA10 indicating its hydraulic connection to infiltration water of the western area. NA4 shows the lighter signature like the wells in the eastern part. The other boreholes NA6, NA13, and NA14 seem to present mixtures of isotopic lighter water and infiltration water from the western area. All of them show traces of Tritium, which is unexpected for the deep horizons (NA13, NA6) and underlying granite water (NA14).

The variations of the isotope signatures might be explained as follows. The water in the deeper granite (NA14) represents a mixture of water infiltrated in the western area and water infiltrated in the south western area. Additionally, there is a hydraulic connection between western infiltration area and water bearing horizons in the northern area of the Tertiary (NA12). Furthermore, in this area (with low kaolin thickness and probably also fault zones), local connections between water bearing horizons in the Tertiary and underlying granite are likely. Therefore the waters (NA13, NA6) might show mixtures of underlying granite water and infiltration water from western area.

The concentration of Cl supports the assumption that NA-14 water represents some mixture from water infiltrated in the western area (NA8, NA10) and water infiltrated in the south western area (RP1). The Cl concentration is with values of approx. 5 mg/l rather similar in both boreholes situated in western infiltration area (NA8 and NA10). There is no strong change downgradient and in the clay/lignite horizon. However, it is remarkable that RP1 granite water exhibits with about 20 g/l higher Cl concentrations than the granites from western part and most clay/lignite waters. Higher Cl-concentrations are also observed in the wells NA14 and NA13 with 10 and 14 g/l, respectively. If we take RP1 as representative for southern water, this is an indication that NA14 water represents a mixture of water infiltrating in the western part (NA10,NA8) and water from the southern part (RP1). The elevated concentrations in NA13 indicate interaction of deep granite water with clay/lignite horizon in this area.

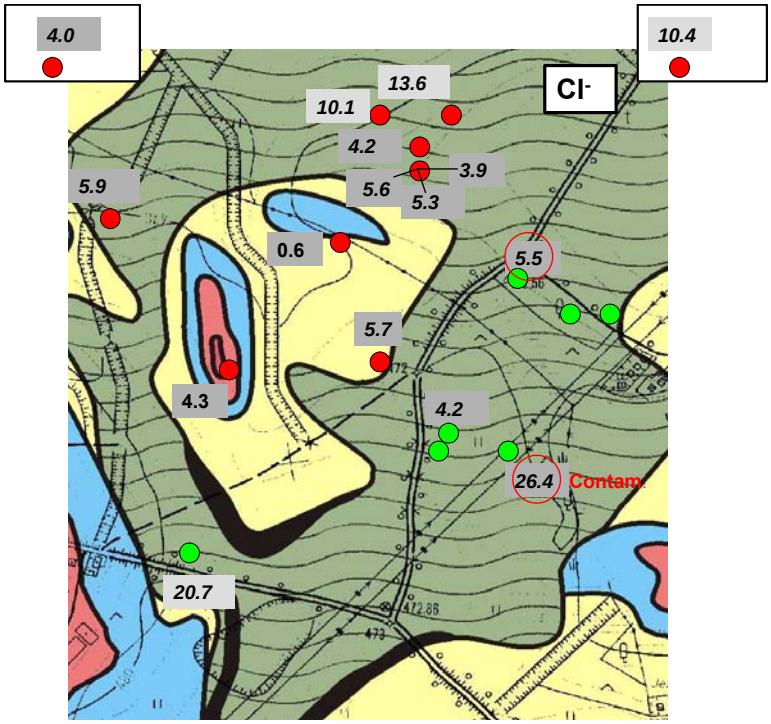

Fig. 4.8: Chloride concentration [mg/l] for distinct wells at Ruprechtov site

The water from RP1 corresponds to infiltration in higher altitude which is probably in the outcropping basalt and granites in the south-west. Several boreholes in the SE part as RP2, RP3, RP5 and also NA4 show similar light signatures as RP1. This indicates hydraulic connection between RP1 and the SE part of the area. PR4 and HR4 are older drillings, which are not well documented. Their $\delta^{18}O$ ratios are higher, which might be caused by contamination with surface water. This is very likely for PR4, where the filter

horizon covers a depth of 32 to 5 m. Another strong indication for such a contamination is the tritium content of 9.7, and 1.2 TU in PR4 and HR4, respectively.

The wells Na15 and NA11 are more than 1000 m away from the model area. Due to the heterogeneous structure at the site including fault zones and strong morphology of the tertiary basis it is difficult to judge, if and (if so) how they are hydraulically connected to the model area. Therefore, they are not included into the considerations.

Based on all results a conceptual model for hydrogeological conditions has been developed which is shown in Fig. 4.9. It illustrates that water inflow occurs from the western part covering the middle and north of the model area. Ground water infiltrated in the SW area flows into the eastern part of the site.

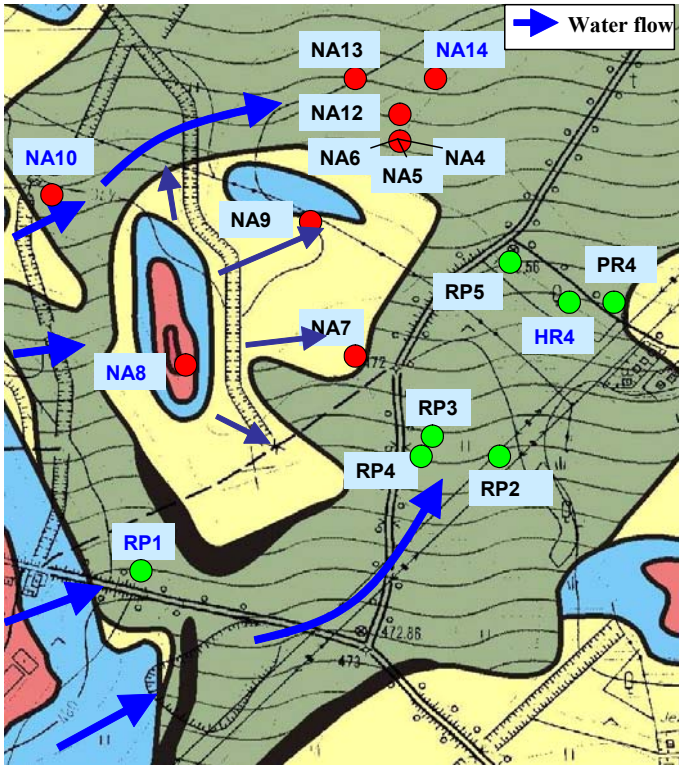

Fig. 4.9: Hydrogeological flow regime proposed from information about tritium and stable isotope data

As already mentioned, hydraulic interaction between granite and Tertiary is also possible via fault zones. An indication for an impact of fault zones is given by comparison of fault zones observed in the area with observations so far. Such fault zones are mentioned in reports from Czech geological survey to occur in the North and East of the investigation (see Fig. 4.10) area and could impact boreholes in northern and eastern part of clay/lignite horizon.

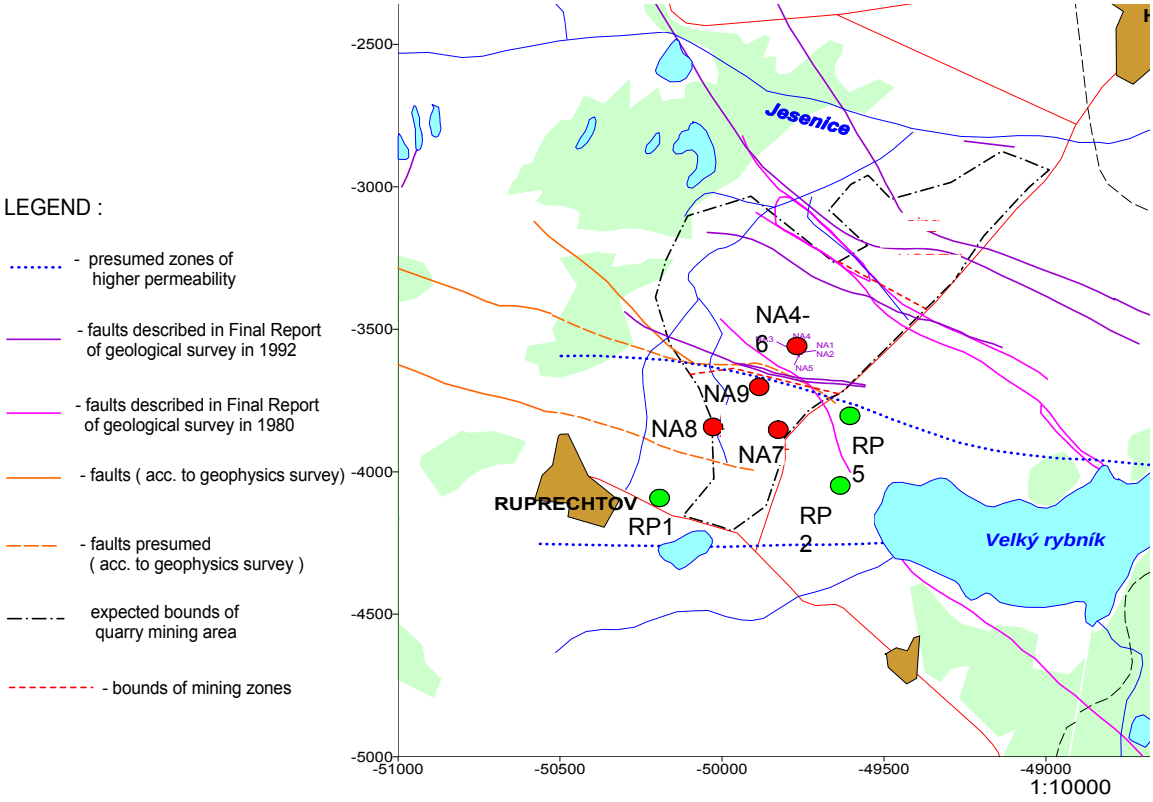

Fig. 4.10: Map with tectonic faults at Ruprechtov site due to Czech geological survey

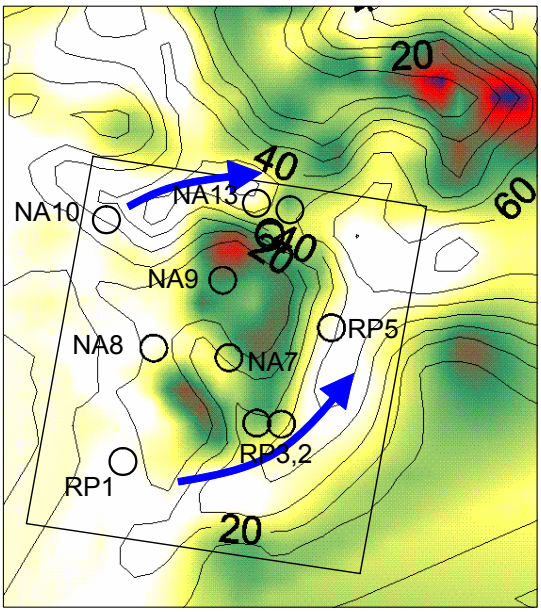

Fig. 4.11: Correlation of the flow regime with the morphologic structure of the tertiary/kaolin-interface. Investigation area is indicated

4.3.2 Carbon isotopes

Carbon isotopes are measured in order to identify water ages, and/or to characterise water mixing processes as well as reactions within the carbon cycle. The ages of the waters calculated with non corrected ^{14}C values are within 1,000 to more than 25,000 years. For interpretation of DIC measurements additional isotope data from SOC, DOC, SIC and CH_4 have been determined in selected wells. These data are listed in Tab. 4.4.

Tab. 4.4: Additional Isotope data from selected boreholes

	$\delta^{13}C_{SIC}$	$\delta^{18}O_{SIC}$	$\delta^{13}C_{SOC}$	$\delta^{13}C_{DOC}$	$\delta^{13}C_{CH4}$	$\delta^{18}O_{SO4}$	$\delta^{34}S_{SO4}$
NA4				-16.9	-26.9		
NA5	2.6	29.3		-25			
NA6				-26.8		-6.7	2.5
NA7B				-27.3			
NA8				-27.8			
NA9				-27.1			
RP2			-26.5 / -24.9				
RP3				-26.6			
RP5	1.8 / 1.9	25.6 / 25.7					
HR4				-26.2			

Typical $\delta^{13}C$ values for endogenous CO_2 found in literature are in the range of -3 and -6 ‰. Values determined in Eger rift area are -2.7 ‰ /WEI 01/. Based on these data development of carbon isotopes are discussed. The most important reactions influencing ^{14}C and $\delta^{13}C$ ratios in dissolved inorganic carbon (DIC) are the following ones:

1. Dissolution of sedimentary inorganic carbon (SIC). Sedimentary inorganic carbon from the tertiary will have 0 pmc ^{14}C. This reaction will lead to a decrease in ^{14}C and increase in $\delta^{13}C$ of infiltration waters.

2. Microbial degradation of dissolved organic carbon (DOC) depends on geochemical conditions. Under anaerobic conditions, if no oxidants are available, degradation can take place by fermentation and methanogenesis which could be described in a simplified way as $2CH_2O = CH_4 + CO_2$. If oxidants like SO_4^{2-} or NO_3^- are involved

sulphate reduction and/or denitrification will occur. In this case only CO_2 and no CH_4 is generated. At Ruprechtov site sulphate reduction is expected to be the preferred reaction because

- Sulphate is available in distinct amounts in all boreholes. Concentrations vary between 0.1 and 2 mmol/l (cf. Fig. 4.12), which is far above a critical concentration of 5 µmol/l, below which no microbial reaction occur /BUC 00/.
- Sulphate reducing bacteria are present in the clay/lignite horizon. Their existence was shown in core material from NA4 (cf. Chapter 5.4.2).

In case of sulphate reduction the $\delta^{13}C$-ratio in generated CO_2 should reflect the $\delta^{13}C$-ratio of DOC. In this case the isotope signature will develop in direction of low 13C-values (around -27 ‰) and 0 pmc ^{14}C expected for organic material from Tertiary.

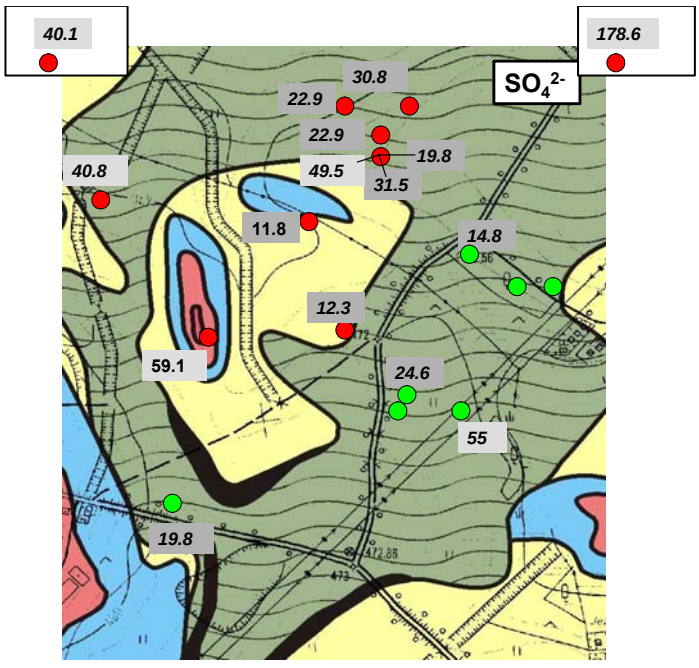

Fig. 4.12: Sulphate concentration [mg/l] in distinct boreholes from Ruprechtov site

3. Input of endogenic CO_2 from exhalation. Concerning carbon isotopes this reaction will show a similar trend as dissolution of SIC, i.e. decrease in ^{14}C and increase in $\delta^{13}C$ of infiltration waters.

A schematic description of the evolution of DIC versus $\delta^{13}C$ was given by Buckau et al. /BUC 00/ and is shown in Fig. 4.13. If CO_2 is generated it will slightly acidify the

solution. This could lead to additional dissolution of sedimentary carbonates, if present. At Gorleben site CO_2 generation by microbial degradation was observed together with dissolution of sedimentary carbonates. This process is denoted as equimolar mineralization in Fig. 4.13 and will lead to $\delta^{13}C$ values of -13.5 ‰. At Gorleben site the degradation process of SOC resulte in the release of DOC, preferentially as humic and fulvic acids /BUC 00/.

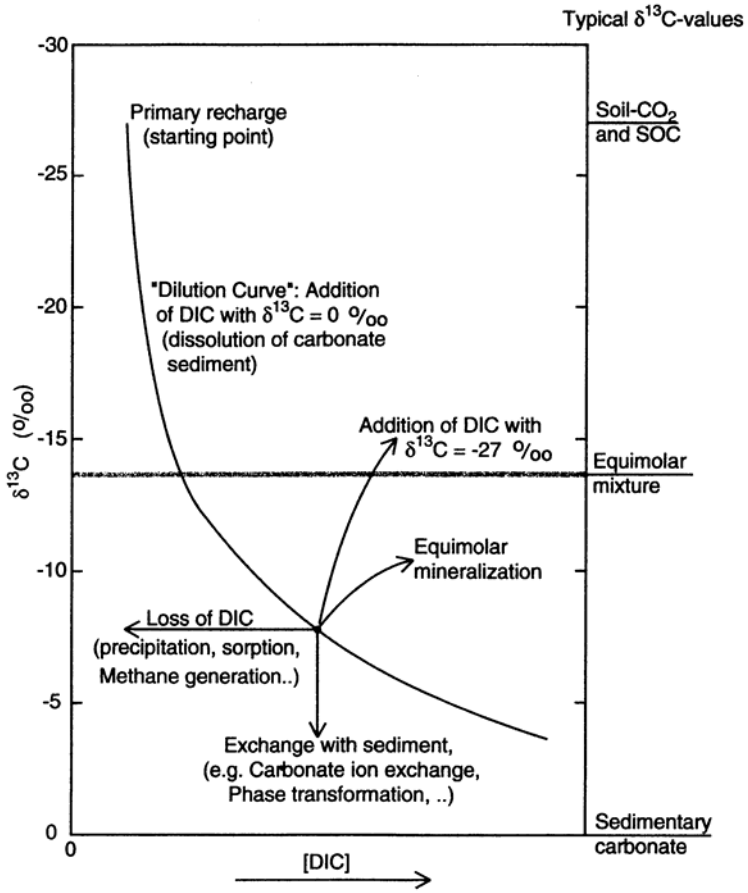

Fig. 4.13: Schematic description for evolution of $\delta^{13}C$ versus DIC in groundwater /BUC 00/

Fig. 4.14 shows the general trend for the development of $\delta^{13}C$ ratios as a function of DIC at Ruprechtov site. The $\delta^{13}C$ values increase from well NA8 with the lowest values of -22 ‰ to well NA11 with the highest value of -9.6 ‰ with increasing DIC. Furthermore, as shown in Fig. 4.15, ^{14}C-values decrease with increasing $\delta^{13}C$ values.

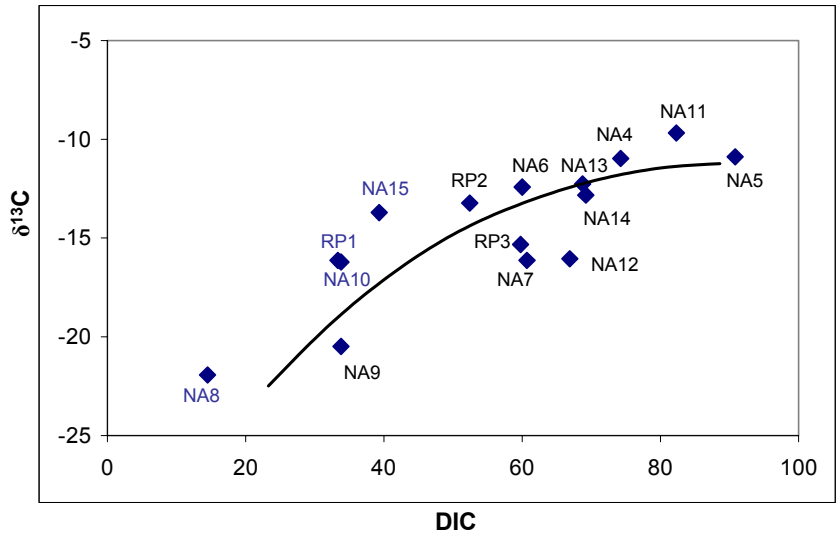

Fig. 4.14: DIC vs $\delta^{13}C$ in different boreholes from Ruprechtov site

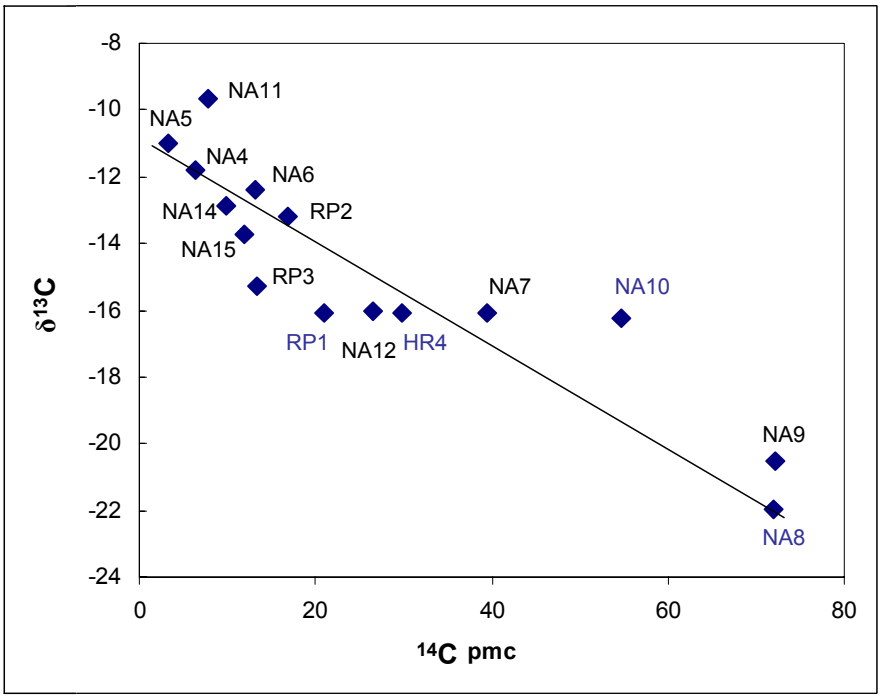

Fig. 4.15: ^{14}C vs $\delta^{13}C$ in different boreholes from Ruprechtov site

Primary recharge water typically shows ^{14}C values of 100 pmc and $\delta^{13}C$ ratios of approx. -25 ‰. At Ruprechtov site highest radiocarbon concentrations are observed in NA8 and NA9 with about 72 pmc corresponding to lowest $\delta^{13}C$ ratios around -21 ‰ as illustrated in Fig. 4.16. This supports the hypothesis of infiltration water in these boreholes in the western area. However, in well NA10, which is supposed to represent

infiltration water, ^{14}C content is slightly decreased along with an increase in $\delta^{13}C$ ratio and DIC. It is already an indication for input of SIC and/or endogenous CO_2.

The well RP1 in the granite in south-eastern area also indicates a different origin by carbon isotope data compared to granite water from NA8 and NA10. The second infiltration area is assumed to be in the granites extending to the SW from RP1 as mentioned in section 4.1. The low ^{14}C and higher $\delta^{13}C$ values (compared with NA8 well) could result from mixing with deeper water, dissolution of low amounts of DIC and/or gaseous CO_2 exhalations.

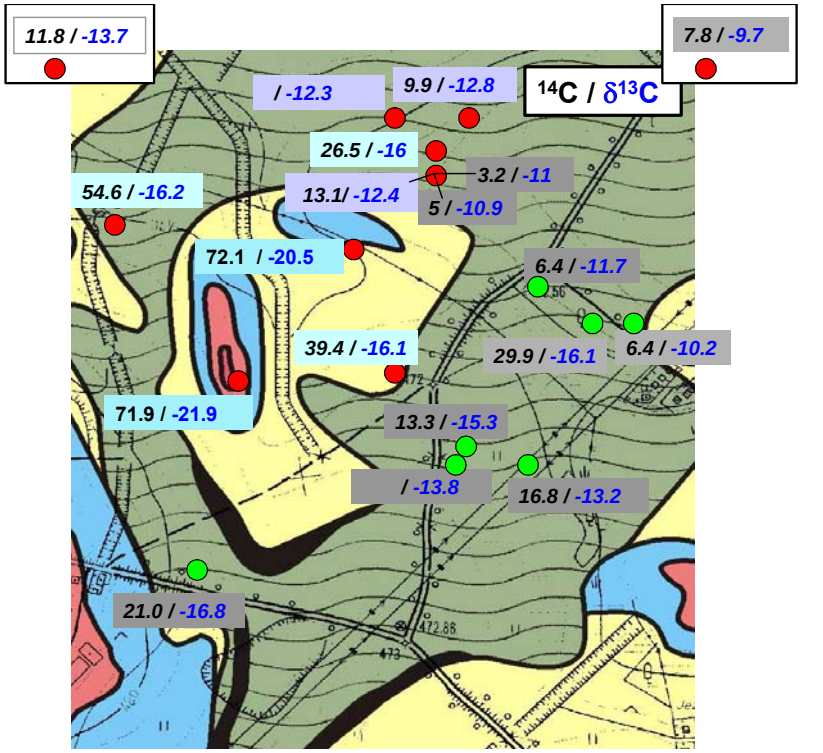

Fig. 4.16: Distribution of ^{14}C and $\delta^{13}C$ in different boreholes at Ruprechtov site

Assuming ground water flow from area around RP1 into the eastern part of the site, we recognise an evolution with decrease of ^{14}C and increase of $\delta^{13}C$ values into flow direction. The lowest ^{14}C and highest $\delta^{13}C$ values are found in the most NE part, i.e. in wells PR4, RP5, NA4 and NA5. An exception is well HR4, which is assumed to be water from underlying granite. A similar value for $\delta^{13}C$ as in RP1 is observed but increased ^{14}C value. However this is very likely caused by inflow of near-surface water due to the long filter horizon and might be indicated in fact by the occurrence of tritium.

Assuming flow from W part (NA10) into the N part of the site, a reduction of ^{14}C with nearly no change in $\delta^{13}C$ is observed for NA12. The ^{14}C values in boreholes NA6, NA12 and NA14 are decreased with increased $\delta^{13}C$ values of -12 to -13 ‰.

The evolution of carbon isotope data is typical for dissolution of sedimentary carbon and/or input of CO_2 by exhalation. There are indications for both processes. An indication for dissolution of sedimentary carbon is the fact that ground water in a number of wells reaches saturation for carbonate minerals, which is shown in Fig. 4.17. The saturation indices for carbonate bearing minerals were calculated for selected waters. The infiltration waters NA8, RP1 and NA12 are undersaturated with regard to carbonate bearing minerals. All other waters show (within a range of uncertainty) saturation of carbonate minerals.

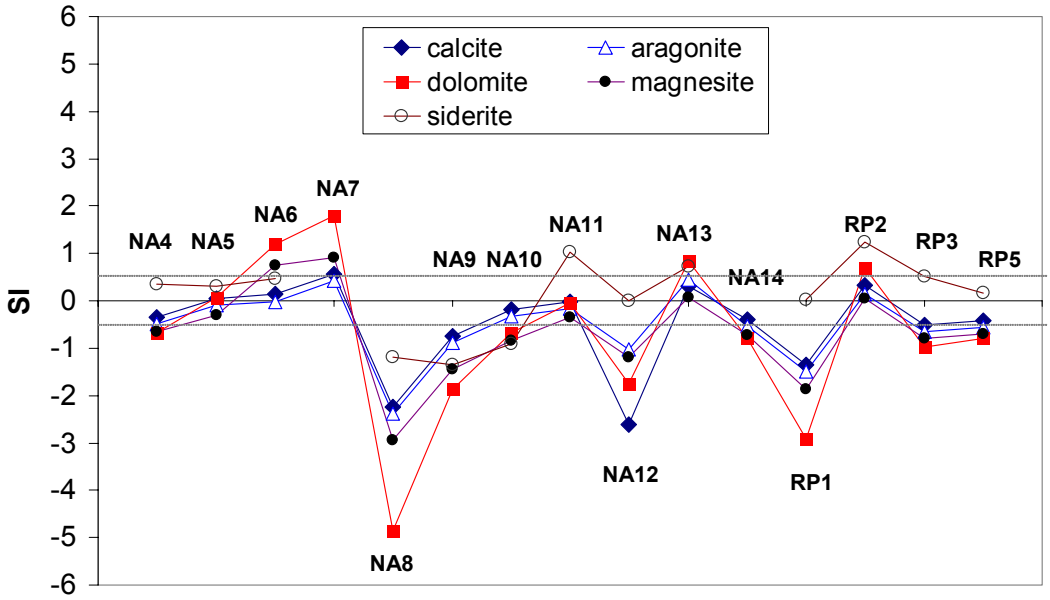

Fig. 4.17: Saturation indices for carbonate bearing minerals in selected groundwaters from Ruprechtov site

But, there are also indications for input of mantle gases, especially CO_2. Firstly, in the whole Ohre rift areas strong CO_2 exhalation are found. In Karlsbad, which is about 10 km away from the investigation area, water is enriched in CO_2 from exhalations (cf. Chapter 2.6). Secondly, methane concentrations measured in well NA4 are about 1 mg/l. The $\delta^{13}C_{CH4}$ value of -27 ‰ is a typical value for thermogenic source, i.e. such methane is very likely brought to the shallow zone by the CO_2 of mantle origin. Methane generated by microbial degradation shows much lower values, << -50 ‰.

Furthermore it is questionable that methane would be generated by microbial reaction, if enough sulphate is available for degradation of organic matter by sulphate reduction.

Thirdly, ^{3}He and ^{4}He has been determined in boreholes NA4 and NA5. It is usually presented as R/R_a ratio. The R_a-value denotes the $^{3}He/^{4}He$-ratio in atmosphere, which is $1.385 \cdot 10^{-6}$. R/R_a-values in the crust are <0.1, normally about 0.02. Values measured in the Ohre rift area for mantle Helium are 8. The values at Ruprechtov site are

- NA4: R/Ra = 0.4
- NA5: R/Ra = 0.72

Fig. 4.18 shows typical values for waters in the Ohre rift /WEI 99/. The values measured in NA4 and NA5 are typical for areas more than 30 km away from so-called escape centre for mantle CO_2 with low but still visible impact of CO_2 exhalation.

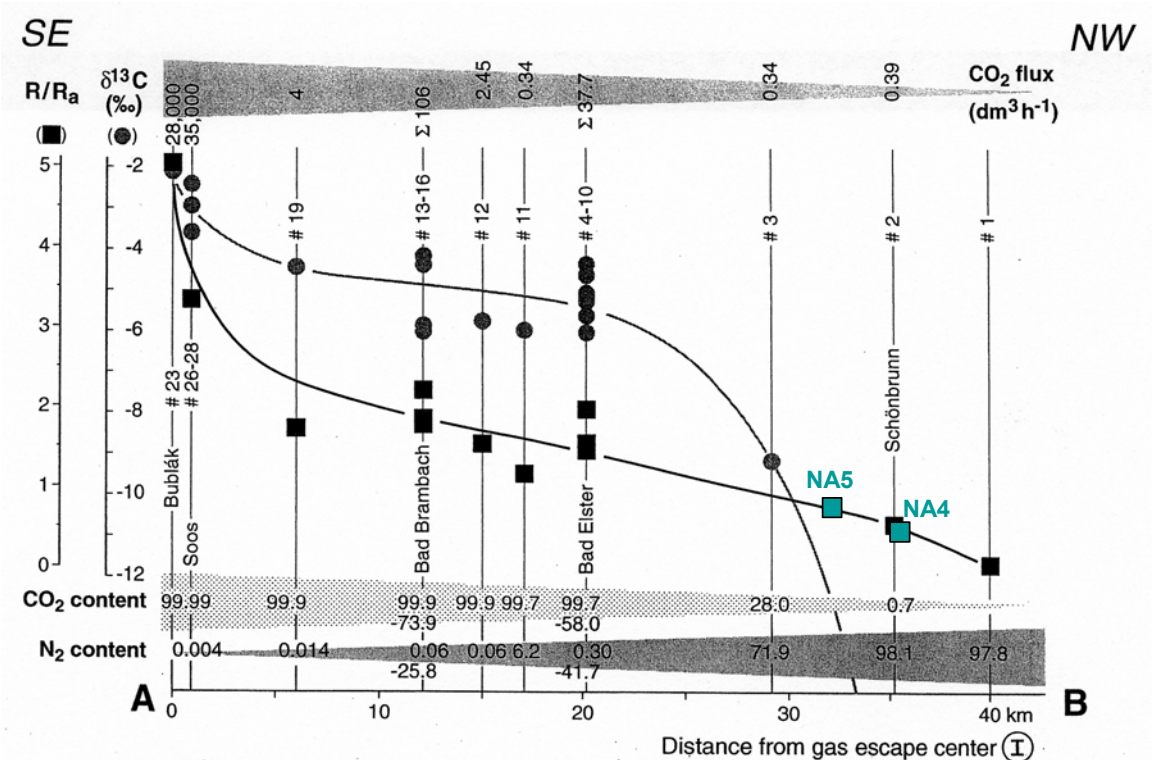

Fig. 4.18: $\delta^{13}C$ and R/R_a-values in groundwaters in the Ohre rift area /WEI 99/

Mineralisation by microbial degradation of organic matter only seem to play a minor role, if at all, because it would decrease the $\delta^{13}C$ ratio by input of inorganic carbon with values of -27 ‰.

4.4 Conclusions

A conceptual model for water flow has been developed. Main features are two infiltration areas in W and SW part of investigation area and an altogether much more complex situation than could be estimated initially. Indications for water exchange between underlying granite and Tertiary, probably in areas with low kaolin thickness, as well as via fault zones are found by stable isotope and hydrochemical results. This agrees with knowledge of fault zones in the area and strong heterogeneity in kaolin thickness.

The carbon isotope data indicate complex carbon chemistry, with different processes affecting DIC and its $\delta^{13}C$ and ^{14}C signature: dissolution of sedimentary inorganic carbon, microbial degradation of organic carbon and input of endogenous carbon by exhalation. At this stage quantification of the processes is not possible. This hampers the use of carbon isotope data for determination of water ages.

Further work for clarification will be done in FUNMIG project /EUR 05/. In order to identify, whether microbial reaction still takes place, ^{34}S isotope measurements in dissolved sulphate and in sulfide minerals are planned. Analyses of ^{14}C in organic matter from dissolved organic matter will additionally be performed in order to distinguish between the source of DOC, i.e. from recharge area and/or from lignite in the Tertiary and therewith to judge, whether microbial degradation in the clay/lignite-horizon leads to generation of DOC today.

Detailed analysis of sedimentary organic material is planned to determine the composition of the sedimentary organic matter from Ruprechtov site and to elucidate degradation processes leading to release of DIC and DOC. This is planned to be done in international co-operation, to compare the results with properties of organic matter from other argillaceous sediments.

5 Uranium at the site

In order to understand the uranium transport and mobilisation / immobilisation processes occurring at Ruprechtov site a detailed characterisation of various samples from the uranium enrichment zone in the clay/lignite-sand horizon and of few selected samples from granite and kaolin was performed using a number of analytical techniques.

Additionally groundwater samples from corresponding water bearing horizons have been analysed on pH, Eh, content of major and trace elements, activity ratios in the uranium decay chain. Furthermore, first water samples have been analysed on content of colloids.

Besides site characterisation sorption / desorption experiments on samples from the clay/lignite-sand horizon have been performed to judge the impact of sorption reactions on uranium immobilisation.

5.1 Granite as uranium source

The compiled information of the surrounding rocks at Ruprechtov site had identified the Erzgebirge granites as the potential uranium source. Knowledge of the chemical composition of the host rocks and their accessory-mineral assemblage is essential in understanding the processes, which control the distribution and mobility of radionuclides during alteration of granitic rocks. In this respect, a collection of six representative samples from the Ruprechtov site have been sampled and analyzed by *H.J. Förster* (for major and trace elements using state-of-the-art analytical techniques as well as the assemblage of accessory minerals, which constitute the main hosts for U and Th in granitic rocks.

The samples comprise both drill-core samples and samples from superficial outcrops. From the granite body penetrated by the boreholes NA6 and NA8, two representative samples from different depths (roughly 75 m and 64.5 m, and 23 m and 12 m, resp.) were collected from each. The granite intrusion exposed by drilling, crops out superficially at the lake Velky Rybnik. For comparison one sample VR1 from this surface exposed granite was taken. The collection of samples was completed by a

biotite granite genetically distinct from the Ruprechtov granite, which was collected near the village of Oděř, about 2 km NW of the Ruprechtov site (sample OD1).

A variety of analytical techniques at the GFZ Potsdam were used to obtain whole-rock geochemical data on homogenised rock powders. Several trace elements were analyzed by various methods, which allows for checking on dissolution procedures and inter-technique calibrations for a given element in a certain concentration range. The major elements, and some trace elements (Zn, Ga, Rb, Sr, Y, Zr, and Ba) were determined by wavelength-dispersion X-ray fluorescence spectrometry (XRF) using fused lithium tetraborate discs. All XRF analyses were made with an automated Siemens SRS303AS spectrometer using a Rh tube operated at 50 kV and 45 mA. Analysis for fluorine was performed using ion-selective electrodes. Total water and CO_2 were determined by combustion - infrared detection. The rare earth elements (REE) plus Rb, Sr, Y, Zr, Cs, Ba, Hf, Pb, Th, and U were analyzed by inductively coupled plasma-mass spectrometry (ICP-MS; Perkin-Elmer/Sciex Elan Model 500) according to the method and with the precision and accuracy outlined by /DUL 94/.

Quantitative analyses of accessory minerals in polished thin sections were performed using CAMEBAX SX-50 and SX-100 electron microprobes at the GFZ Potsdam operating in wavelength-dispersive mode. The operating conditions during analysis of accessory minerals were as follows: accelerating voltage 20 kV, beam current 40–60 nA, and beam diameter 1–2 µm. Counting times, data reduction, analyzing crystals, standards, analytical precision and detection limits are described in detail in *Förster* /FOE 98a, FOE 98b/.

5.1.1 Granite alteration

The granite from Ruprechtov, and its superficial equivalent VR1, is an evolved peraluminous monogranite belonging to the group of late-collisional, F- and P-rich Li-mica granites of the Krušné hory/Erzgebirge in the sense of *Förster et al.* /FOE 98, FOE 99/. The coarse- to medium-grained, weakly porphyritic granite represents a relatively less fractionated subintrusion, comparable to the main intrusion forming the huge plutons of Eibenstock, Pobershau and Satzung in the German Erzgebirge (e.g. /FOE 99/). The group of F- and P-rich Li-mica granites displays a remarkable homogeneous composition with respect to immobile elements in the entire Erzgebirge. This permits an investigation of the intensity of alteration that the various samples from

Ruprechtov have experienced by comparison with unaltered samples from other areas of Erzgebirge granite. Such unaltered samples from the neighbouring Eibenstock massif in the German Erzgebirge were investigated by *Förster et al*. in previous studies /FOE 99/.

In Fig. 5.1 and Fig. 5.2 content of selected elements and oxides is plotted as function of the reciprocal of TiO_2, because Ti is much less susceptible to alteration than Si, which is commonly used as measure of the degree of granite fractionation. The unaltered granites are shown as blue unfilled squares and represent the “magmatic pathways”. Deviations from these indicate whether an element or oxide became enriched, depleted or remained unaffected by alteration.

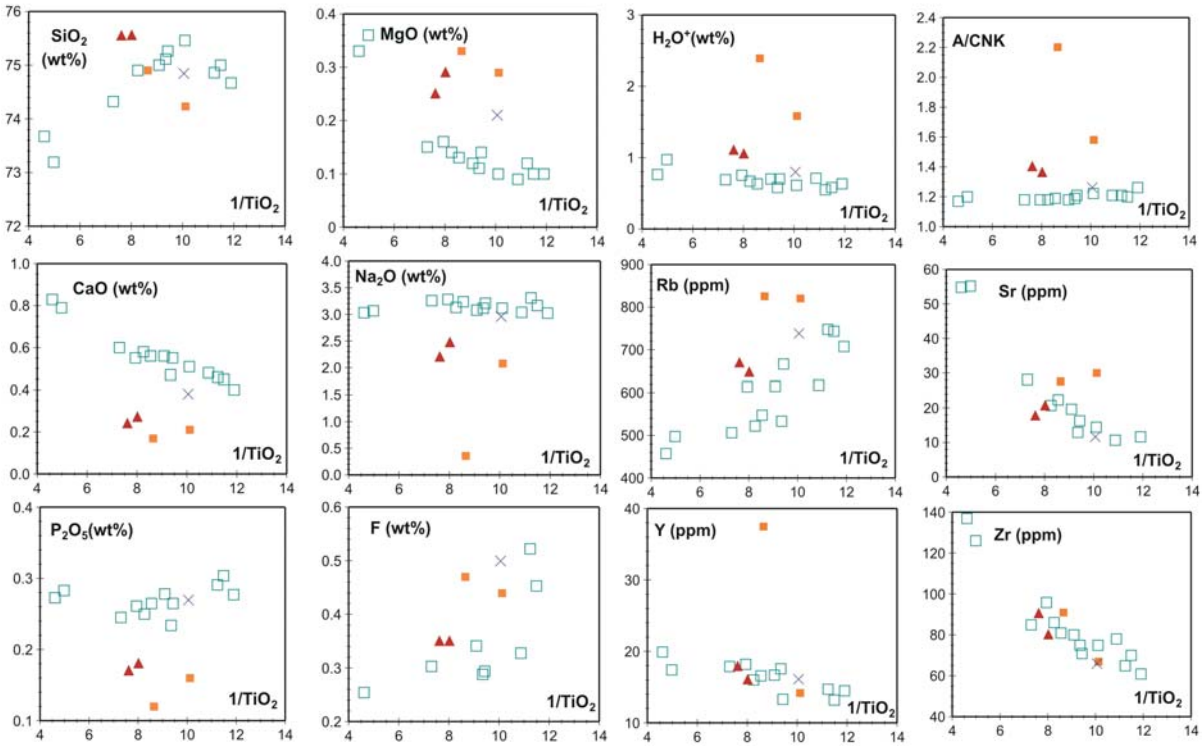

Fig. 5.1: Plot of various oxides and elements versus $1/TiO_2$ for the samples VR1 (cross), NA6/75 and NA6/64 (filled triangles) and NA8/23 and NA8/12 (filled squares) from Ruprechtov site. The composition of unaltered, F and P rich Li-mica granites from the German Erzgebirge is shown for comparison (blue unfilled squares)

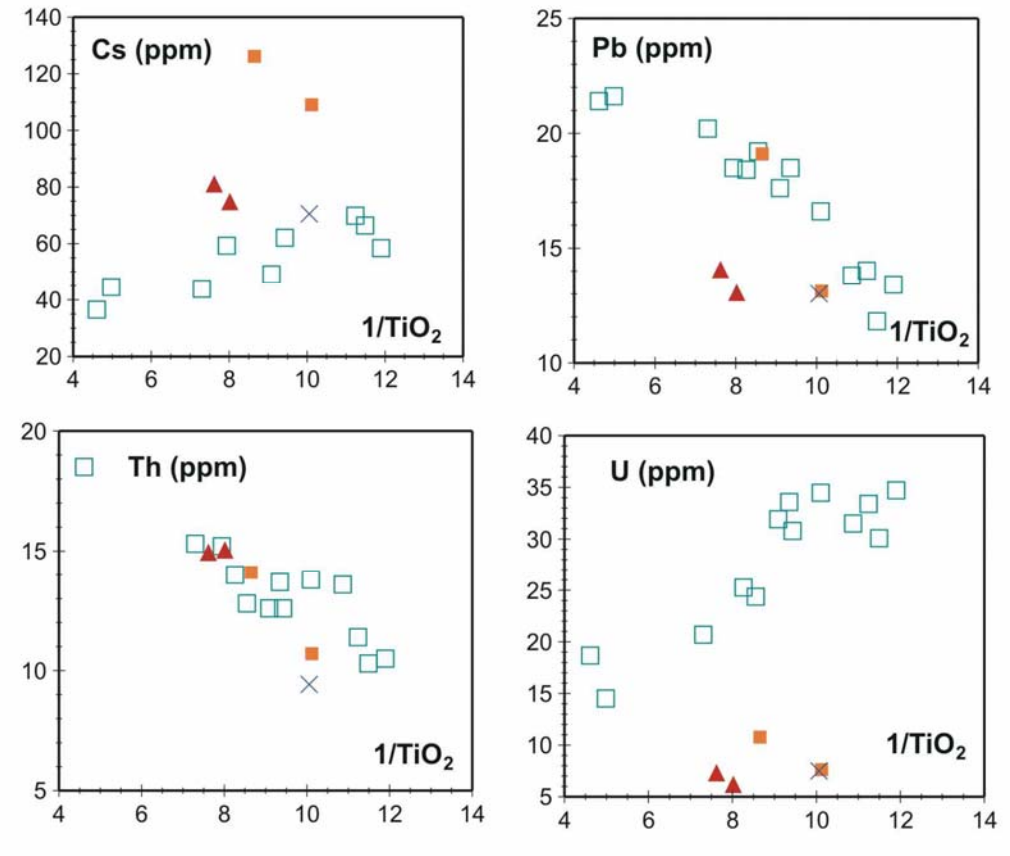

Fig. 5.2: Plot of Cs, Pb, Th and U versus $1/TiO_2$ for the samples VR1 (cross), NA6/75 and NA6/64 (filled triangles) and NA8/23 and NA8/12 (filled squares) from Ruprechtov site.

Comparison of the composition of the Ruprechtov samples with that of virtually unaltered, compositionally equivalent granites clearly documents that all five show disturbances in their original elemental pattern, however, with different intensity. The superficial sample VR1 constitutes the least altered and most fractionated rock (indicated by the highest value of $1/TiO_2$), i.e., the five samples possess slightly different degrees of fractionation. The most striking alteration features of sample VR1 consist in a moderate enrichment of MgO and a severe depletion in U. The four drill core samples are moderately to strongly depleted in CaO, Na_2O, P_2O_5, and U. Oxides and elements enriched include MgO, H_2O^+, F, Rb and Cs. The granites from borehole NA6 additionally are depleted in Pb and enriched in SiO_2, whereas the NA8 granites show additional enrichment in Al_2O_3, Zn, and Sr. The most intensely altered granite is represented by sample NA8/12, which most strongly deviates from the magmatic trend with respect to Al_2O_3, MgO, CaO, P_2O_5, H_2O, F, Ba, Rb, Cs, and Y. In neither sample, do the contents of Zr, Hf, Th, Nb, and Ta show displacement from their original magmatic pathways.

5.1.2 Composition of radioactive accessory minerals

In peraluminous granites, between 60 and 90 percent of U, Th, and the REE are hosted in accessory minerals /BEA 96, FOE 98/. Major minerals like feldspars and micas carry only insignificant proportions of the radionuclides in this type of granites.

The magmatic radioactive accessory-mineral assemblage of the Ruprechtov granite comprises uraninite, monazite–(Ce), xenotime–(Y), zircon, and fluorapatite. Apatite was not studied because it commonly contains Th and U in abundances of several 10 to a few 100 ppm only, which cannot be accurately determined by electron microprobe and requires analysis by LA-ICP-MS or SIMS. In sample NA8/12, two or more unidentified secondary REE minerals are present in altered biotite. Accessory minerals in the biotite granite OD1 include apatite, monazite–(Ce), zircon, and minor xenotime–(Y).

5.1.2.1 Monazite–(Ce)

Monazite–(Ce) is the main carrier of the light rare-earth elements (LREE) and present in all six samples investigated in this study. However, monazite–(Ce) from Ruprechtov is distinct from that of the Oder biotite granite.

Monazite (Ce) from Ruprechtov varies in size from less than 10 µm to (rarely) more than 100 µm in sample NA6/64. It is mostly included in mica, but is also present in the feldspars and quartz. In addition to forming single crystals, monazite is observed intergrown with zircon and apatite. Monazite appears usually homogeneous in the back-scattered electron (BSE) image, but grains displaying weak zonation also occur. Electron-microprobe analyses of monazite from Ruprechtov are listed in the (Annex 4 Tab. 3–7). Monazite from the surface sample VR1 is chemically indistinguishable from monazite from the granites exposed by boreholes NA6 and NA8. This LREE mineral is distinguished by a wide variation in the contents of Th, U, and the (HREE+Y). The concentration of Th ranges from 6.78 wt% ThO_2 in the dark interior of M9 in sample NA6/64 to 20.4 wt% ThO_2 in M3/1 in sample VR1. The content of U is lower than that of Th, but scatters likewise. The lowest U content (0.13 wt% UO_2) was measured in M9/2d and M11/2 (sample NA6/64). Monazite M3 from sample NA8/23 is highest in U (4.3 wt% UO_2). Another distinguishing feature of monazite from Ruprechtov and other high-F, high-P_2O_5 granites from the Erzgebirge is the relatively high content of Y (e.g.

/FOE 98a/). A content of 4.9 wt% Y_2O_3 as measured in M12 (sample NA8/23) is exceptional in peraluminous granites.

Monazite–(Ce) from sample OD1 displays an elemental pattern that is unambiguously different from that characterizing monazite–(Ce) from the Ruprechtov site (Tab. A.4.8). First, it is, on average, lower in Th (6.61 < ThO_2 < 10.3 wt%). Secondly the abundances of U (0.12 < UO_2 < 0.26 wt%), are mostly, those of Y (0.13 < Y_2O_3 < 0.71 wt%) always lower than the respective contents in monazite–(Ce) from Ruprechtov. Finally, the bulk of Th and U in the OD1 monazite is substituted as huttonite ($ThSiO_4$), whereas the brabantite component [$CaTh(PO_4)_2$] is essential for the incorporation of (Th+U) in the monazite from Ruprechtov.

5.1.2.2 Xenotime-(Y)

Xenotime-(Y) is abundant in all five samples from the Ruprechtov granite, where the mineral constitutes the main host of Y and the heavy rare earth elements (HREE), Only a single xenotime grain could be observed in the biotite granite OD1.

Xenotime-(Y) varies in size between <10 µm and 30 µm. It forms individual crystals of anhedral to subhedral shape, but more commonly it is intergrown with zircon. The xenotime grains are usually homogeneous in the BSE image. Zoned crystals are less common. The results of electron-microprobe analyses of xenotime are listed in the Tab. A.4.9-A.4.12. Xenotime has a Th/U ratio < 1, in contrast to what is observed in monazite. The highest (5.68 wt% UO_2) and lowest (1.74 wt% UO_2) concentrations of U were measured in a zoned grain from sample NA6/75. The variation in Th is less significant (0.09 < ThO_2 < 1.01 wt%). Xenotime also displays some variation in the Y/HREE ratio and the relative abundances of the individual HREE. However, with the exception of one grain (X5) included in biotite from sample NA6/64, the ratio of (Gd–Ho)PO_4/(Er–Lu)PO_4 is always above unity. Grain X5 with (Gd–Ho)PO_4/(Er–Lu)PO_4 = 0.85 probably did not crystallise from the granite melt, but rather represent unmelted material from the magma protolith or a fragment of country rocks assimilated by the uprising and solidifying melt.

5.1.2.3 Zircon

In the Ruprechtov granites, zircon is the accessory phase most complex in composition. In every sample, Th–U–REE–P poor, unaltered euhedral to subhedral zircons of ideal stoichiometry exists together with Th–U–REE–P rich, heavily altered and metamict, hydrated and fluorinated zircon grains. Only a selection of zircon grains could be probed. Thus, the zircon compositions reported in the Tab. A.4.13-A.4.17 are unlikely to correctly reflect the proportions between fresh and altered zircon grains within each sample.

Unaltered zircon grains usually display weak oscillatory zoning indication crystallization from the melt. Altered zircon grains often display patchy zoning, are cracked and contain a bunch of voids. Altered portions of zircon grains quickly decompose under the electron beam indicating the presence of water in the crystal structure. Zircon–xenotime assemblages are common.

Chemically, fresh zircon of ideal stoichiometry does contain elements other than Zr and Si in abundances at or below their detection limits. Uranium and Th are present at concentrations <0.1 wt%. Altered zircons typically contain U in excess of 1 wt%, with a maximum of 5.9 wt% UO_2 measured in the dark portion of zircon Z5 in sample NA8/23. Alteration of zircon also was accompanied by a decrease in Th up to 3.6 wt% ThO_2 in Z7 from sample NA8/23. Other features distinct of alteration include locally extreme enrichment in (P+HREE), Al, Sc, Ca, Fe, and F. Enrichment in (P+REE) and concomitant depletion in (Si+Zr) suggest the coupled substitution reaction $Si^{4+} + Zr^{4+} \Leftrightarrow P^{5+} + REE^{3+}$ to be operational. Of further interest are the relatively high concentrations of Pb, particular in some of the zircons analysed in sample NA8/12. These high Pb abundances cannot be considered as fully radiogenic formed during radioactive decay of U and Th from the zircon itself, but must be due to addition of lead during alteration of these zircons.

Zircon from the neighbouring biotite granite OD1 is less magnificent. Unaltered zircon grains predominate over altered grains. In altered zircon, enrichment of P, Sc, Y, REE, and F is less significant than in zircon from the Ruprechtov granite suite.

5.1.2.4 Uraninite

Uraninite could be identified in all samples studied from the Ruprechtov granite, but appears to be missing in the biotite granite. It usually forms perfect euhedral crystals of cubic or hexagonal appearance enclosed in quartz. The grain size of uraninite is small; it ranges from 5 x 5 µm to a maximum of 20 x 15 µm. Initially, uraninite was much more frequent at Ruprechtov, but only those grains inside of the relatively insoluble quartz (and not those hosted in easily attackable micas and feldspars) survived the widespread fluid-induced dissolution of uraninite in Permian time.

Chemically, uraninite is poor in Th (2.0–5.2 wt% ThO_2) and very low in (REE+Y) (Table 2). Elements such as P, Si, Ca, and Fe are present at levels at or below their microprobe detection limits. Its composition resembles that of uraninite from the Eibenstock, Pobershau and Satzung high–F, high–P_2O_5 Li-mica granites in the German Erzgebirge as well as that of uraninite from the more highly evolved Podlesi granite-pegmatite system in the western Czech Erzgebirge (/FOE 99, FOE 01/). The low abundance of Th is responsible for the high susceptibility of the Ruprechtov uraninite for destabilization and dissolution during the Permian interaction with oxidizing fluids, e.g. /FOE 99/.

5.1.3 Mineralogical mass balance

Assuming that 5% of U and Th are contained in major minerals and that the composition of apatite from Ruprechtov and Oder is similar to that of apatite from chemically equivalent granites in the German Erzgebirge, the contribution of the individual accessory minerals to the bulk-rock actinide and lanthanide budgets could be calculated. This was done exemplarily for samples VR1 and OD1.

In sample VR1, uraninite plus U deposited along grain boundaries account for about 60% of the bulk-rock U budget. Zircon, monazite, and xenotime contain 10%, 12%, and 15%, respectively, of the total U. Almost all of the Th (90%) is contained in monazite–(Ce), the predominant LREE mineral (containing 90% of the Ce budget). Xenotime–(Y) accounts for 65% of the Y and most of the HREE. Zircon hosts important proportions of the small-size REE, i.e. about 30% of Yb. Less than 10% of the REE resides in fluorapatite.

Xenotime accounts for about 30% of the U in sample OD1. It is followed by apatite (20%), zircon and monazite (15% each). Ten percent may be related to U along grain boundaries. 93 percent of total Th resides in monazite (and about 82% of Ce). Xenotime accounts for 45% of the bulk-rock Y budget, followed by fluorapatite (40%).

5.1.4 Conclusions

Even the macroscopically most “unaltered” portions of the Ruprechtov granite are not devoid of alteration-induced elemental disturbances. Temporally, two or more events of alteration can be distinguished. Enrichment of (F+Rb+Cs) is related to late- to postmagmatic crystallization of Li-micas during or shortly after crystallization of the granite melts in the late Carboniferous (e.g. /FOE 99/). Widespread depletion in U is likely associated with the regional interaction of near-surface portions of the granite bodies in the Erzgebirge with oxidizing meteoric fluids in the Permian, between 280 and 270 Ma (e.g. /FOE 99/). The elemental patterns of the borehole samples indicate operation of a third alteration event, probably related to Tertiary/Quaternary events affecting the Sokolov basin. These low-T processes are responsible for the depletion in CaO, Na_2O, P_2O_5 and (Pb) and the enrichment in (Al_2O_3), MgO, H_2O^+, (Sr), and (Y). X-ray diffraction analysis of the samples is required to verify the nature of the secondary minerals that host the enriched elements. “Hot” candidates are OH-bearing clayey and micaceous minerals. Depletion of (Ca+Na+P) would indicate destruction of plagioclase and apatite. The process that caused the depletion in Pb remains obscure.

A large amount of the removal of the U in all five samples studied is associated with Permian activities. However, by comparison with samples from outcrops of Erzgebirge granite from Eibenstock, Pobershau and Satzung it can be deduced that probably during Tertiary a second phase with an again significant removal of uranium occurred (cf. chapter 6.1). The proportion of the total leached uranium is enormous. From the U *vs.* 1/TiO_2 plot in Fig. 1 it could be deduced that in sample VR1, the original U content was about 33 ppm implying that almost 80% of the U got lost. In the fresh granite VR1, about 88% of the U resided in uraninite. The contents of Th, Zr, and Y (with the exception of sample NA8/12) were little, if at all, affected by the overprinting. Monazite-(Ce) and xenotime-(Y) mostly remained stable during alteration. Zirconium leached from altered and dissolved zircons became not efficiently removed from the system.

The investigation of accessory minerals in the sedimentary cover of the granite exposed in borehole NA6 supposes that monazite-(Ce) in the sedimentary layer is detrital and derived from weathered granite (cf. chapter 5.2.2.1). The results are confirmed by the study of granite minerals. Moreover, the similarity in the elemental patterns of monazite-(Ce) from the sediments and the underlying granite unambiguously define the Ruprechtov granite itself as the source of the monazite. The detrital monazite did not come from the neighbouring biotite granites represented by sample OD1.

5.2 Uranium in sedimentary layers

Uranium enrichment with concentrations up to several 100 ppm is observed in the tertiary basin of Ruprechtov site. The spatial distribution of uranium in the area is rather unevenly, clearly correlated to the strong morphology of the interface between kaolin and pyroclastic sediments and to the kaolin thickness. This is exemplary shown in Fig. 5.3 for the correlation with kaolin thickness. This circumstance is discussed in detail in chapter 6.

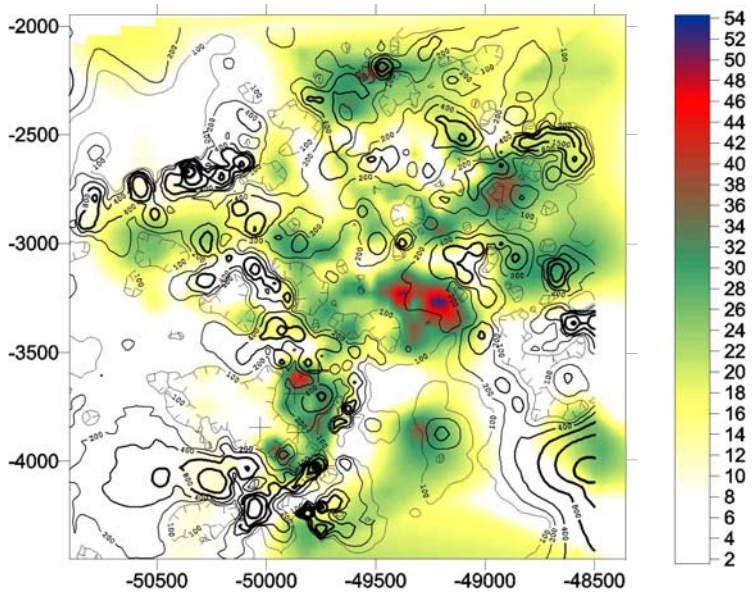

Fig. 5.3: Uranium distribution (indicate by isolines) correlated to kaolin thickness

Furthermore, the uranium is unevenly distributed in vertical direction, which is illustrated in Fig. 5.4**.** The main uranium enrichment occurs in the clay/lignite layers, which are found at the interface between kaolin and pyroclastic sediments in the so-called clay-lignite-sand horizon. Its extension is limited to only a few metres. Fig. 5.4

shows also that the position of the peak varies in depth. The most surface-near peak is obtained in NA7 around 15 m and the deepest peak in NA14 below 60 m. This is due to the strong morphology of the top of the kaolin and therewith the depth of the clay/lignite-sand layer, which is illustrated in Fig. 5.5. NA14 and NA13 are situated more north in a valley where the depth of the kaolin top is around 60 m, whereas NA7 is more south in an area with depth of kaolin top around 20 m.

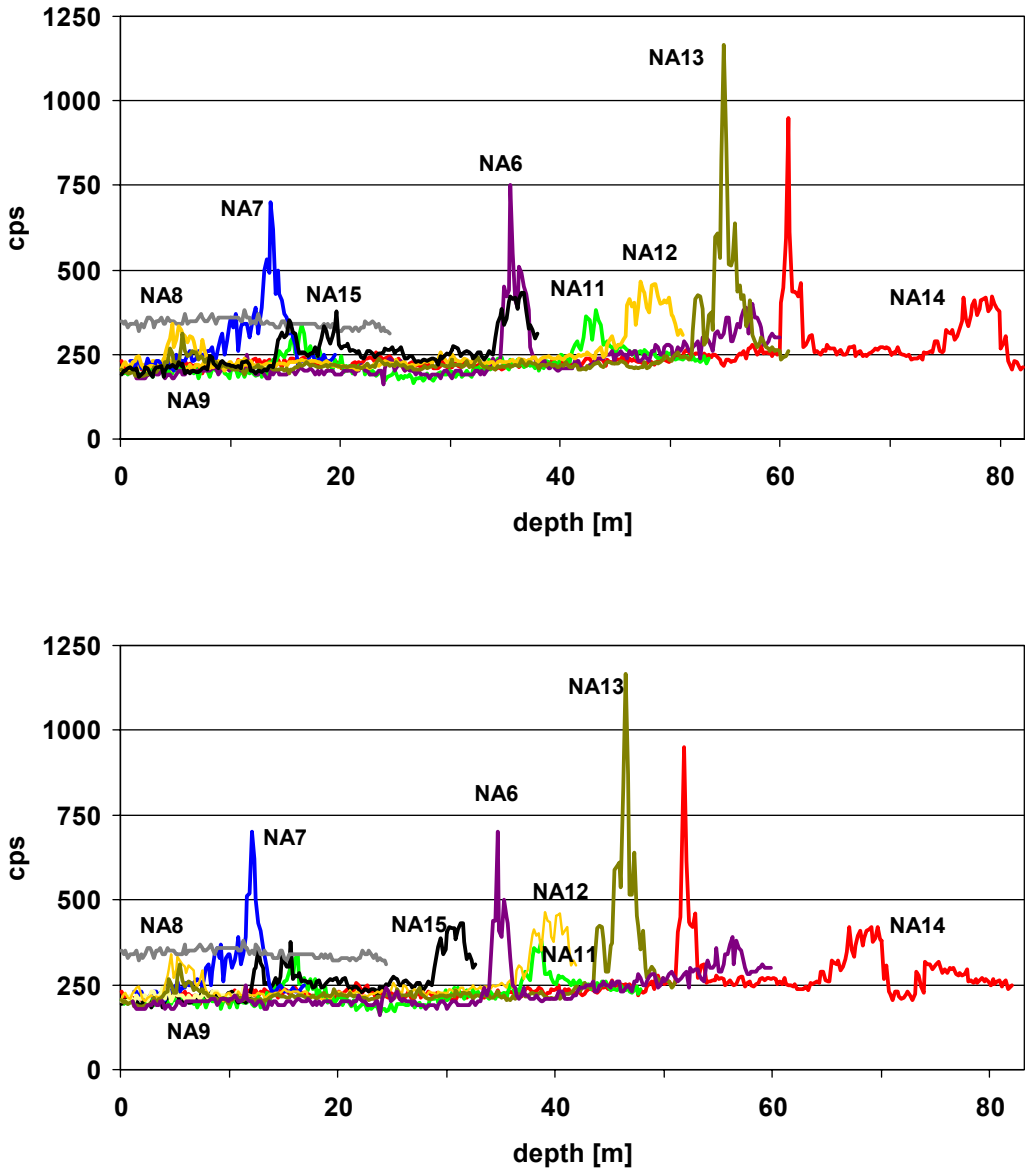

Fig. 5.4: Extension of the uranium enrichment in the clay/lignite horizon in different boreholes detected by on site gamma log directly after drilling. Uncorrected values (top) and corrected values (bottom)

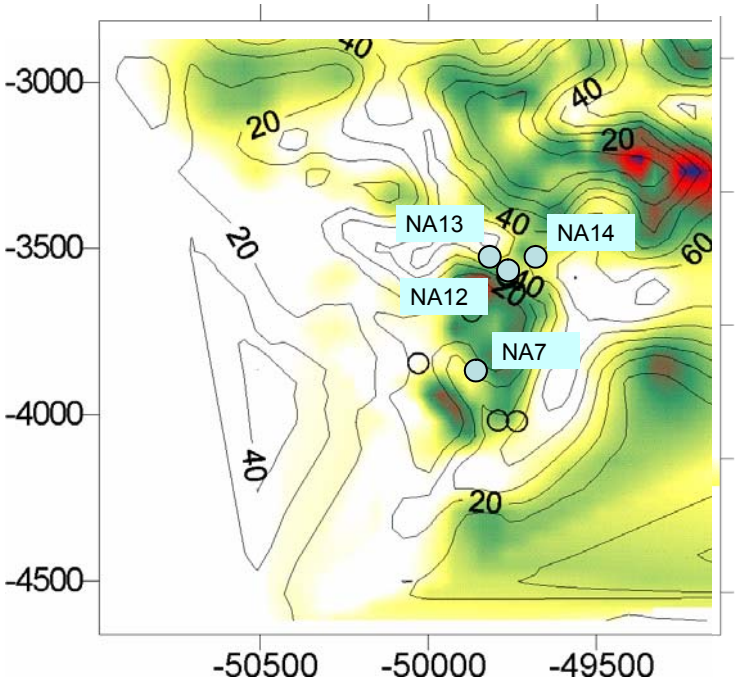

Fig. 5.5: Position of single boreholes versus top of kaolin indicated by isolines

One main observation is that uranium is predominantly found in lower part of clay/lignite horizon and below, in sediments with low concentration of or even no organic matter (Fig. 5.6).

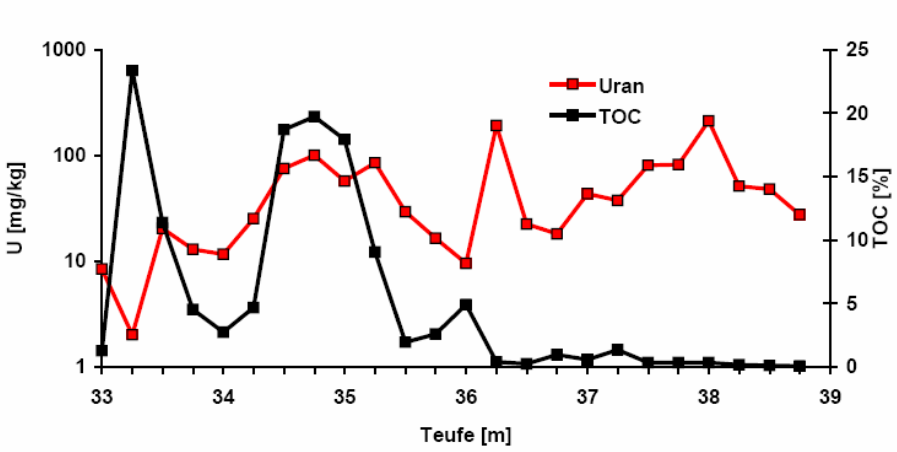

Fig. 5.6: Correlation of U- and TOC-content in sediment samples from drillhole NA3 in different depths [m] (from /BRA 98/)

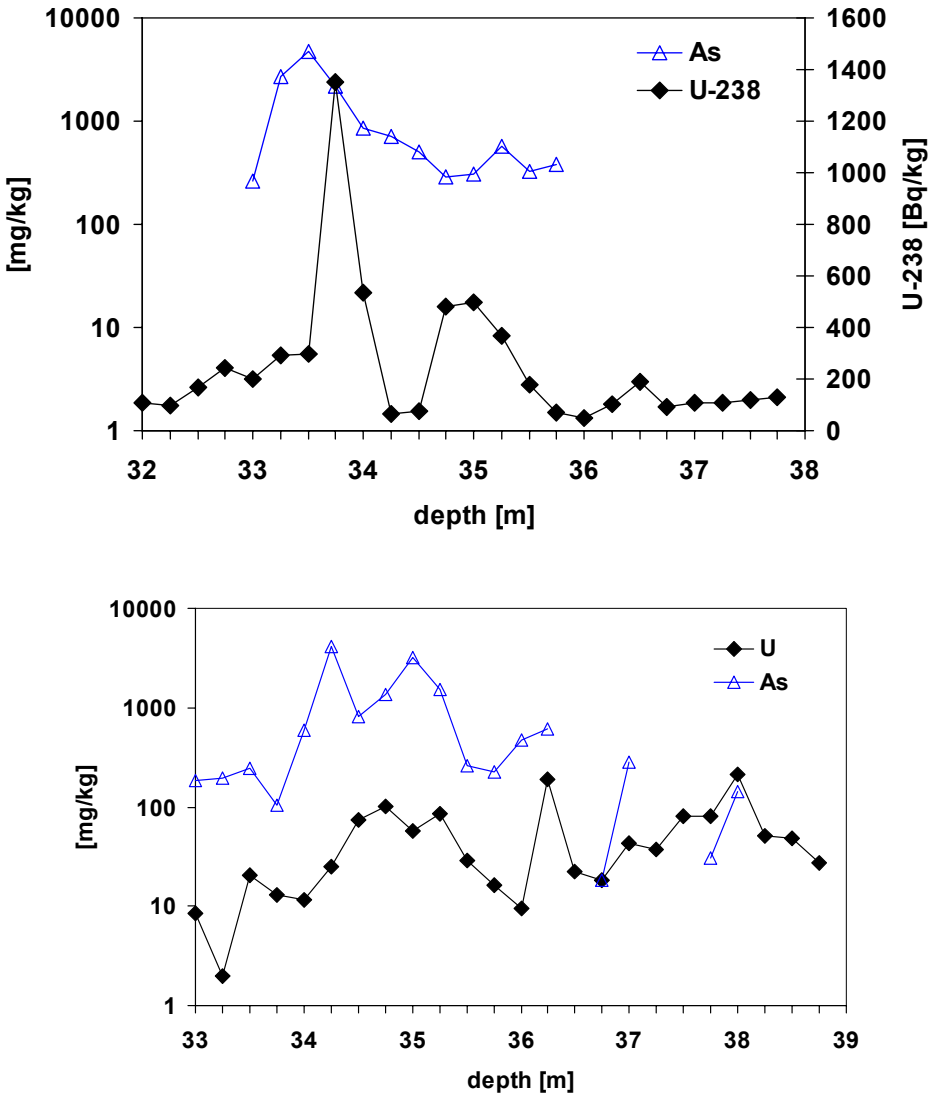

Fig. 5.7: Correlation of U content with content of As in samples from drill core NA2 (top) and drill core NA3 (bottom).

Fig. 5.7 shows the correlation of uranium content with As concentration in bulk samples from 25 cm pieces. The data from NA2 and NA3 show positive correlation between both elements. The occurrence of As seem to be important for the reduction process of uranium as discussed in Chapter 5.2.3.2.

5.2.1 Mineralogical features of the sedimentary layers

The mineralogy of the pyroclastic sediments, the clay-lignite sand layer and the kaolin has already been described in detail in /NOS 02/. Here we will only summarise the most relevant information

The typical distribution of major minerals in the clay lignite horizon is shown in Fig. 5.8. Highest content of lignite is found in the upper part of this layer. The content of organic matter can be up to 50 wt.%. With increasing depth the amount of organic matter decreases and the amount of kaolin and quartz increases. Highest quartz contents are found in the bottom parts where the sandy layer of the Staré Sedlo formation is deposited.

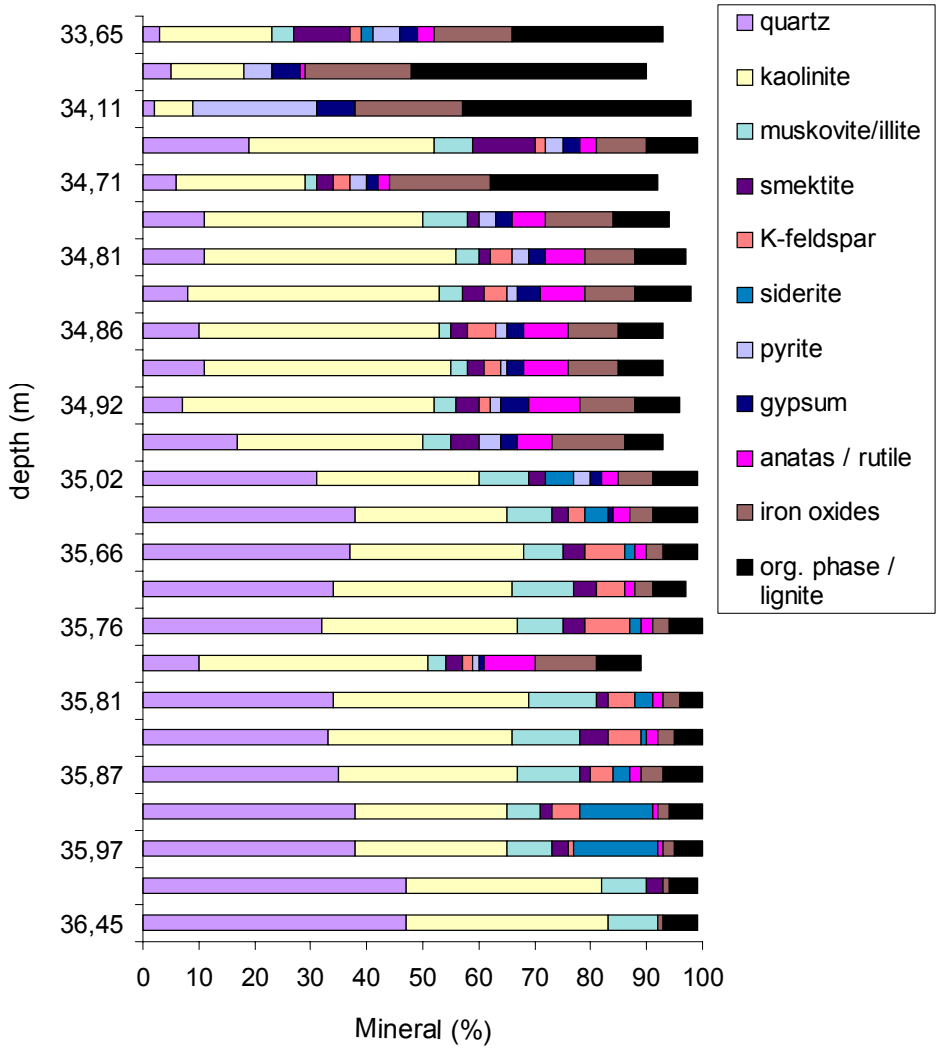

Fig. 5.8: Mineral phase distribution in the clay/lignite-sand horizon

The composition of clay minerals changes above the clay lignite layer. In the argillized pyroclastic sediments the content of smectite is significantly higher, reaching concentrations of up to 40 %. The content of kaolin in the pyroclastic sediments is extremely low. Elevated contents are only found in rarely occurring small water bearing layers where kaolin was enriched as resistant mineral.

Typical cation exchange capacities (CEC), measured in sample NA4 are shown in Fig. 5.9 and Fig. 5.10. The CEC-values in the clay lignite horizon vary roughly between 40 and 65 mmol/z/100g. At the top of the clay/lignite-sand layer CEC-values increase due to higher content of TOC (samples from lower part) and higher content of smectite (samples from upper part).

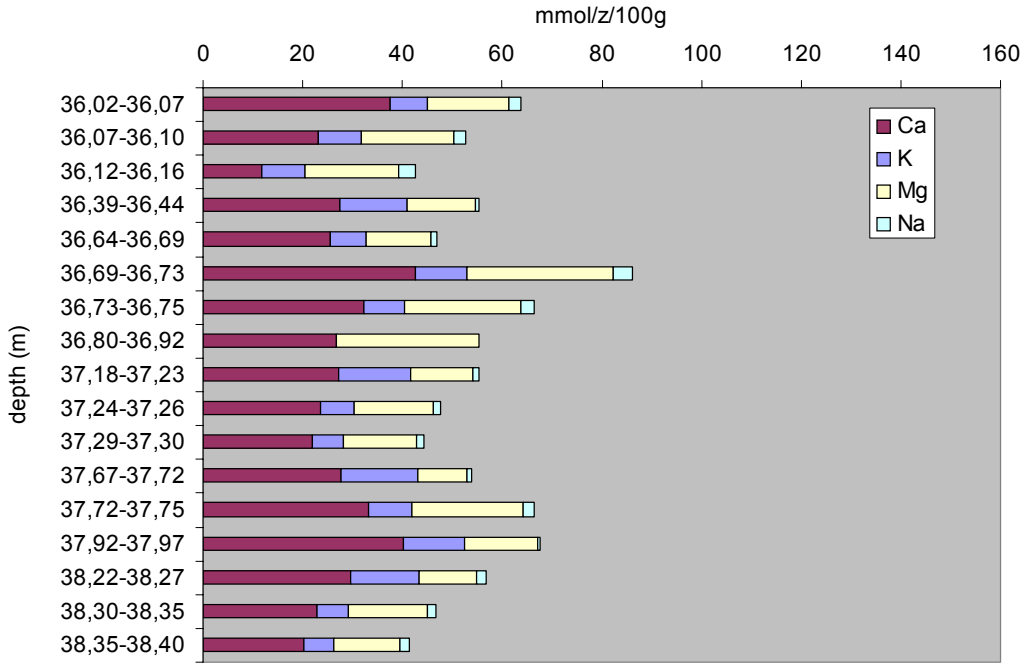

Fig. 5.9: CEC-values from of clay/lignite-sand horizon (NA4)

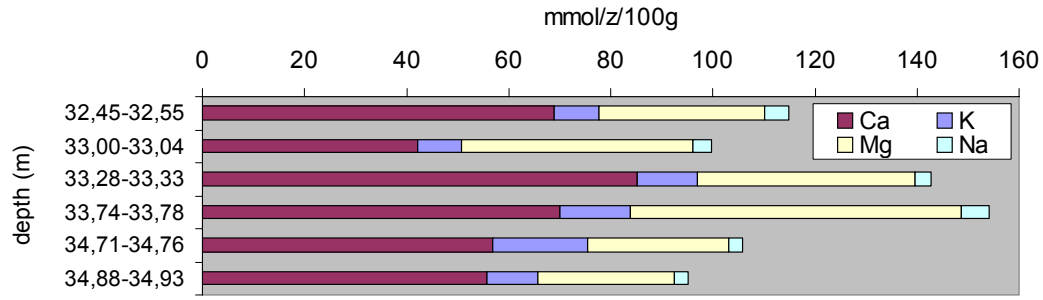

Fig. 5.10: CEC-values from interface clay/lignite-sand / argillized tuffs (NA4)

5.2.2 Uranium bearing mineral phases in sedimentary layers

On few samples from borehole NA5 uranium bearing minerals uraninite and ningyoite were already identified by SEM-EDS in the last project phase /NOS 02/. The aim of this

project phase was to check if other uranium bearing mineral phases are present and to quantify uranium content in the different phases.

Major investigations were made on drill cores from NA6 from the segments 35.90-36.00 and 37.62-37.72. The sample preparation was performed by *J. Janeczek*. They were immersed in liquid polymers prior to cutting. Three sub-samples were drilled out from each segment (totalling six sub-samples) covering the top, middle and bottom portions of each drill core (Fig. B). Sub-samples formed rounded blocks, which were stabilised with resin. Their flat surface was gently polished and covered with a carbon layer of a few micrometer.

Analysis and images of accessory minerals in the clay/lignite-sand horizon were performed by Analytical scanning Electron MicroscopyASEM and electron microprobe. ASEM observations were performed by *J. Janaczek* using ESEM-XL30TMP (Philips/Fei) scanning electron microscope equipped with EDAX detector. Quantitative analyses were mainly performed by *H.J. Förster* as described in chapter 5.1 using electron microprobes at the GFZ Potsdam operating in wavelength-dispersive mode. The samples manufactured by *J. Janeczek* were used but re-polished and re-coated at the GFZ. The operating conditions during analysis of accessory minerals were as follows: accelerating voltage 20 kV, beam current 40–60 nA, and beam diameter 1–2 µm.

In comparison bulk-rock geochemical work was done on a powdered sample from the clay-lignite horizon (borehole NA6, depth 35,80-35,90 m) directly neighboured to the samples investigated by ASEM and electron microprobe. This sample comes from a horizon between 5 and 6 meters above the zone, from which the polished sections were made. The contents of the rare earth elements (REE) plus Rb, Sr, Y, Zr, Cs, Ba, Hf, Pb, Th, and U were analyzed by inductively coupled plasma-mass spectrometry (ICP-MS; Perkin-Elmer/Sciex Elan Model 500) according to the method and with the precision and accuracy outlined by Dulski (2001).

As uranium bearing minerals zircon, xenotime, rhabdophane, monazite, uraninite and ningyoite were observed. The single mineral phases are described in the following with emphasise on uranium content and origin of the minerals, i.e. to answer the question whether they are primary or secondary minerals. The chemical composition of the accessory minerals analysed by microprobe are listed in Annex 5.

5.2.2.1 Monazite-(Ce)

Monazite-(Ce) constitutes the most frequent REE mineral in both samples. It is usually homogeneous or weakly zoned and occurs in variable sizes, from less than 10 µm to (exceptionally) 70 µm. The grains are typically subhedral, fractured, corroded, and contain vacuoles. Small anhedral, rounded or elongated grains also occur. Chemically, monazite-(Ce) contains between 3.4 and 15.5 wt% ThO_2, and between 0.06 and 2.65 wt% UO_2 (Tab. A.5.1 and A.5.2). Yttrium is present at concentrations ranging from 0.27 to 5.6 wt.% Y_2O_3.

In thin section NA6/37.62, a single monazite grain (M1, Tab. A.5.2) was measured, which distinctly differs in composition from the bulk of the monazite grains studied. It contains Th, U, and Pb below their detection limits. The dearth of the two actinides is inconsistent with the composition of granitic monazite of magmatic origin. The origin of this grain remains obscure. It either formed in response to the hydrothermal alteration of the granite in Variscan time, or during the kaolinisation of the granite in the Tertiary.

Most of the monazite occurs as angular grains up to 25 µm in diameter. The grains are often fractured and regions along fractures appear darker in BSE images than the unfractured portions of grains (s. Fig. 5.11). The angular shape of the monazite grains including shards suggests that the grains are broken fragments of larger crystals. Idiomorphic grains of monazite are rare.

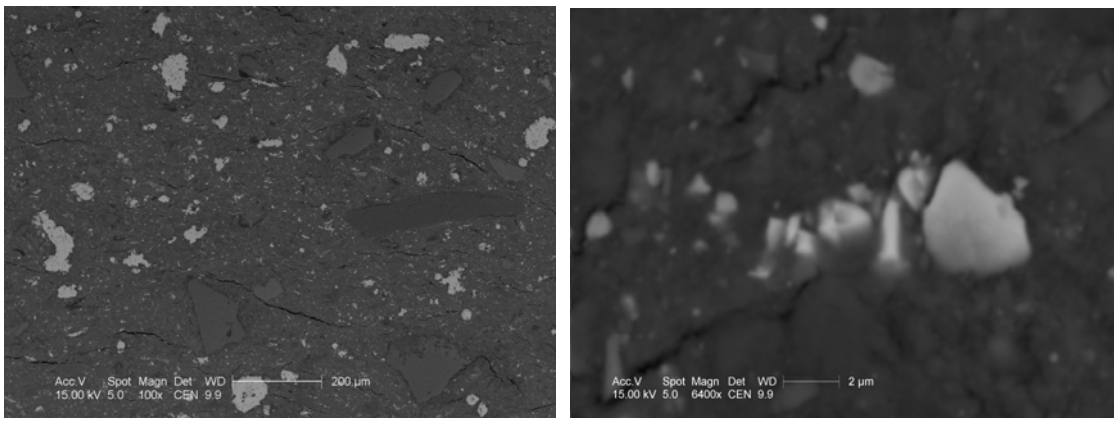

Fig. 5.11: Image of monazite minerals in sample 36 m of borehole NA6

5.2.2.2 Rhabdophane-(Ce)

In section NA6/37.67, one grain of a LREE-dominant mineral was observed, which was originally identified as monazite. However, this grain only totalled to about 94–94.5 wt% and differs significantly from monazite-(Ce) in various elemental abundances. It is richer (in wt.%) in Y ($5.8<Y_2O_3<6.0$), the HREE with the lowest ionic radio (Er, Yb), P, Al, and Fe, but poorer in Th ($0.19<ThO_2<0.00$) and, consequently, Pb, and displays a weak negative Ce-anomaly. These chemical characteristics suggest the mineral being rhapdophane-(Ce), ideally (Ce, LREE)PO_4 x (H_2O). Members of the rhabdophane group are evidently of secondary origin, formed during low-T alteration processes. Therefore, formation of this hydrous LREE phosphate is likely attributed to the weathering of the Ruprechtov granite during Tertiary time.

5.2.2.3 Xenotime-(Y)

Xenotime-(Y) occurs in all sections in low, but generally higher abundances than reported by Janeczek (2004). It forms overgrowths on zircon or independent grains usually less than 20 µm in size. Xenotime-(Y) always contains Th and U in concentrations (in wt.%) well above their detection limits, i.e., $0.06<ThO_2<1.18$ and $0.89<UO_2<3.93$ (Table 2). Its REE abundances and patterns are indistinguishable from xenotime-(Y) in the deeper part of the borehole (cf. chapter 5.1.2.2).

5.2.2.4 Zircon

Zircon constitutes a minor accessory phase. In almost every sample, Th–U–REE–P-poor, unaltered euhedral to subhedral zircons of ideal stoichiometry exist together with Th–U–REE–P-rich, heavily altered and metamict, hydrated and fluorinated zircon grains. Unaltered zircon grains may display weak oscillatory zoning indication crystallization from the melt. Altered zircon grains are cracked, embayed, or otherwise corroded, contain a bunch of voids, and decompose under the electron beam indicating the presence of water in the crystal structure.

Chemically, fresh zircon of ideal stoichiometry does contain elements other than Zr and Si in abundances at or below their detection limits (Tables 3a and 3b). Chemical features distinct of alteration include enrichment in P, (Y+HREE), Al, Sc, Ca, Fe, and F, and depletion in Zr and Si. Uranium and Th are usually present at low concentrations

(in wt.%), $0.01<UO_2<1.29$ and $0.00<ThO_2<0.41$, respectively. Zircon from this, kaolinized portion of the granite is compositionally indistinguishable from zircon from the weakly altered Ruprechtov granite (e.g., Förster, 2004).

Uraninite

Occasionally observed bright (in the backscattered-electron image) spots < 8 μm in size probably indicate the occurrence of uraninite in some of the sections, but only two single, idiomorphic grains (8 x 8 μm in size) could be probed. These grains have a near-end member composition, containing only Si, Ti, and Al in minor abundances. Whether these 3 elements form part of the structure or represent analytical artefacts from adjacent phases is impossible to resolve due to grain-size restrictions. The most important chemical feature of this uraninite is the presence of Th, Pb, and (Y+REE) in contents below their detection limits. Fig. 5.12 shows a SEM image with uraninite.

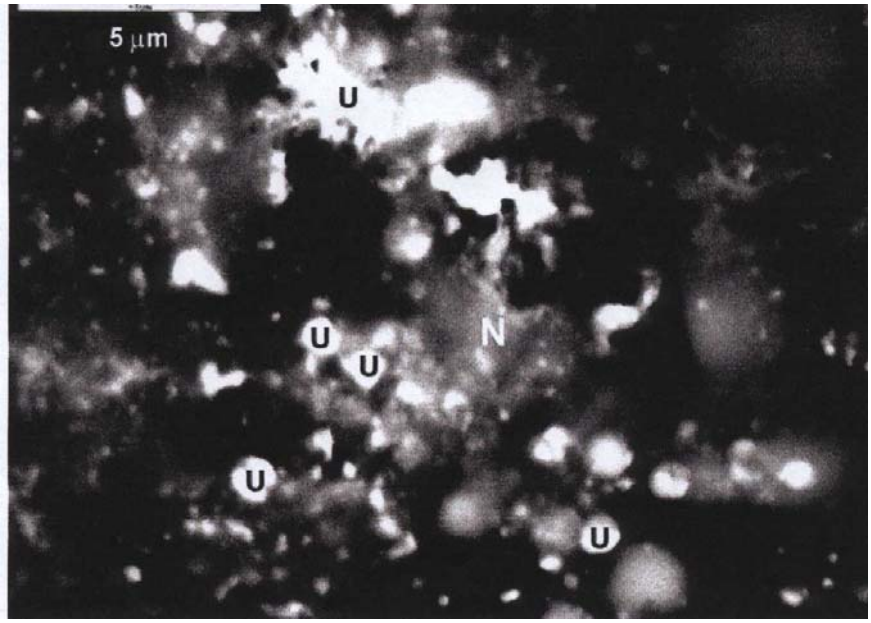

Fig. 5.12: Sketch of uraninite from SEM-EDX investigation at NA5. U denotes uraninite and N denotes ningyoite minerals

5.2.2.5 Ningyoite

A single grain of U- and REE-bearing phosphate, most probably ningyoite (nominally $U,Ca,Ce)_2(PO_4)_2 \cdot 1\text{-}2H_2O$) was found in NA6 36.00. The grain of ningyoite, some 7 μm in diameter is rimmed by a few μm thick layer of organic matter, s. Fig. 5.13.

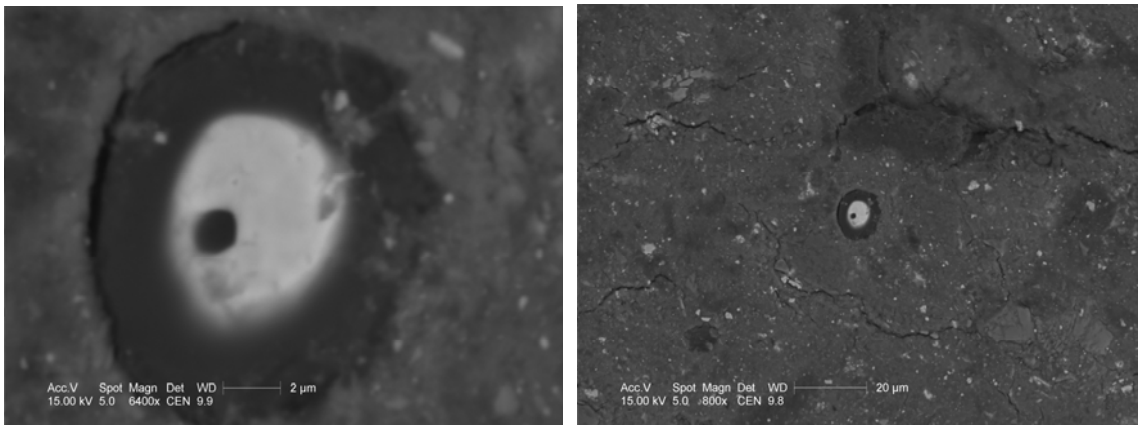

Fig. 5.13: Image of phosphate (probably ningyoite) mineral in sample 36 m of borehole NA6

5.2.2.6 Mineralogical mass balance of U and Th

Identification of the accessory minerals responsible for the highly radioactive zone within the kaolinized granite is an important, but complicated issue. One major problem arises from the presence of minerals other than primary zircon, monazite-(Ce), xenotime-(Y), and uraninite, which control the radioactivity in common granitic rocks. In addition to Th-U-poor monazite-(Ce), rhabdophane-(Ce), (?) ningyoite, and unidentified secondary accessory minerals may be present in this zone. Furthermore, monazite-(Ce) and zircon display a large scatter in their Th and U abundances, which complicates determination of average contents necessary for the mass-balance calculations.

An important observation from the bulk-rock composition is the great predominance of the LREE and U over Th in the U-rich zone. This proportion contrasts with that in the weakly altered Ruprechtov granite as well as in the magmatic monazite-(Ce), the most important carrier of the LREE in common granitic rocks. In the non-kaolinized Ruprechtov granite, almost 90% of the Ce and Th is contained in magmatic monazite. In contrast, to account for all the Th in the U-rich zone, only about 25% of the LREE can reside in detrial magmatic monazite (with calculated weighted averages of 22.5 wt.% Ce and 7.6 wt% Th)! The contribution of magmatic monazite to the U budget of the rock would then be less than 5%! This relation underscores that newly formed LREE minerals poor in Th (but eventually rich in U) must be present in substantial amounts in this particular zone. The three previously mentioned late-magmatic and secondary LREE minerals would be good candidates, but other may occur as well.

The primary minerals monazite, xenotime, and zircon control less than 10% of the U content of the rock. The bulk of the U must reside in secondary uraninite and other accessories. Additionally important appears to be the presence of U along grain boundaries or absorbed on organic matter,

5.2.2.7 Conclusions

A crucial question is whether the identified accessory minerals are inherited from the granite or represent species newly formed in the course of alteration. This study shows that the monazite-(Ce) is detrital and derived from the weathered Ruprechtov granite itself. Moreover, the broad correspondence in composition implies that this mode of origin also apply to xenotime-(Y) and zircon in the kaolinized granite. However, the presence of perfectly rounded grains of particularly monazite may suggest that part of the primary accessories were transported to the site of their deposition over certain distances from more distant portions of the superficially exposed Ruprechtov granite.

In contrast, the composition of uraninite in samples NA6/36.00 and NA6/37.72 is distinctly different from that of uraninite in the deeper, not-kaolinized portion of the pluton. This uraninite contains several oxide weight percentages of Th and Pb, Y contents between 0.1 and 0.3 wt%, and yields a Th–U–total Pb age of 315.1 +/– 2.8 Ma (2-Sigma STDW) (cf. chapter 5.1.2.4). Thus, the uraninite in the clay/lignite sand horizon comes either from a different source or constitutes a newly formed mineral. The absence of measurable Pb in this uraninite, which suggests a very young (subrecent) age, lends support to the second alternative. In the bulk rock, uranium has the greatest enrichment factor (20.7) in the rich-ore zone relative to the unaltered granite and thus, constitutes by far the most mobile element during most of the alteration process. Decomposition of the Th-poor, and thus easily soluble uraninite in the Ruprechtov granite (cf. chapter 5.1.4 and /FOE 99/ seems to be a more appropriate process to explain the formation of this secondary uraninite. Remnants of the magmatic uraninite were not yet observed to have survived the kaolinization process. Finally, formation of rhabdophane-(Ce) implies also a certain mobility of the REE during alteration. Its precursor phase may have been monazite-(Ce), but it could also have incorporated elements from other sources. Assuming that rhabdophane-(Ce) formed from breakdown of monazite-(Ce), significant Th, but only minor U would have added to the fluid.

The results available at present suggest that micrometer or sub-micrometer-sized secondary uraninite and other U-rich alteration minerals like ningyoite largely account for the enriched U-content in the clay/lignite-sand horizon. The only weak enrichment of Th relative to U argues against a substantial fraction of undetected sub-micrometer monazite, as does the LREE: Th ratio of the bulk rocks (24.8:1 in sample NA6/31 versus 4.3:1 in sample NA6/64.5 and below). If significant amounts of LREE-rich species are missed because of small grain size, then these are rhabdophane-(Ce) rather than detrital monazite-(Ce).

5.2.3 µ-XRF and XANES

Besides Scanning electron microscope and electron microprobe first measurements by a newly developed confocal µ-X-ray fluorescence (µ-XRF) and X-ray absorption fine structure spectroscopic (µ-XANES and EXAFS) method have been performed on a sample from borehole NA4 by *M. Denecke et al.* (FZK-INE) in order to gain additional information about the uranium mineralisation. This work is described in detail in /DEN 05/. In the following the main results will be summarised.

5.2.3.1 Information about the experiments

The main feature of the method is a set up with two polycapillary half-lenses, which are used in a confocal geometry for these experiments. The confocal geometry was developed in order to restrict the volume inside the sample from where fluorescent radiation can reach the detector. It allows probing of defined volumes below the surface of the sample with a µm scale resolution /JAN 04/. By scanning arbitrary sample areas (x,y scans) at different depths (z), stacks of tomographic cross sections can be recorded. A detailed description of the method can be found in /DEN 05/. Measurements were performed at the Beamline L experimental station at the Hamburger Synchrotronstrahlungslabor (HASYLAB) using synchrotron light from the DORIS storage ring operating at 4.436 GeV with ring currents between 85 and 150 mA.

The bore core section stems from NA4 from 34.5 m depth. The bore core of near 20 mm diameter is embedded / impregnated in acrylic plastic (see Fig. 5.14). Uranium-rich areas at the sample surface were identified by autoradiography and the content of uranium therein quantified to ~150 µg ^{238}U/g material. A microscopic image of the large hot spot located to the lower left of the sample is also shown on the left in of Fig. 5.14.

The pyrite nodules found to be typically in the areas of high uranium activity are visible as round orange areas in the image. The pyrite is obviously oxidized on the exposed surface. A lignite inclusion is seen as a blackish formation.

Fig. 5.14: Image of the borecore sample NA4 34,5 m (middle) autoradiographic image (left) and optical microscopic 2.1 mm x 2.1 mm image of the lower left area with hot spot (pyrite nodules appear orange, lignite black and clay white)

5.2.3.2 Results

µXRF-Spectra were taken in 60 µm depth below the surface and a area of 700x700 μm^2 was scanned. The elemental distribution maps for Fe, As, Sr, Zr, U and Cu are shown in Fig. 5.15 (for details see /DEN 05/). Dark pixels represent areas of high concentration and lighter pixels areas of low concentration, and white of no detectable concentration.

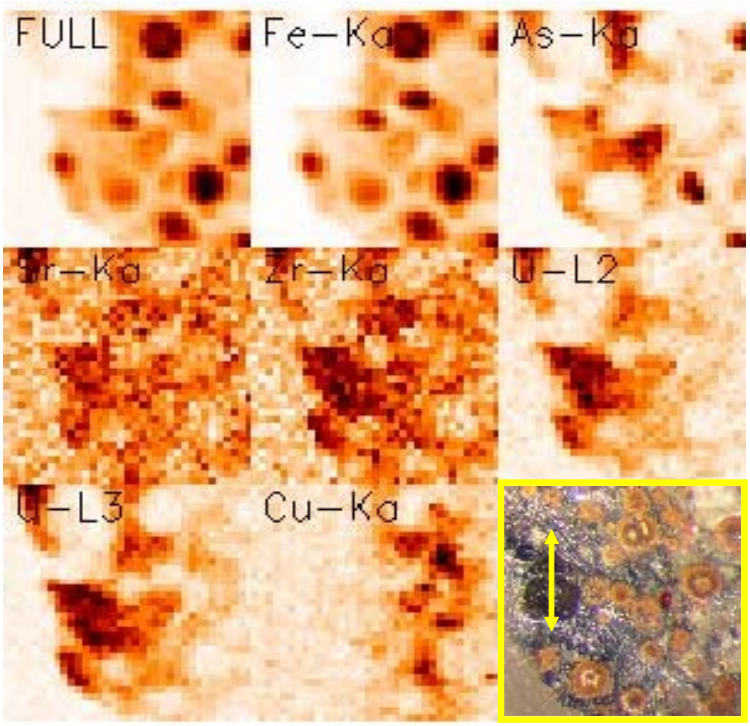

Fig. 5.15: Element distribution as (left to right) total incoming fluorescence counts in the multi-channel analyzer (labeled as "Full") and measured fluorescent intensities for Fe Kα, As Kα, Sr Kα, Zr Kα, U Lβ, U Lα, and Cu Kα radiation in an approximately 700 × 700µm area (optical micrograph shown at bottom right) at a depth of -60µm.

The pyrite nodules are visible as round-shaped areas of high Fe fluorescence intensity. Volumes with high As Kα-intensity appears in areas bordering the Fe(II)nodules. The U distribution is found very similar to the As distribution. However, it is not the same. For example, highest uranium concentration corresponding to highest Lα,β intensity is located on the right half of the lower left quadrant. Arsenic is also found in this area but not with highest concentrations. Since uranium mineral ningyoite and tristramite containing Ca have been identified by SEM-EDS in the clay-lignite horizon (cf. chapter 5.2.2.5) the distribution of Ca was checked. The Ca Kα,β peaks are at energies too low to be detected in this depth due to self absorption. Therefore Sr as indicator for Ca was detected. Indeed, Fig. 5.15 shows that the Sr distribution strongly correlates to the uranium distribution. The tetravalent element Zr also shows a similar distribution as uranium, indicating the oxidation state IV of uranium.

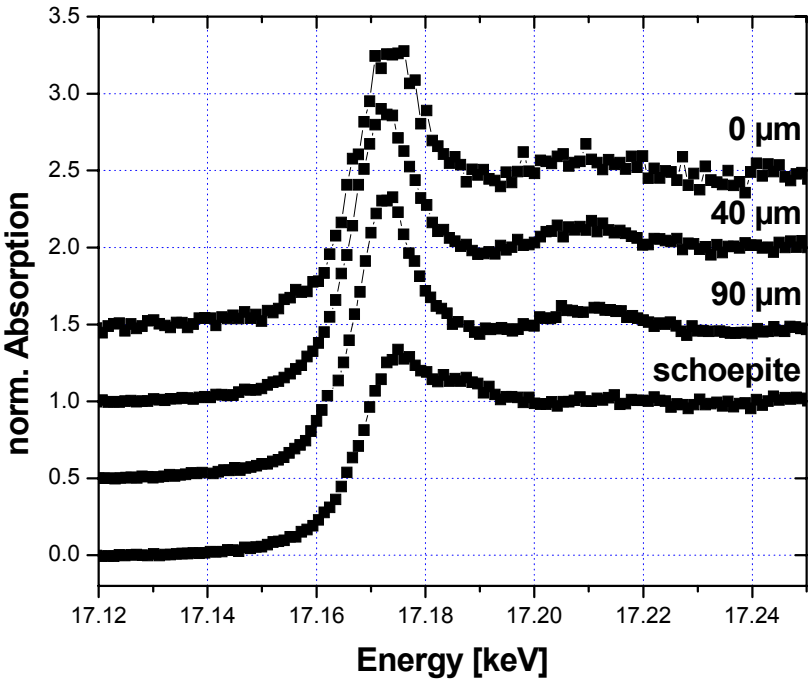

Fig. 5.16: U L3 µ-XANES recorded at various depths of the sample NA4. For comparison reference XANES of UO_2 for U(IV) and schoepite for U(VI) are presented /DEN 05/

To assess the oxidation state of uranium U L3 µ-XANES spectra at the hot spot on and below the surface at depth of 40 and 90 µm are recorded (Fig. 5.16). The shape and intensities show the average valence state of the sampled volume to be tetravalent, i.e. U(IV). All three curves do not show the multiple scattering feature 10-15 eV above the white line (WL) characteristic for U(VI) nor do they show a significant decrease in the WL intensity, which would be expected for U(VI) as be seen in the schoepite spectrum in Fig. 5.16. The small apparent shift in the U edge white line energy in the XANES spectrum recorded on the sample surface is likely an artefact due to loss in the DCM θ angle stepping motor steps and not any real energy shift, as this spectrum's features are characteristic for U(IV). From XANES there is no spectral evidence for U(VI) at the surface or below.

In addition a µ-EXAFS-spectrum was recorded in the hot spot area in a depth of about 90 µm. The results are discussed in detail in /DEN 05/. This spectrum confirms uranium to be in oxidation state IV, since there is no evidence for the short uranyl oxygen distance indicative for the presence of U(VI). It was not possible to identify the uranium mineral doubtless as ningyoite. But it is concluded that the uranium mineral is not uraninite and likely a phosphate.

The qualitative, general inverse relationship between the signals observed for Fe, As and U is evaluated by correlation plots of the measured intensities in each pixel of the images shown in Fig. 5.15. The results are shown in Fig. 5.17. The highest counts for U are all associated with no or negligible Fe signal and vice versa. In the correlation plot of the As Kα signal versus Fe Kα it can be seen that a portion of the pixels with high Fe counts are associated with no or negligible As signal. However, there are two other correlations between As and Fe. There are pixels with significant As intensity associated with up to 20000 Fe counts, as well as another linear dependency between As in pixels with higher Fe intensity. As expected from qualitative evaluation of the images, the U counts are correlated to the As Kα signal, but there are also pixels with high As counts (up to ~640), which are not correlated to pixels with any U Lα intensity.

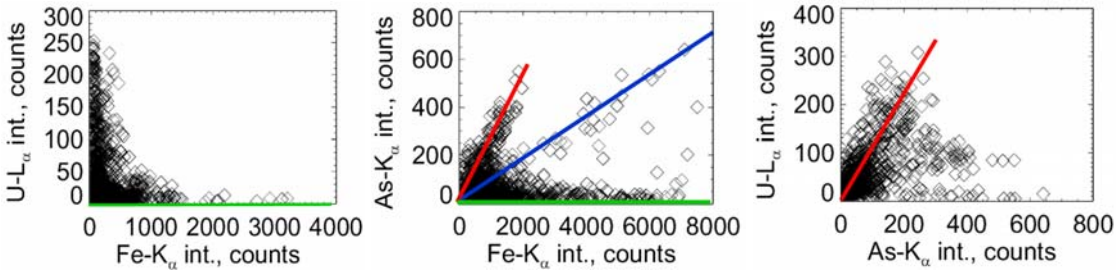

Fig. 5.17: Correlation of intensities Fe Kα, As Kα and U Lα measured in each volume element shown in Fig. 5.15. The lines indicate linear dependencies between element pairs

Because the U distribution is first observed to be generally found in areas void of Fe, but associated with the As distribution, and because sequential extraction experiments suggest a correlation between the total organic carbon (TOC) and the uranium concentration, μ-XRF images near both a lignite inclusion and Fe(II) nodules are recorded to ascertain if uranium is in any way preferentially located near one of these candidates capable of reducing the U(VI) to U(IV) during geogenesis. For this purpose, the fluorescence intensities for U, Fe, and As are recorded in 300 μm^2 images at different depths perpendicular to the depth scan (Fig. 5.18).

In the map recorded at -180 μm, a round Fe nodule is evident near the center of the image. A U hot spot is located just to the left of this nodule, as is an area of high As concentration. Both As and U appear to show low or no intensity in the location of the nodule, similar to the observations discussed above. Another region of high U intensity is at the lower left hand part of the image. The Fe nodule at the center of the image is

reduced in size in the next image, 30 µm closer to the surface, indicating a view of the cross section near the nodule top. Also evident are two more nodules at the top right and lower part of the image. Again high U Lα intensity at the lower left is observed. It is now evident that this high U intensity region borders a Fe nodule, lying just to the right, and the emerging lignite inclusion, which is visible as an area void of U, As, and Fe. The As Kα intensity appears to border the pixels with high Fe concentration. Following the nodule Fe Kα signal, which is clearly seen in the lower right quadrant from –180 µm up to –30 µm and comparing it to the development of the As Kα fluorescence, gives the impression that As appears to cover – or envelope – the Fe nodule. This particular nodule is not yet entirely evident at the lowest depth of -180 µm. In this image, the As signal is seen concentrated on or directly bordering the pixels, where, in the next image 30 µm closer to the surface (-150 µm), the nodule is seen. The areas with As being concentrated seem to “close” over the nodule, as the successive recorded images encompass the upper hemisphere of the Fe nodule with smaller cross-section diameters. In the final image of the series, -30 µm below the surface, the As exhibits high intensity above the pixels where the Fe nodule is located. If we follow the U distribution in this same series, the U fluorescence appears near, but not on top of As or Fe.

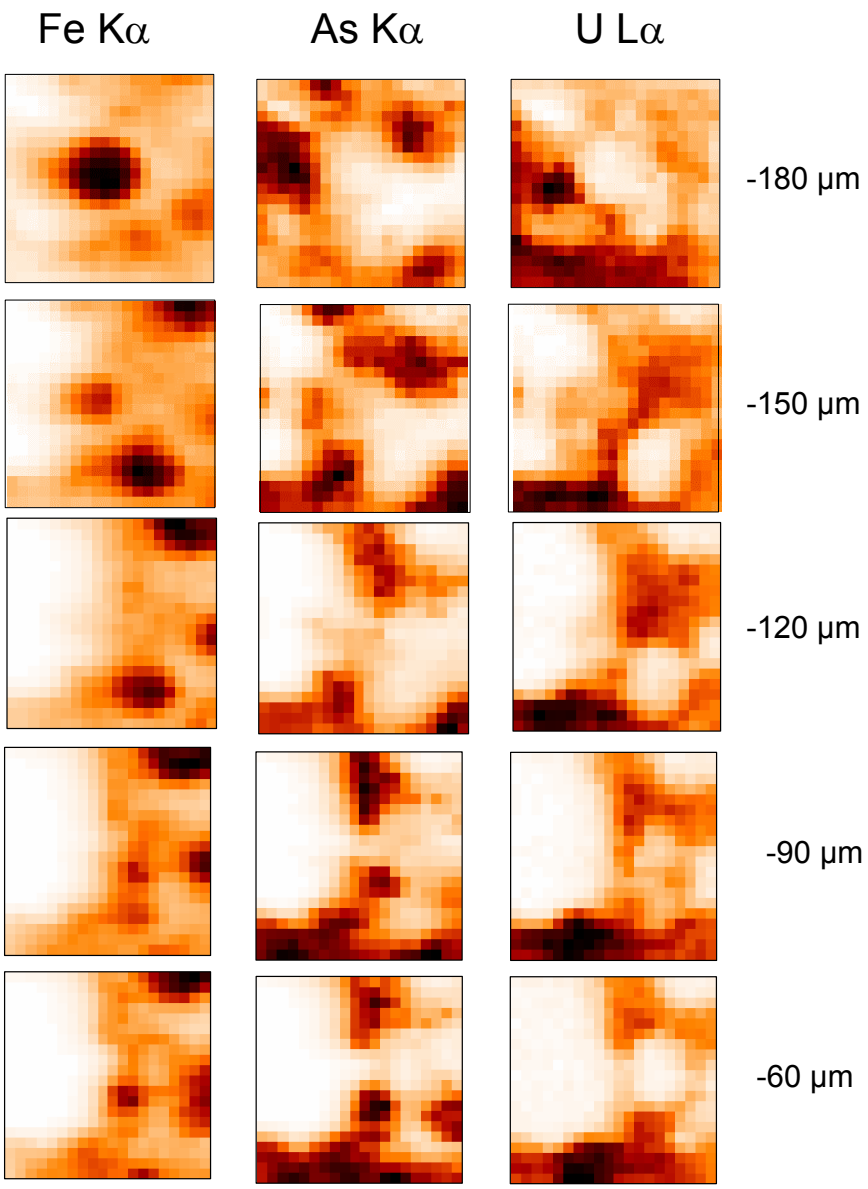

Fig. 5.18: Elemental map images for Fe, As, and U recorded at different depths below the surface /DEN 05/.

To identify the As species in the bore core sample, a number of As K XANES spectra were recorded at various locations in the bore core and at depths varying from near the surface to more than 200 µm below. The measured XANES are depicted in Fig. 5.19. This figure includes the energy positions of the WL for As in the 0, III, and V valence states (11.864 keV, 11.867 keV, and 11.870 keV, respectively) measured at HASYLAB by *M. Denecke at al.* /DEN 96/. Spectra A through E are recorded near or on different uranium hot spots, visible as black areas at the lower left and in the upper right quadrant of the autoradiogram in Fig. 5.14 (left). By comparison of the energy position of the WL of these spectra with that expected for As in different valence states, it is

found that spectra A, B, C, and E have WL corresponding to As(V) and spectrum D that for As(0). Spectra B and E clearly exhibit a XANES features, with a small peak also corresponding to As(0). In spectra A and C this feature is reduced to a shoulder, indicating a lower As(0):As(V) ratio at the particular bore core volume sampled. As both arsenic oxidation states are found below the sample surface, the presence of As(V) in the spectra can be safely ruled out to be an artefact resulting from surface oxidation. Spectrum E and B, both with mainly As(V) are from the exact same pixel position also having high U Lα,β counts.

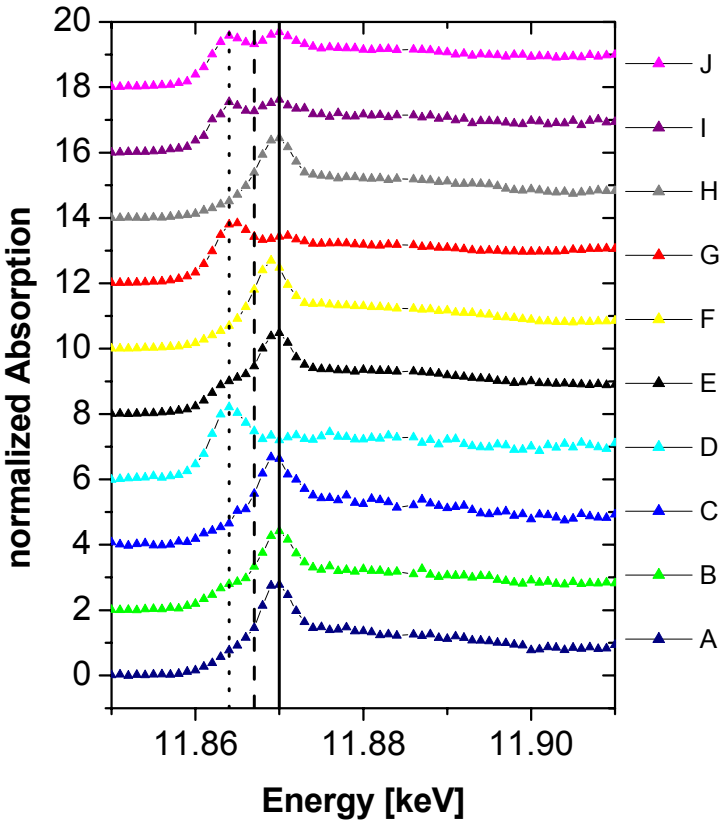

Fig. 5.19: As K μ-XANES recorded at various depths below the surface. Vertical lines denote energy positions for As(0) (· · ·), As(III) (- - -) and As(V) (——)

It is proposed that arsenic was involved in the uranium immobilisation process during diagenesis since As(V) is found in addition to As(0) even below the surface and is always associated with uranium. As hypothesis for the uranium mineral formation it is supposed that arsenopyrite reacted as reductant of dissolved U(VI) leading to precipitation of low soluble U(IV) mineral phases and thereby forming As(V).

5.2.3.3 Conclusions

The µ-XRF, µ-XANES and µ-EXAFS measurements clearly show U(IV) being the predominant oxidation state of uranium in the investigated hot spot in sample NA4. There is no spectral evidence for U(VI), neither from XANES nor from EXAFS. Uranium is observed to exist as a poorly crystalline phosphate (or sulfate), possibly ningyoite. Ningyoite is reported to be found as small crystals with dimensions around 5 µm, most commonly associated with iron sulphides /PAS 93/. For the uranium enrichment in sample NA4 a mechanism with involvement of arsenopyrite is postulated. Arsenopyrite, which covers pyrite nodules, might have formed from dissolved arsenic species, initially sorbed on pyrite surfaces. In a later stage As(0) reduced probably dissolved U(VI)-species to low soluble U(IV) which precipitated in form of phosphate minerals like ningyoite.

Further work is needed to test this hypothesis. Investigations to produce tomographic maps of Fe, As and U with much higher resolution can help to identify Fe-FeAs-A-boundaries on the pyrite nodule surface. Furthermore it is desirable to perform additional measurements on some other uranium-rich samples from the clay-lignite horizon in order to check if similar observations can support the hypothesis or if additionally other mechanisms play a role in uranium immobilisation. Such investigations are planned to be performed within the integrated European project FUNMIG.

5.2.4 U(IV)/U(VI) separation

The results from analysis of uranium bearing minerals described in the previous chapters showed only uranium in oxidation state IV. In order to check if additionally uranium in oxidation state VI occurs in the system, a wet chemical separation method for uranium (IV) and uranium (VI) was applied by *J. Suksi*. Two samples from drill core NA 6 from 35.87 m and 37.74 m depth were used.

The method consists of two main steps /ERV 96/. Firstly, uranium was extracted in a mixture of an anoxic 4.5 M HCl / 0.03 M HF-solution under Ar-atmosphere in ultrasonic bath. The extraction solution had been purged of oxygen by bubbling with Ar. Ar was also led into the reaction vessel during the extraction. The solution obtained from extraction was divided into two parts: one for total U analysis and the other for oxidation state analysis. In the second step both solutions were filtered and the solution

for the oxidation state analysis was loaded into an ion exchange chromatographic column where U(IV) and U(VI) were separated, due to sorption of U(VI) and elution of U(IV) complexed by fluoride.

During the extraction not all uranium was mobilised. Therefore, the residue was extracted first in boiling concentrated HNO_3 acid and then in aqua regia to dissolve the residual U. For all phases - uranium (IV), uranium (VI) and residual uranium - the $^{234}U/^{238}U$-ratio was determined. The results are summarised for sample NA6 37.74 m in Tab. 5.1.

The first major observation is, that the residual uranium phase, which is not extracted in the first step, amounts to 10-30 % of total uranium. Since a very strong solvent is used to get it into solution, this phase very likely consists of uranium (IV). This assumption is supported by the $^{234}U/^{238}U$-ratio in this phase, which is very similar to the ratio measured for uranium (IV).

Tab. 5.1: Amount of uranium and $^{234}U/^{238}U$-activity ratios in the different phases from uranium separation NA6 sample from 37.74 m. Total U concentration of the samples are in a range between 35 and 48 ppm.

sample	U(IV)		U(VI)		U(residue, IV)		U(IV) $_{total}$
	[%]	$^{234}U/^{238}U$	[%]	$^{234}U/^{238}U$	[%]	$^{234}U/^{238}U$	[%]
1	73.7	0.79	15.7	2.66	10.6	0.73	84.3
2	66.2	0.52	9.0	3.37	24.8	0.86	91.0
3	51.3	0.58	19.8	2.56	28.9	0.71	80.2

Secondly, the $^{234}U/^{238}U$-ratio in the U(IV) and U(VI) phase is significantly different. Both values clearly diverge from unity. In case of U(IV) the values are distinctly lower going down to 0.52, whereas the values for U(VI) are significantly above unity in the range of 2.5-3.4.

With the assumption that uranium in the residual phase is U(IV) the amount U(IV) in this sediment sample makes up about 80-91 % of total uranium. This, in general confirms the results from mineral analysis and µ-EXAFS/XANES measurements that major amount of uranium is in oxidation state IV.

The observed low $^{234}U/^{238}U$-ratios in the sediments are caused by a preferential dissolution of ^{234}U. A preferential dissolution of ^{234}U can only be caused by processes connected with radioactive decay. The radioactive decay of ^{238}U follows the scheme:

$$^{238}U \xrightarrow{\alpha} {}^{234}Th \xrightarrow{\beta^-} {}^{234}Pa \xrightarrow{\beta^-} {}^{234}U \xrightarrow{\alpha} {}^{230}Th$$

With the short lived daughter nuclides ^{234}Th (half life 24,1 d), and ^{234}Pa (half life 1,18 m). By α-decay of ^{238}U recoil energy of 72 keV is transferred to ^{234}Th resulting in the following effects:

- The α-recoil process leads to local lattice defects, breaking of chemical bonds and localisation of ^{234}U in inter-lattice positions. This is one reason for a preferred mobilisation of ^{234}U.
- The α-recoil can also lead to transfer of ^{234}Th from the immobile into the mobile phase. ^{234}Th decays within short time via ^{234}Pa into ^{234}U. The range of the recoiled atoms in the solid is about 0.01 – 0.1 μm. This direct transfer in the liquid phase is therefore limited to surface near mineral layers /OSM 83/. However, since SEM/EDS-analysis indicate that a large number of radionuclide bearing mineral grains in the clay/lignite-sand horizon have sizes of 1 μm and below, this process can significantly impact the ^{234}U/^{238}U-ratio in the U-bearing mineral phases at Ruprechtov site.
- As third process oxidation of U(IV) to U(VI) plays a role (e. g. /ADL 91/). Due to the recoil process radicals are formed along the trajectory of the recoiled atoms. By reaction with oxygen radicals daughter atoms are oxidized. As a consequence the more mobile ^{234}U(VI) is built by α-decay of ^{238}U(IV) and twice repeated β-decay of ^{234}Th (IV) and ^{234}Pa (V).

It is difficult to quantify these processes. However, they definitely cause ^{234}U/^{238}U-activity ratios below 1 in the solid phase. If such low ratios are observed, it is clear that no chemical leaching of the uranium phases occurs and has occurred over long time frames, since chemical leaching would have covered the effects of radioactive decay. Therefore the uranium(IV) phases in the clay/lignite-sand horizon occur to be stable as expected under the prevailing reducing conditions (see chapter 5.3.1).

Due to the experiments a small fraction of uranium is U(VI). However, it needs to be checked, whether it is really U(VI) or whether it is an effect of oxidation during the separation procedure. Currently this is investigated by experiments with further samples, in particular by studying the impact of high iron content in the samples. However, clear difference in ^{234}U/^{238}U-ratio indicates that this phase significantly differs from the U(IV) phases. It is also evident that the ^{234}U/^{238}U-ratio measured in the U(VI)-

fraction is similar to the ratio measured in the liquid phase in groundwater from the clay/lignite-sand horizon. This is an indication that the U(VI)-fraction is easily accessible and therefore in equilibrium with uranium groundwater. If this is the case, uranium in the groundwater is expected to be U(VI). This is discussed in chapter 5.3.2.

A correlation between the uranium mineral phases and the different fractions from separation is not reliably possible on the basis of only one measurement. It might be possible that the residual uranium fraction is represented by monazites and the other U-bearing detrital primary minerals, since they are expected to be rather resistant. The uranium amount in this fraction lies between 10 and 30 %, which is slightly above the amount estimated by mass balancing for the detrital uranium minerals (cf. chapter 5.2.2.6). It has to be mentioned that the uranium concentration and the U/Th ratio in this sample (37.74 m) is quite lower than typical contents of 100 to 300 ppm measured in the peak areas in the clay-lignite horizon. Therefore the fraction of detritic uranium minerals could be higher than 10 % in this distinct sample.

In order to confirm the results from these measurements more samples will be investigated in the frame of the EC project FUNMIG. These analyses will be accompanied by specific sequential extraction and sorption / desorption experiments using ^{233}U tracers on neighboured samples.

5.2.5 Bulk sample radiometric analyses

Besides measurement of $^{234}U/^{238}U$-ratios in separated fractions a number of bulk samples from clay/lignite-sand horizon and few from granite and kaolin have been analysed on activity ratios in the uranium decay chain, including analysis of ^{230}Th. Fig. 5.20 show the results for two samples from more near surface granite NA8 and two samples from underlying granite NA6. The uncertainties are relatively high due to lower uranium concentrations in the granite. The values of the samples scatter around unity, except the value for NA6 75.8 m, which shows a high $^{230}Th/^{238}U$-ratio of 1.34. This value with increased ^{230}Th activity compared to ^{238}U and ^{238}U would indicate an ongoing leaching process. However, it is only one value. Due to the scattering of the four values it general indicates that there is no U-enrichment (certainly not expected) and no strong uranium leaching going on today.

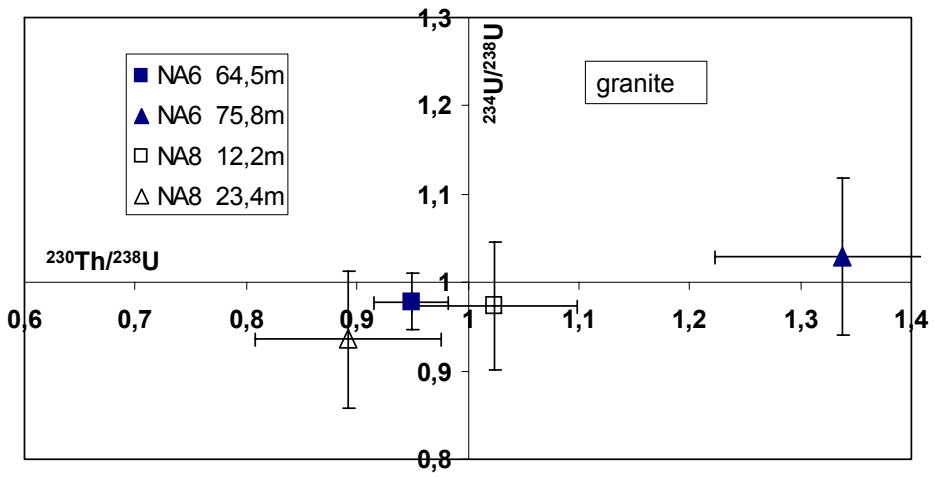

Fig. 5.20: Activity ratios of the uranium decay chain plotted in a Thiel diagram for samples from granite

The activity ratios in samples from new boreholes in the clay-lignite horizon are shown in Fig. 5.21. These results are in agreement with those from previous analyses in boreholes NA2, NA3, NA4 and NA5 /NOS 02/. They show $^{230}Th/^{238}U$-ratios below 1 and $^{234}U/^{238}U$-ratios around or slightly below 1. The $^{230}Th/^{238}U$-ratio lower 1 is a clear indication that some enrichment of uranium occurred during the last several 100 000 years and/or still occurs today.

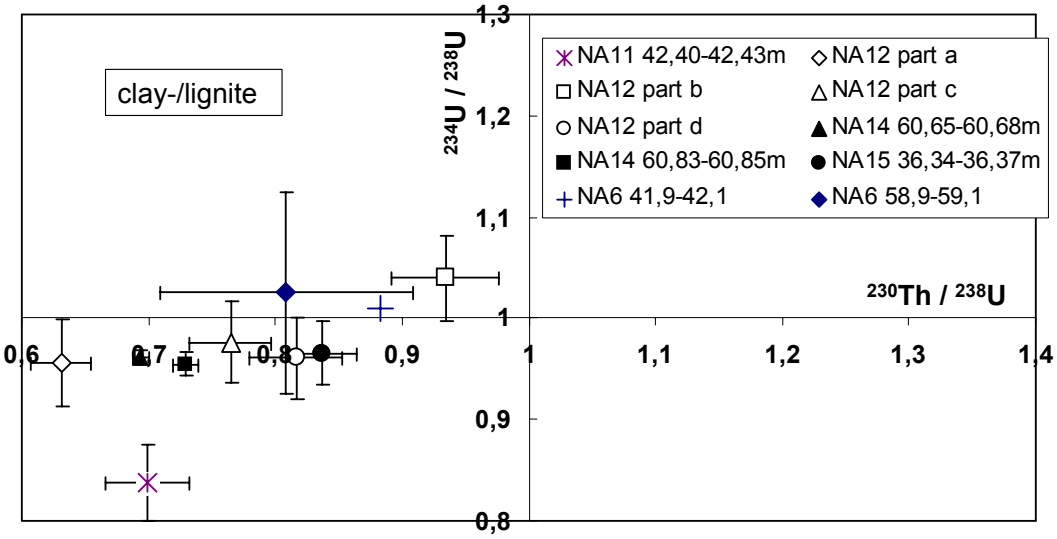

Fig. 5.21: Activity ratios of the uranium decay chain plotted in a Thiel diagram for samples from clay-lignite horizon

5.3 Description of groundwater

The wells including position of filtered horizons available for groundwater probing at the site were already described in chapter 4. A sketch with the denotation of the boreholes and supposed groundwater flow is shown again in Fig. 5.22. There are three wells in near-surface granites (NA8, NA10 and RP1) in the western part of the area, one well in underlying granite (NA14) in the northern part and all other wells are situated in the water bearing horizons in the clay/lignite-sand horizon. However, the filter horizons of wells RP2-RP5, HR4 and PR4 are several tens of metre and therefore might not represent pure water from clay/lignite-sand layer but a mixture with water infiltrating from other water bearing layers.

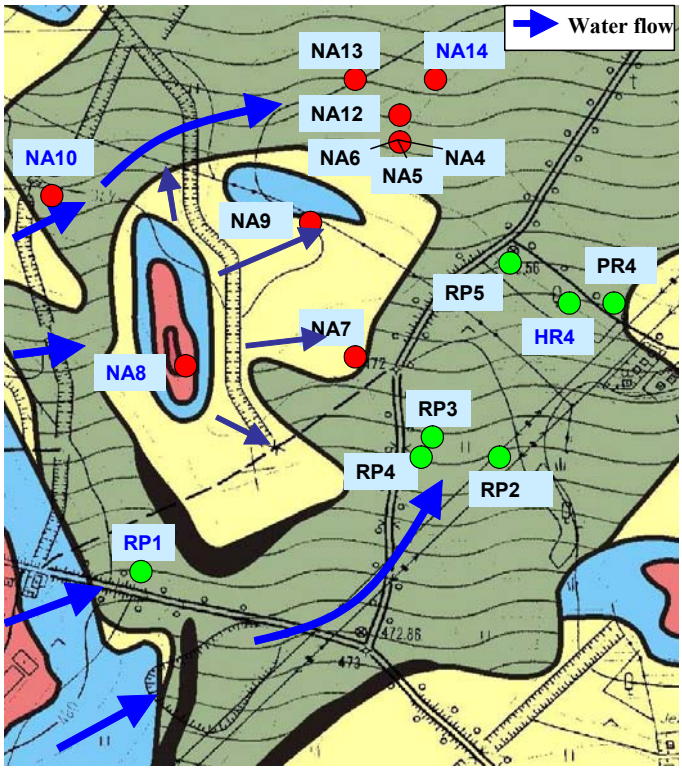

Fig. 5.22: Wells available for groundwater sampling at Ruprechtov site

5.3.1 Groundwater Geochemistry

The chemical composition of the waters including major and trace elements is listed in tables in Annex 6. A first categorisation of the groundwaters can be done by use of piper diagrams, which is shown in Fig. 5.23. Waters from nearly all boreholes of

clay/lignite-sand horizon except NA12 have a higher alkalinity than waters from NA8 and RP1, falling in the field of the Ca-HCO_3-type waters in a Piper diagram. In the case of the granite waters NA8 and RP1 and groundwater NA12 the alkalinity as well as the concentration of Ca is significantly lower than in previous boreholes and thus, this water is defined as Ca-SO_4-type water.

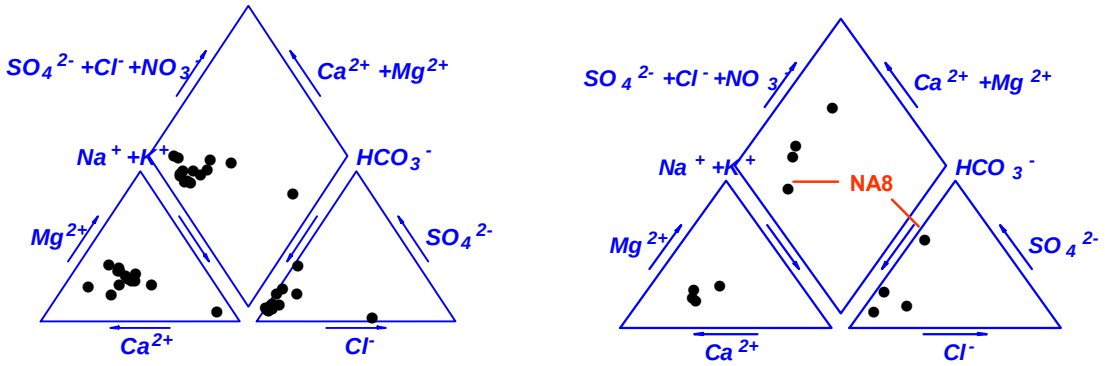

Fig. 5.23: Piper diagrams for groundwater from clay/lignite-sand horizon (left) and granite (right)

Geochemical calculations presented in the following have been performed with PHREEQC and NAGRA thermodynamic database /HUM 02/.

All samples seem to be in equilibrium with quartz. With regard to carbonate minerals (Fig. 5.24) it must be pointed out that water from most boreholes is in equilibrium with calcite except in the case of water from borehole RP1, which is slightly undersaturated and boreholes NA8 and NA12, which are clearly undersaturated with respect to this solid phase. This behaviour is similar for other carbonate minerals such as magnesite ($MgCO_3$), dolomite ($CaMg(CO_3)_2$) and siderite ($FeCO_3$). For NA8 and RP1 it is a clear consequence of the lithology where it has been sampled and of its shorter residence time, since both boreholes correspond to the granitic located wells. Accordingly the pH-values of these boreholes are slightly lower (6.2- 6.5) than the values obtained in water from the clay/lignite-sand horizon (7-8).

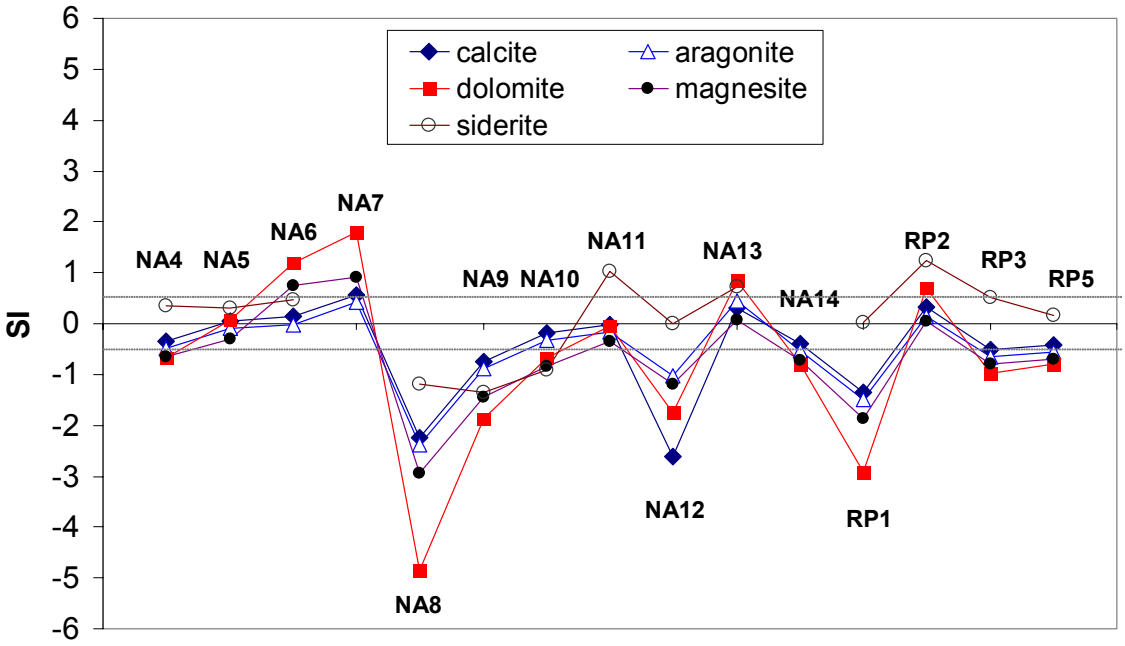

Fig. 5.24: Saturation indices of carbonate minerals

Sample NA8 shows equilibrium with hematite while the NA4, NA5 and NA6 samples are in equilibrium with microcrystalline $Fe(OH)_3(s)$ and NA7, RP1 and RP2 are in equilibrium with the more amorphous ferrihydrite solid phase. Gibbsite saturation index is close to zero in borehole NA8 and this solid phase is oversaturated in boreholes NA4 and NA6.

5.3.2 Uranium speciation

The uranium speciation is strongly dependent on the Eh/pH characteristic of the groundwater as shown for carbonate rich water in Fig. 5.25. Therefore, especially the determination of the Eh-value is of major importance. Eh- values have been measured by different techniques, i.e. on-site in a flow through cell isolated against atmosphere, in-situ with a multiparameter probe and for selected boreholes long-term in-situ measurements have been performed. It was shown that the on-site values are affected probably due to pumping effects

Data from borehole NA6 showed an on site Eh value of -110 mV and an in situ Eh value of -150 mV. In the long-term the redox-value in NA6 decreased within one and a half month down to -281 mV. It is not uncommon to find lower Eh values when measuring in-situ compared with values obtained on-site. This situation was reported from the Oklo natural analogue project, during which the Eh of some of the samples

was measured at depth and on surface, and important differences among the values obtained were found. As groundwater is pumped oxygen is being dissolved and, therefore, on-site Eh values are usually more oxidising than in-situ measurements.

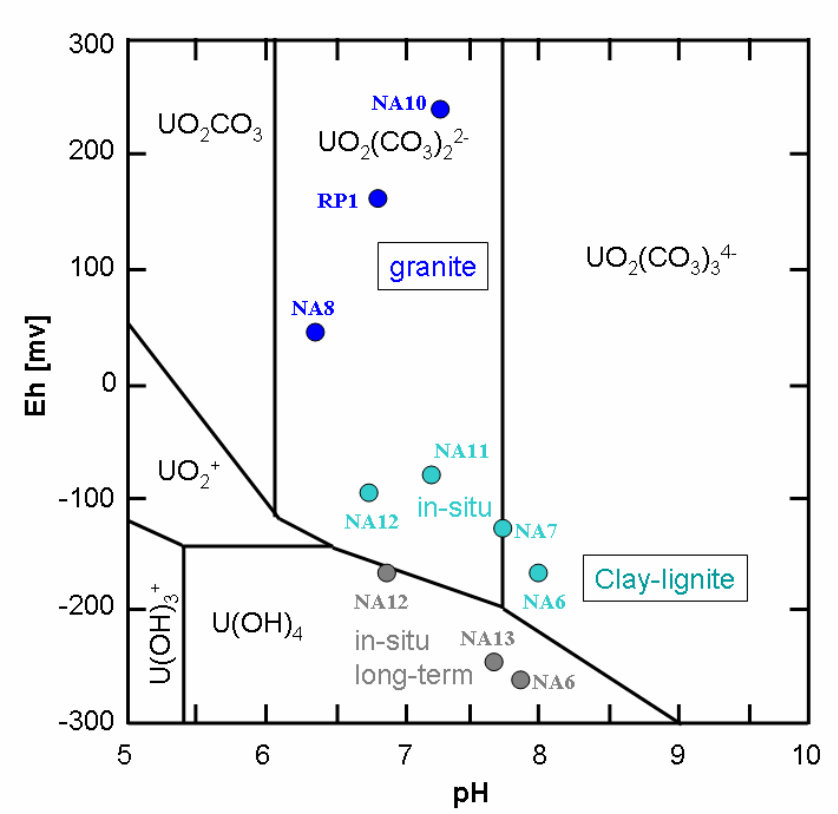

Fig. 5.25: Eh-pH diagram of the aqueous uranium species compared to values measured in different wells from Ruprechtov site

Also in other wells from the clay-lignite horizon we can recognize a strong long-term effect leading to an increase of pH and decrease of Eh-values in groundwater over a time frame of one / two months under undisturbed conditions of the system. If we consider the long-term in-situ values as most realistic ones, and ignore the other values uranium(IV) will be the predominant oxidation state in the aqueous phase of the waters from clay/lignite horizon. $UO(OH)_4$ represents the major uranium species, In the granite waters U(VI)-carbonate complexes, i.e. $UO_2(CO_3)_2^{2-}$ are the dominating species.

The surface near granite waters, which are assumed as infiltration water show lower pH values around 6.5 and positive Eh-values along with elevated uranium concentrations. However, pH-value in NA10 is already increased, which might be a local effect. Water from underlying granite (NA14, HR4) show lower Eh-values and only

slightly increased pH-values around 6.8 going along with lower uranium concentrations (cf. Fig. 5.27).

In tertiary sediments the Eh-value is generally low (especially in the northern area and RP2). The water from RP3 and RP5 might be influenced by inflow of surface near water due to the large filter horizon (cf. Chapter 4). The pH-values are increasing, but not uniform. In NA12 and NA4 the values are <7. Higher pH-values are found in NA6, NA13 and NA14.

The redox state of the system may *a priori* be controlled by different redox couples. From groundwater data, several pairs of ions susceptible to poise the redox state can be proposed: N(-III)/N(V), C(-IV)/C(IV) and Fe(II)/Fe(III). Saturation indexes suggest equilibrium with $Fe(OH)_3$(mic) in boreholes NA4, NA5 and NA6, with $Fe(OH)_3$(am) in boreholes NA7, RP1 and RP2 and with hematite in borehole NA8. Taking into account that these minerals could control the aqueous concentration of Fe(III) and that Fe(II)/Fe(III) have an important associated analytical uncertainty, it was preferred to study the redox pairs Fe(II)/$Fe(OH)_3$(mic) and Fe(II)/Hematite instead of Fe(II)/Fe(III). Additionally the redox pair Pyrite/S(VI) is considered given that the presence of pyrite in several samples from the clay/lignite horizon.

For boreholes NA4, NA6 and NA8, the theoretical Eh value is calculated responding to each one of the plausible redox pairs in the system (see Fig. 5.26).

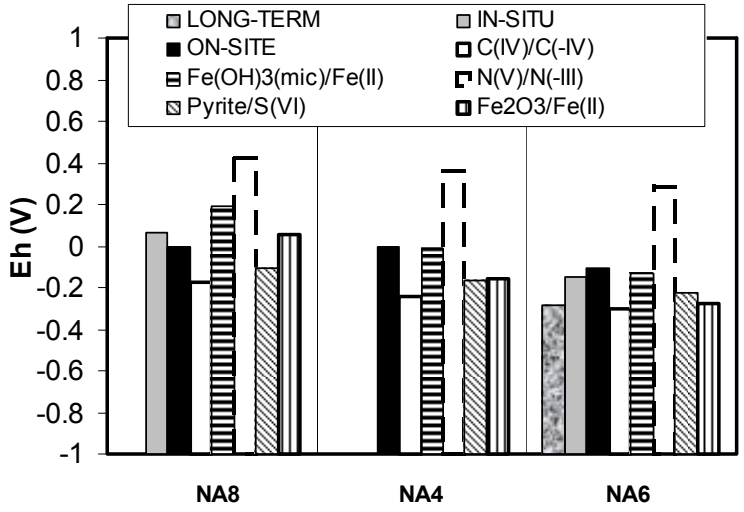

Fig. 5.26: Eh values (field and calculated assuming different redox equilibrium) for boreholes NA4, NA6 and NA8

Typical uranium concentrations at the site are presented in Fig. 5.27. The values show a clear tendency: values in the granite waters appear to be one order of magnitude higher than values in the clay/lignite-sand horizon. The more oxidising conditions in water

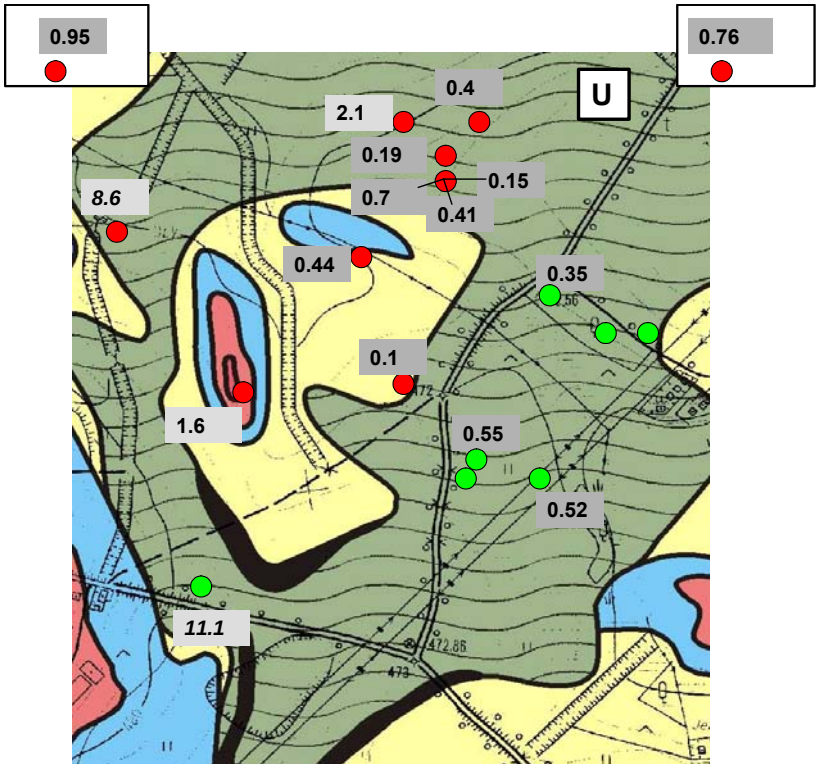

Fig. 5.27: Typical uranium concentrations in wells from Ruprechtov site

Geochemical calculations with PHREEQC show that uranium concentrations in the clay/lignite horizon are likely controlled by the mineral phase of amourphous uraninite, due to the reducing conditions. The granite waters are more oxidising and contain uranium (VI) dominated by the uranium carbonato species $UO2(CO_3)_2^{2-}$. The concentration is probably controlled by some very slow input from granite.

5.3.3 Activity ratios

In selected groundwaters and two pore-waters from core material of NA4 $^{234}U/^{238}U$-activity ratios have been determined. Measurements have been performed using 100 ml samples obtained by evaporation of 5 l water. These concentrated solutions have been analysed by alpha spectrometry and ICP-MS for concentration of ^{234}U and ^{238}U.

Pore water solutions were obtained by squeezing of core material from NA4. These solutions have been directly used and analysed by alpha spectrometry.

The results from all measurements are shown in Fig. 5.28. The two granite waters NA8 and RP1 show $^{234}U/^{238}U$-activity ratios around 1. Most of the waters from the clay/lignite horizon show $^{234}U/^{238}U$-activity ratios above 1 reaching values up to 4.

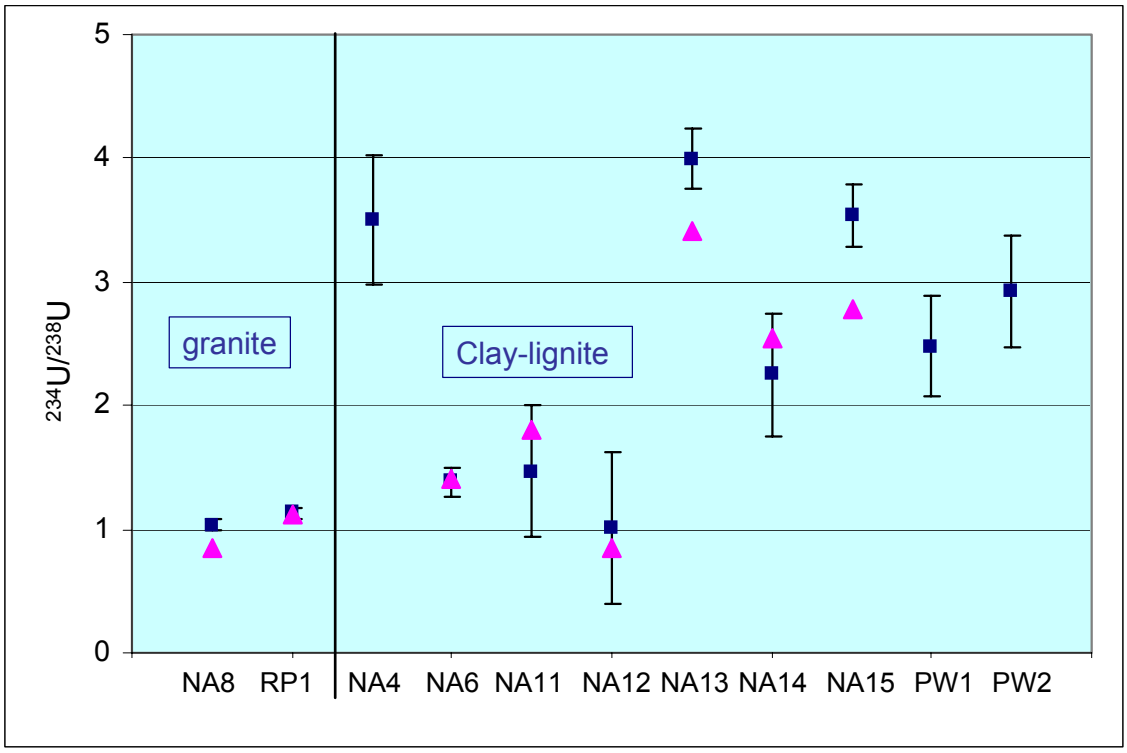

Fig. 5.28: $^{234}U/^{238}U$ activity ratios in groundwater and two pore-waters (PW1, PW2) measured by alpha-radiometry (blue) and ICP-MS (magenta)

The high $^{234}U/^{238}U$ activity ratios in groundwater from clay/lignite sand water agrees with very low $^{234}U/^{238}U$ activity ratios in uranium(IV) phases. The occurrence of the α–recoil and partial oxidation process by radioactive decay leads to a preferred dissolution of ^{234}U compared to ^{238}U from the sediment (cf. chapter 5.2.4). In systems with slow water flow, as in the clay/lignite-sand horizon, a $^{234}U/^{238}U$ activity ratio above unity will arise the mobile phase.

In the granite water system, probably very low dissolution of uranium from the granite still takes place and leads to uranium concentrations of about 10 ppb in solution. This slow chemical solution leads to $^{234}U/^{238}U$ ratios similar to one as they exist in the

granite (cf. Fig. 5.21). However, this leaching process is supposed to occur very slow, no disequilibria in granite bulk rock sample were detected.

5.3.4 Impact of colloids

In order to check the impact of colloids on the mobility of uranium groundwater from selected wells have been analysed for their colloid content.

Up to now colloids have been detected in five selected ground waters from Ruprechtov site with Laser induced Breakdown detection. The waters from three wells (RP2, NA6 and NA7) are in direct contact with the clay/lignite-sand horizon. As shown in Fig. 5.29, in all waters rather low colloid concentrations between 170 and 450 µg/l were observed, where most of the particles have sizes >450 nm. These particles might not be mobile at low ground water velocities.

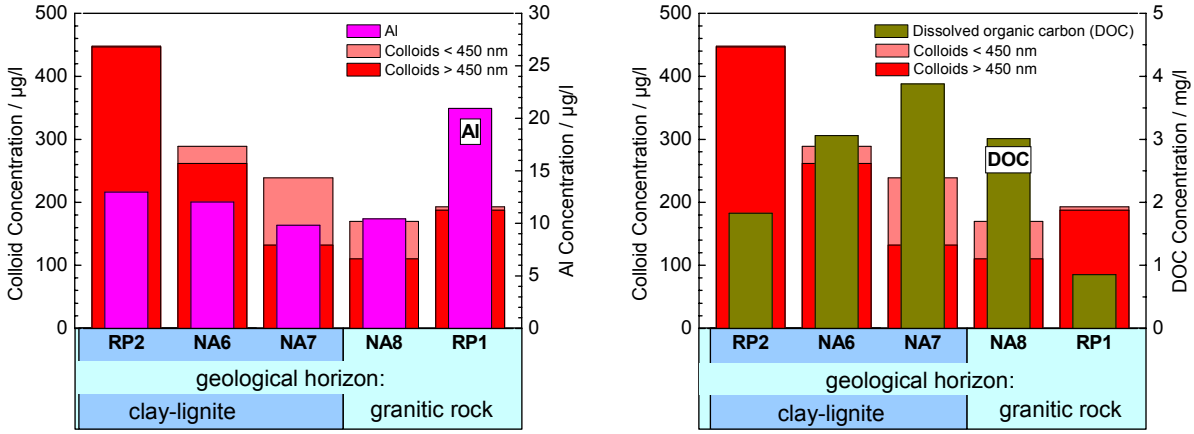

Fig. 5.29: Comparison of colloid concentration determined by LIBD (left) with the Al content of the groundwater (analysed by ICP-MS) and with the dissolved organic carbon concentration (right)

There is no clear correlation between colloid concentration and element concentrations. Furthermore a dependency of colloid concentrations on the geological situation of the sampling location is also not distinctive from these five samples.

DOC measurements revealed rather low concentrations with no correlation with LIBD data on colloid concentrations. Different to the Gorleben aquifer we are facing conditions at the Ruprechtov site, where significant content of lignite-like solids are

found in the sedimentary layers, however very low soluble organic species, and especially very low concentration of humic and fulvic acids if at all, in the ground water.

5.4 Sorption/Desorption experiments

In order to estimate the impact of sorption processes on the uranium immobilisation sorption experiments with selected samples from the clay/lignite-sand horizon were performed by A. Abdelouas et al. at Ecole de Mines, Nantes. Four samples, two from drill core NA6 from 35.60-35,70 m depth (denoted NA6-35) and from 37.82-37.92 m depth (denoted NA6-37) and two from drill core NA7 from 11,35-11.45 m depth (denoted NA7-11) and from 15,55-15.65 m depth (denoted NA7-15) were selected and stored under anoxic conditions before use. For practical purposes a synthetic groundwater with composition similar to that found at the studied site was used. All batch experiments were performed with H_2S to keep the conditions reducing.

Sorption experiments were performed with U(IV) under nitrogen atmosphere, since long-term in-situ Eh/pH-measurements gave rise for $U(OH)_4$ as major species in solution. Suspensions of sediments with groundwater and U-IV synthesized by electrochemical reduction of uranyl nitrate were used. Moreover, reduced ^{232}U was used as a tracer to study the stability of U-IV in groundwater within the time selected for equilibrium to be reached between sediments and groundwater (48h). The results showed that, for U-IV concentrations between 10^{-6} and 10^{-9} M, no significant precipitation of U-IV was observed unlike experiments with U-IV concentration of 10^{-5}M.

Synthetic groundwater representing the relevant features of Ruprechtov groundwater was used for all experiments. The composition is shown in Tab. 5.2. The sediments were equilibrated with groundwater until no more changes in groundwater composition occurred.

Tab. 5.2: Chemical composition of synthetic groundwater (mg/l)

Na	K	Mg	Ca	Cl^-	SO_4^{2-}	HCO_3^-	NO_3^-	pH	Eh (mV)
27.1	10.9	19.2	52.8	141	65	190	16	8.5	-252

The results of the sorption experiments show that uranium is strongly sorbed on all sediments. In Fig. 5.30 the sorbed amount of U is plotted against the U-concentration in solution for different mass/volume ratios. There is no impact of the m/v-ratio for U-

sorption on samples from NA6. For NA7 the values scatter but without clear about a factor of 5 but do not show a clear tendency, since experiments with m/v-ratio of 0.1 g/l show highest sorption values, whereas experiments with m/v-ratio of 1 g/l show lowest sorption values, and experiments with m/v-ratio of 10 g/l are in-between.

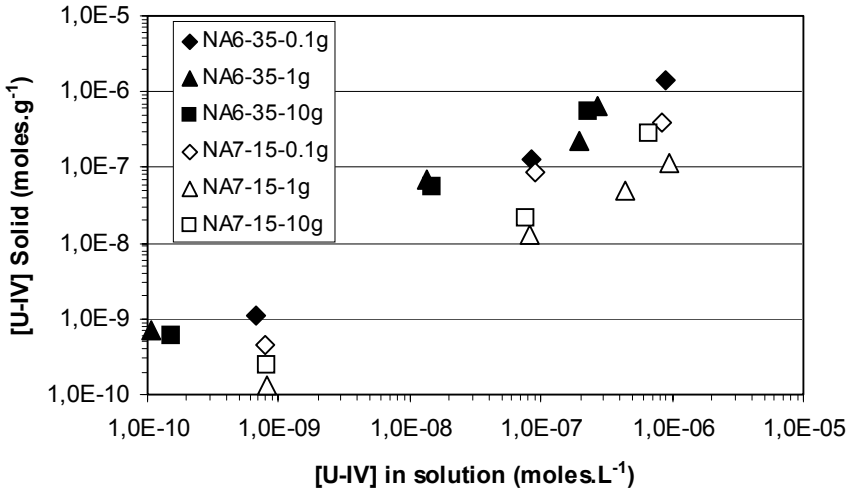

Fig. 5.30: Sorbed amount of uranium versus uranium in solution for different sediments and different mass/solid ratios (0.1 g/l, 1 g/l and 10 g/l).

The pH dependence is shown in Fig. 5.31. A plateau is obtained in a range from pH 6 to 7.2. The sorption decreases with increasing pH values above 7.2 and is a factor of 150 lower than for maximum sorption.

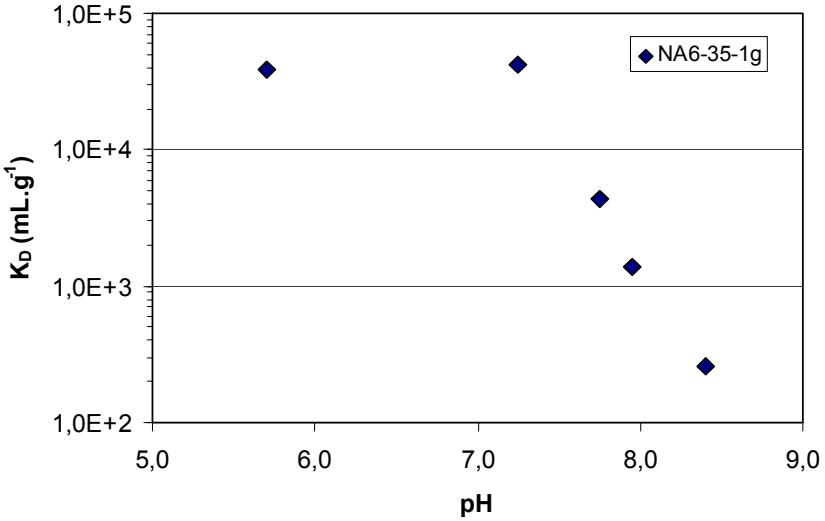

Fig. 5.31: pH dependence of U(IV) sorption on sediment NA6-35 m measured at m/v ratio of 1 g/l

An additional cycle of sorption experiments was performed with injection of a certain amount of humic acids in order to estimate the impact of humic colloids on the sorption behaviour of uranium(IV). Humic substances were extracted from the sample with the highest amount of organic carbon (NA6-35m) with 0.1 M NaOH and purified with DAX-8 and XAD-4 resins. 10 grams of sediments are mixed with 100 mL of 0.5 M NaOH under N_2 atmosphere. The bottle is wrapped in aluminium foil and shacked for 3 days. Following centrifugation the supernatant is separated from the sediment and filtered through 0.45 µm silver filters. The solution pH (pH 12) is decreased to pH 2 by addition of 6 M HCl for chromatography. The humic acids are then separated in column packed with DAX-8 resin. Prior to separation the resin was washed in a soxhlet apparatus with organic solvents methanol and ether. Then, the resin is packed in the column and rinsed again with ethanol. Before introduction of solution for humic acids separation the resin is rinsed with HCl until getting pH 2. The humic substances retained in the column (brown color) are then eluted with 0.1 M NaOH. The eluted solution is then introduced in a column packed with a cationic resin to purify the solution from sodium and replace it with hydrogen. At this step the humic substances are ready to use in sorption experiments.

The results are shown for sorption on the two sediments NA6-35 and NA7-15 in Fig. 5.32. The Kd-values measured without addition of humic acid are approx. $4 \cdot 10^3$ ml/g for NA6-35 and $1.2 \cdot 10^3$ ml/g for NA7-15. For sorption on NA6-35 the Kd-value do not change in the sample with an amount of humic acids of 5 mg C/l. For experiments with higher humic acid concentrations the Kd-value decreases, due to competing sorption of uranium on humic colloids. For experiments with highest humic acid concentration the sorption value for NA6-35 is reduced by a factor of 150.

The impact of humic acids on uranium sorption on sediment NA7-15 is less, showing a decrerase of sorption values not until concentration of humic acid is increased above 20 mg/l. For experiments with highest humic acid concentration the sorption value for NA7-15 is reduced by a factor of approx. 10 compared to experiments without addition of humic acid.

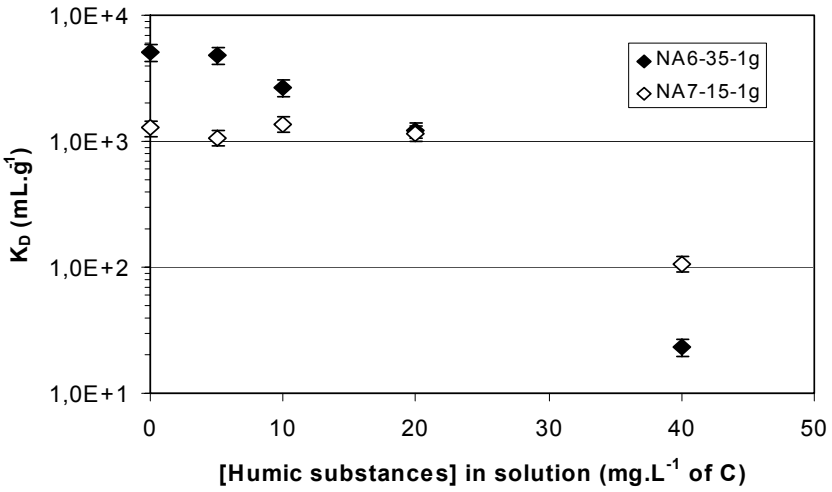

Fig. 5.32: Impact of humic substances on uranium(IV) sorption on sediments from Ruprechtov site

Further work is planned in FUNMIG project, i.e. the application of surface complexation models to describe the sorption behaviour with and without presence of humic substances.

5.4.1 Role of Microbes

Two samples from drill core NA4 were selected for analysis of indigenous microorganisms and additional experiments to identify the potential role of microorganisms in the clay/lignite-sand horizon at Ruprechtov site. The samples stem from 33.16-33.28 m (denoted NA4-33) and 36.24-36.36 m depth (denoted NA4-36). Material from these samples has already been used in previous sorption/desorption experiments performed with U(VI) (see /NOS 02/).

5.4.1.1 Information about the experiments

For microbial growth common aerobic and anaerobic culture media on solid plates or in liquid forms were used. The sulfur oxidizing bacteria were isolated using Stakey medium fungi on DRBC medium (DIFCO) and the iron chelating microorganisms were detected on CAS medium /SCH 87/. In particular, the role of sulfate-reducing bacteria (SRB), which are known to reduce uranium /LOV 92, ABD 00/, was studied. The presence of sulfide in groundwater at 13°C is likely due to activity of SRB. Hence, to stimulate the growth of SRB, batch experiments with NA4-33 and NA4-36 sediments

and groundwater with a v/m-ratio of 0.1 g/ml (50g : 500 ml) were amended with 5 mM lactate, 4 mM sulfate and 20 mg/l phosphate. In this experiment the system was spiked with UO_2^{2+} to reach final uranium concentrations of about 600 µg/l. The organic matter content of the two samples was highly different. The measured values are 8.5 % for NA4-33 and 15.7 % for NA4-36. The inorganic carbon concentrations are similar in the two samples, close to 3.7 %. The composition of the groundwater used and the change in composition after equilibration with both sediment samples is shown in Tab. 5.3. The composition of the sediments and the sorption experiments with uranium (VI) are described in detail in /NOS 02/.

Tab. 5.3: Chemical composition, pH and Eh of groundwater before and after equilibration with NA4-33 and NA4-36 sediments. Concentrations are in mg/l except those of U, Fe and Mn, which are in µg/l. I.C. inorganic carbon; O.C. organic carbon.

	Groundwater	**NA4-33/groundwater**	**NA4-36/groundwater**
	0 day	**31 days**	**31 days**
pH	7.40	7.98	7.31
Eh (mV)	n.m.	308	321
U	0.57	1.8	0.81
Fe	667.3	79.7	31.1
Mn	66.7	23.9	153.6
Si	3.5	2.0	1.3
Ca	32.3	55.0	34.7
Mg	24.4	43.8	23.6
Na	22.0	37.6	20.6
K	13.3	39.5	17.4
I.C.	52.5	57.7	24.8
O.C.	0.7	1.7	3.3
SO_4	20.5	35.7	203

5.4.1.2 Results

The leaching of sediments with sterile solution under aerobic sterile conditions led to a qualitative detection of some microorganisms. The results show the presence of fungi, like *Penicillium* sp. and *Geotrichum* sp., various species of bacteria like sulfur oxidizing bacteria, and various $Gram^+$ and $Gram^-$ facultative bacteria. Some of the isolated fungi

were able to produce iron-chelating molecules. Hence, the presence of many aerobic microorganisms in deep anoxic samples is confirmed and is expected to consume the excess of oxygen in flowing groundwater. By this way microorganisms could play a stabilizing effect on radionuclides deep storage as proposed by /BRO 99/.

The results from batches with stimulated SRB are given in Fig. 5.33 through Fig. 5.36. The evolution of experimental pH is given in Fig. 5.33 and is similar to that observed in the sorption/desorption experiments (see /NOS 02/. The pH in NA4-36 sediment dropped down to 4.5, while the final pH in sediment NA4-33 was 7.4. Fig. 5.33 shows a drastic drop in Eh in sediment NA4-33 due to microbial activity, which is inhibited in the acidic conditions prevailing in sediment NA4-36.

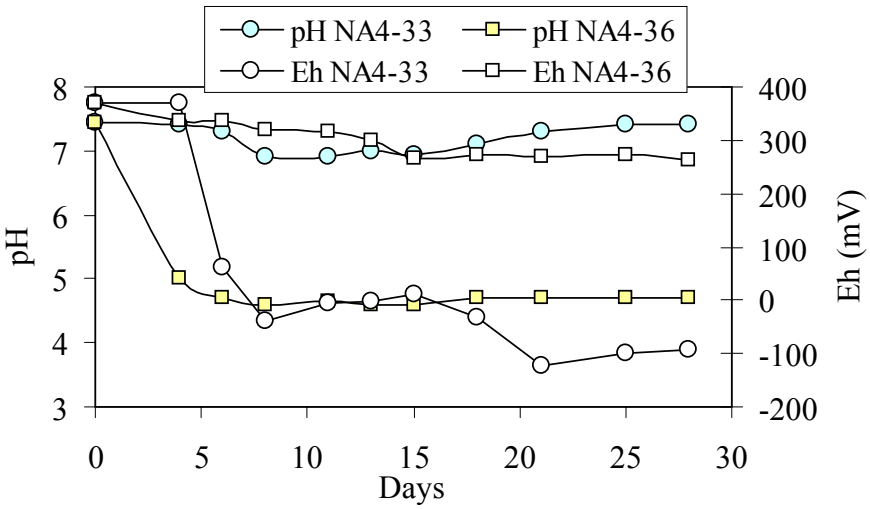

Fig. 5.33: Evolution of pH and Eh in two sediment/GW-systems. Growth of SRB was stimulated by addition of sulfate, lactate and phosphate at 22°C

Fig. 5.34 shows a strong correlation between the drastic drop in Eh and sulfate and the increase in inorganic carbon concentration. This confirms that the strong drop in Eh was provoked by the activity of indigenous SRB. The initial decrease in Eh from 370 mV to about 0 mV between 0 and 15 days is likely due to consumption of oxygen by facultative bacteria and fungi. During this step the uranium concentration and the Eh decreased significantly. The uranium concentration continued to drop during sulfate reduction with final concentrations in the order of 10^{-8} M despite the increase of carbonate concentration originating from lactate oxidation. Calculations based on experimental data including U, pH, Eh and inorganic carbon concentrations show that uraninite is expected to precipitate.

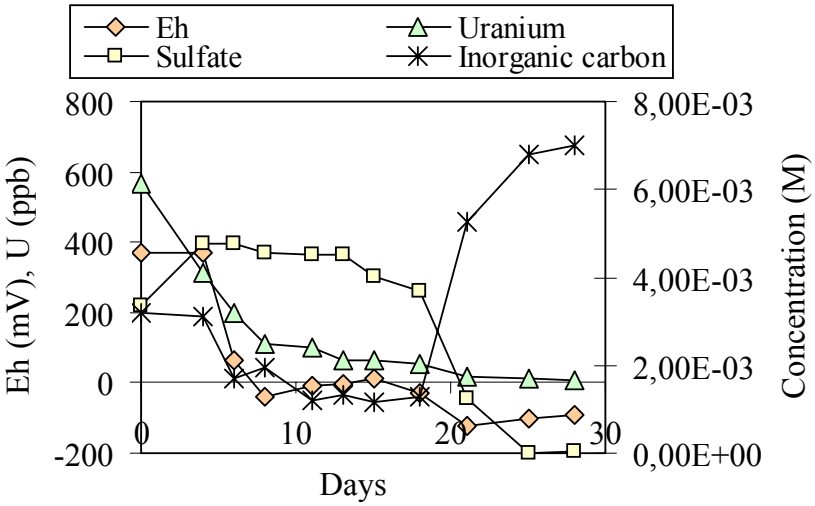

Fig. 5.34: Evolution of Eh, sulfate, uranium and inorganic carbon concentrations in sediment/GW-system NA4-33. Growth of SRB was stimulated by addition of sulfate, lactate and phosphate at 22°C

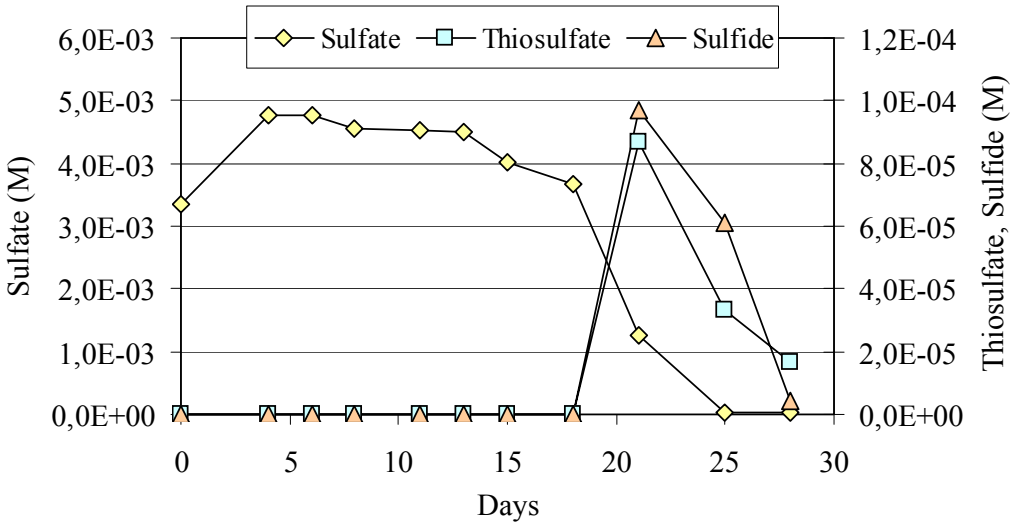

Fig. 5.35: Evolution of sulfate, thiosulfate and sulfide concentrations in sediment/GW-system NA4-33. Growth of SRB was stimulated by addition of sulfate, lactate and phosphate at 22°C.

During sulfate reduction by-products such as thiosulfate (S_2O_3) formed and ultimately were reduced into sulfide (Fig. 5.35). This metabolic utilization of sulfate by SRB is well described by /POS 84/. The drop of sulfide concentration is due to precipitation of sparingly soluble iron sulfide.

Finally, it can be seen in Fig. 5.36 that SRB are more efficient in U-removal via reduction of U(VI) to U(IV) compared to U(VI) sorption (described in /NOS 02/). Nevertheless, all these processes are expected to contribute to the stability of uranium in the Ruprechtov site, which is indicated by the low U-concentrations in groundwater.

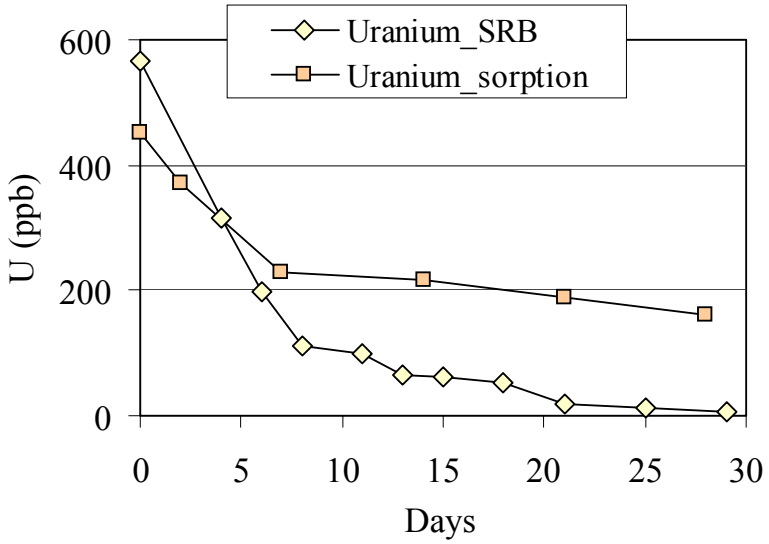

Fig. 5.36: Evolution of uranium concentration during sorption (Uranium_sorption) and sulfate reduction (Uranium_SRB) in sediment/GW-system NA4-33

Microorganisms are expected to play an important role in uranium stability in the field. Hence, aerobic and facultative micro-organisms present in the sediments rich in organic matter can be considered as a sink for oxygen entering with flowing groundwater. In addition, the indigenous sulfate-reducing bacteria were able to grow and maintain reducing conditions leading to U(VI) reduction, precipitation and stabilization.

A variety of microorganisms from the sediments were able to grow on synthetic growth media. Fungi, facultative $Gram^+$ and $Gram^-$ bacteria, sulfur oxidizing bacteria, and sulfate-reducing bacteria (SRB) were identified. During the growth of SRB the uranium concentration dropped significantly with final values in the order of 10^{-8} M.

The present work shows that the reducing conditions in the field, keeping the uranium concentration between 10^{-8} and 10^{-9} M could play a role in control of the U-concentration. Laboratory data suggest that the indigenous SRB help maintaining the redox potential low enough for U(VI) reduction to U(IV) and precipitation. They very likely played an important role during formation of sulphide minerals. Fig. 5.37 shows

an image of framboidal pyrite, which is a strong indication for the mineral growth by activity of microbes. Even if they are not directly involved in reduction of uranium, this formation of sulfide minerals seem to be very important for uranium immobilization at Ruprechtov site, since one major uranium enrichment process is assumed by reaction with arsenopyrite layers on pyrite nodules (cf Chapter 5.2.3.2).

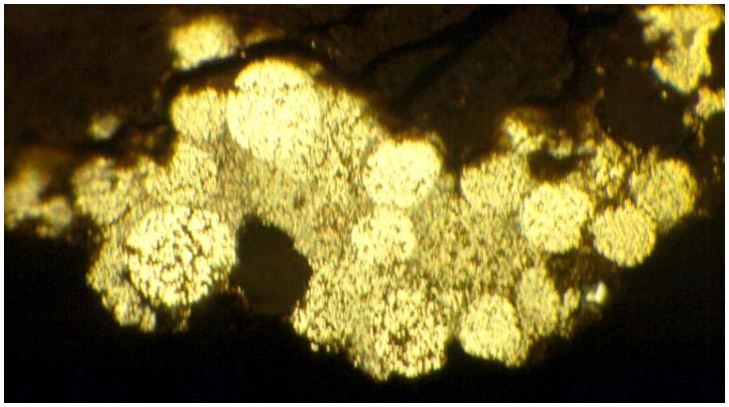

Fig. 5.37: Framboidal pyrite in clay/lignite sand horizon from drill core RP3.

In addition, indigenous aerobic and facultative micro-organisms contribute to the stability of precipitated U(IV) by consumption of oxygen in infiltrating groundwater.

6 Scenario for uranium migration and enrichment

Based on related information available, a scenario for uranium enrichment and transport at Ruprechtov site has been developed. During the detailed site characterization it turned out that geological development and structure of the site are much more complex than could be estimated initially based on profiles and descriptions from nearby Hajek site. Therefore, today still uncertainties concerning the past geological processes including uranium transport and immobilization exist. In On the basis of all information the most probable scenario for uranium mobilization and transport has been evolved and is described in the following. First of all, as a basis for scenario description the geological units and their ages are shortly summarized (see also Chapter 3).

6.1 Description of geological units at Ruprechtov site

The main geological units at Ruprechtov site are (from bottom to top)

- Granite, underlying and surrounding the tertiary basin
- Kaolin layer
- Clay/lignite-sand layer
- Pyroclastic sediments (overlying),

which are shown in Fig. 6.1. Clay lignite seams are developed irregularly and do not provide a continuous horizon, but can be found preferentially near the base of Tertiary sediments. Uranium enrichment mainly occurs within and slightly below the clay/lignite seams.

The Granites date back to Carboniferous. By analyses of accessory minerals the age of the so-called Erzgebirgsgranit (Krušné hory mts. granite, in older publications also cited as granite, Karlovy Vary-type) has been determined to 317±16 My /RHE 96/. Due to its high U-content and U/Th-ratio compared to other rocks in the surrounding (Gebirgsgranit, Neovulkanit) the Erzgebirgsgranit has been identified as the source for uranium, i.e. the weathering and alteration processes of the granite have charged significantly for uranium release in different ways.

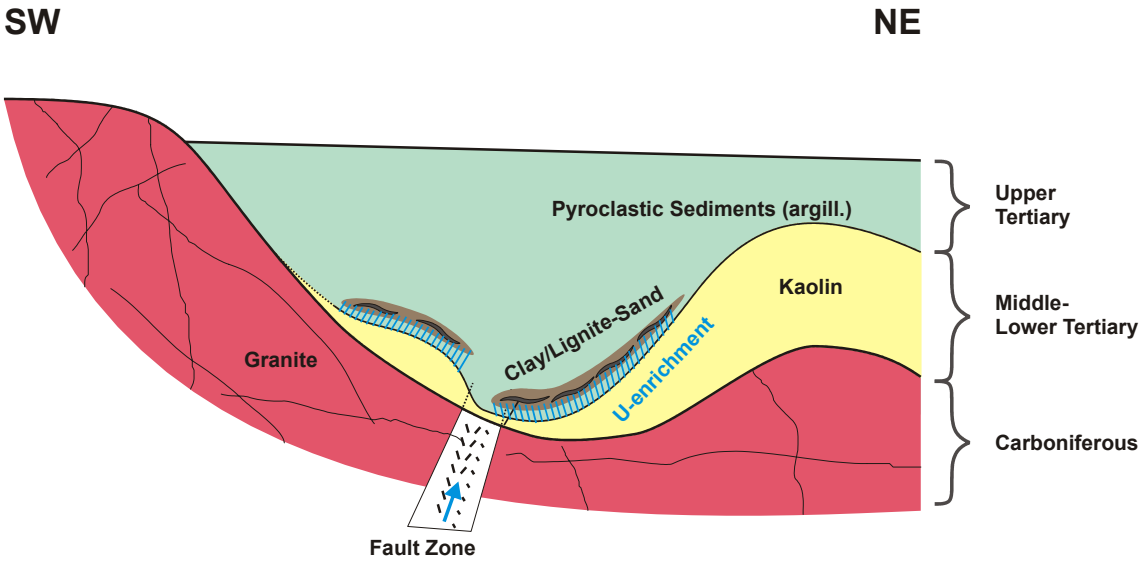

Fig. 6.1: Schematic geological cross section with main geological units of the investigation area

A crucial question for the description of the scenarios is, during which time period major uranium release from the granite occurred. In a first step a rough estimation can be done by a mass balance using information from nearby Erzgebirgsgranit occurrences in Germany, which were characterized in detail by /FOE 99/.

The initial uranium content in the Erzgebirgsgranit from Upper Carboniferous can be estimated from the contents observed in undisturbed granite samples. Such samples have been obtained from very deep boreholes in the German areas Eibenstock, Pobershau and Satzung and yielded an average content of 30.1 ± 5 ppm U /FOE 99/.

In contrast, analyses of uranium in Erzgebirgsgranit from Ruprechtov site resulted in average values of about 7.8 ± 5 ppm U. Therefore app. 75 % of the total initial uranium content of the Erzgebirgsgranit has already been lost at Ruprechtov site. By comparing the concentrations of uranium in different accessory minerals in undisturbed granite samples it becomes clear that major uranium release occurred from uraninite, which contributed up to 88 % of the total uranium content in undisturbed granite and is reduced to a quota of 60 % in the today's granite samples. The distribution of the total uranium content on different accessory minerals is shown in Tab. 6.1.

Tab. 6.1: Distribution of total uranium content in granite samples on different accessory minerals

	Undisturbed Samples (Upper Carboniferous)	Altered Samples (Today)
U concentration	30 ppm	7.8 ppm
uraninite	88 %	60 %
xenotime	3 %	13 %
monazite	3 %	12 %
zircon	2 %	9 %
apatite	<1 %	1 %
others	5 %	5 %

A significant loss of uranium most likely occurred already during Permian /FOE 05/. This loss can be documented in samples from outcropping Erzgebirgsgranit samples. Surface near Eibenstock granites show average uranium contents of 19.1 ± 5.6 ppm, which are attributed to the loss during Permian, i.e. about 35 %. However, the Erzgebirgsgranit samples from Ruprechtov show distinctly lower uranium contents. This indicates an additional uranium loss of again app. 35 % from Erzgebirgsgranit at Ruprechtov site down to 7.8 ± 5 ppm U. It is supposed that this second release took place during Tertiary. It gives evidence for an additional process at Ruprechtov site compared to other parts of the Erzgebirge due to regional pronounced tectonic and volcanic activities. This rough estimation leads to the following uranium balance of Erzgebirgsgranit from Ruprechtov site:

- 35 % of initial uranium was mobilized Pre Tertiary (probably during Permian)
- 35 % of initial uranium was mobilized during Tertiary, and
- 30 % of initial uranium is still contained in granite at Ruprechtov site

6.2 Discussion of the kaolin formation

One central aspect in the geological development of the site is the process of kaolinization, i.e. the alteration of granite to kaolin. This process determines strongly the whole scenario for uranium mobilization, transport and immobilization. Therefore it will be discussed before the whole scenario is described.

There are two completely different possibilities denoted as hypothesis A and hypothesis B in the following. Essential base of hypothesis A is that kaolinization has

occurred after covering of granite by volcanic ashes. In hypothesis B kaolinization proceeded on surface exposed granite before covering with volcanic ashes.

It was tried to determine the age of the kaolin by K/Ar-dating of illites present in the kaolin. Unfortunately, the illite content is too low to permit a dating. Therefore, there is no direct evidence for the kaolin alteration before or after deposition with volcanic ash.

6.2.1 Hypothesis A

The process of kaolin weathering corresponding to hypothesis A is schematically shown in Fig. 6.2. The originally landscape characterized by granitic hills and valleys is covered by volcanic ashes after main volcanic activity during Lower Oligocene to Miocene. Certainly, a large amount of mantle CO_2 was released by the volcanic activity and trapped probably together with oxygen in the deposited volcanic ashes. It is very likely that additionally CO_2 poured out from fault zones. These processes caused CO_2-rich oxidising waters, which were able to strongly alter the underlying granite.

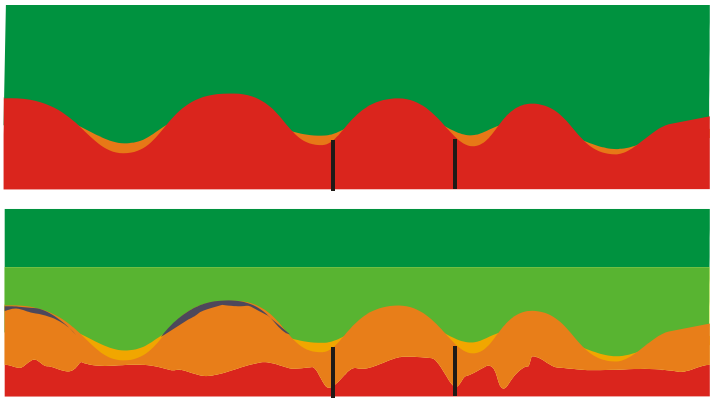

Fig. 6.2: Hypothesis A: Alteration of granite (red) to kaolin (orange) after deposition of volcanic ash (green).

Alteration of the underlying granite mainly occurred by reaction of feldspars with CO_2 rich water and formation of kaolinite according to the generalized formula:

$$2\ KAlSi_3O_8 + 2\ CO_2 + 7\ H_2O \quad = \quad Al_2Si_2O_5(OH)_4 + 4\ SiO_2 \cdot n\ H_2O + 2\ K^+ + 2\ HCO_3^-$$

Bythis reaction kaolin is formed in the place of granites and is widespead with variable thickness. The special characteristic of hypothesis A is, that stronger kaolinisation occurs in elevated granites leading to higher thickness of kaolin in these areas.

6.2.2 Hypothesis B

The process of kaolin weathering due to hypothesis B is schematically shown in Fig. 6.3. The original landscape again is characterized by granitic hills and valleys. Surface weathering of granite leading to formation of kaolin occurs in a warm and humid climate. In such a climate it is very likely that in valley areas at least temporarily small ponds or swamps occur. These water bearing units represent good conditions for granite weathering and formation of kaolin. The elevated areas of the granite are not exposed to standing water bodies and therefore should be less weathered. Even if there is weathering in the elevated areas, it is very likely that the weathered material is mechanically transported down the slopes into the valley areas. Therefore highest kaolin thickness is expected to be found in valleys of the former granitic surface and lowest kaolin thickness in former granitic hill areas.

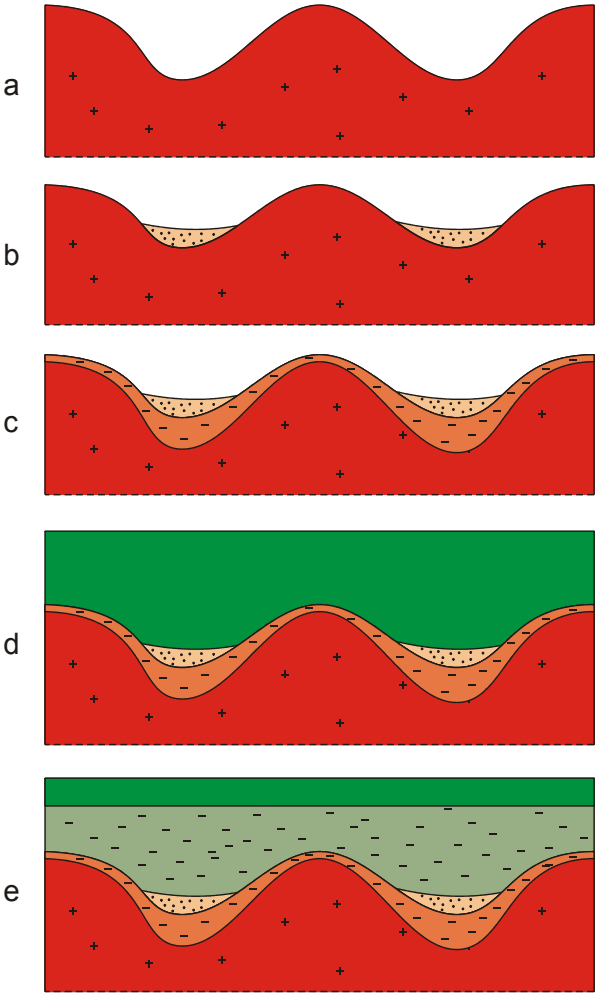

Fig. 6.3: Hypothesis B: Weathering of surface exposed granite to kaolin in warm humid climate. As a result kaolin thickness in valleys of former granite surface should be significantly greater than on hills

To give an imagination of an undulated grantic surface as it is implied in both schemas of scenario A and scenario B, the following arial photograph (Fig. 6.4) shows an outcropping granitic massif which today represents such an inselberg landscape formed by erosion.

Fig. 6.4: Granitic massif dissected by erosion. The inselberg landscape is characterised by bell- /helmet-behaved elevations which are typical for a wet-dry (seasonally humid) climate (taken from /KRO 67/)

6.2.3 Conclusions

One main difference between hypothesis A and hypothesis B is the resulting distribution of kaolin thickness at the site. For kaolin formation due to hypothesis A the thickness of kaolin is expected to be highest in elevated areas and lowest in valley areas of the former granitic surface. For hypothesis B the results would be vice versa, i.e. kaolin thickness should be increased in valley areas and low or nearly not existing in elevated zones. The kaolin thickness observed today at Ruprechtov is shown in relation to the depth of the interface pyroclastic sediments / kaolin in Fig. 6.5. From this map a clear correlation between both parameters is visible: High kaolin thickness is found in elevated areas of interface pyroclastic sediments / kaolin and low kaolin thickness in depressions. This gives strong indication for kaolin alteration process having occurred corresponding to hypothesis A, namely by alteration of a system covered with volcanic ash.

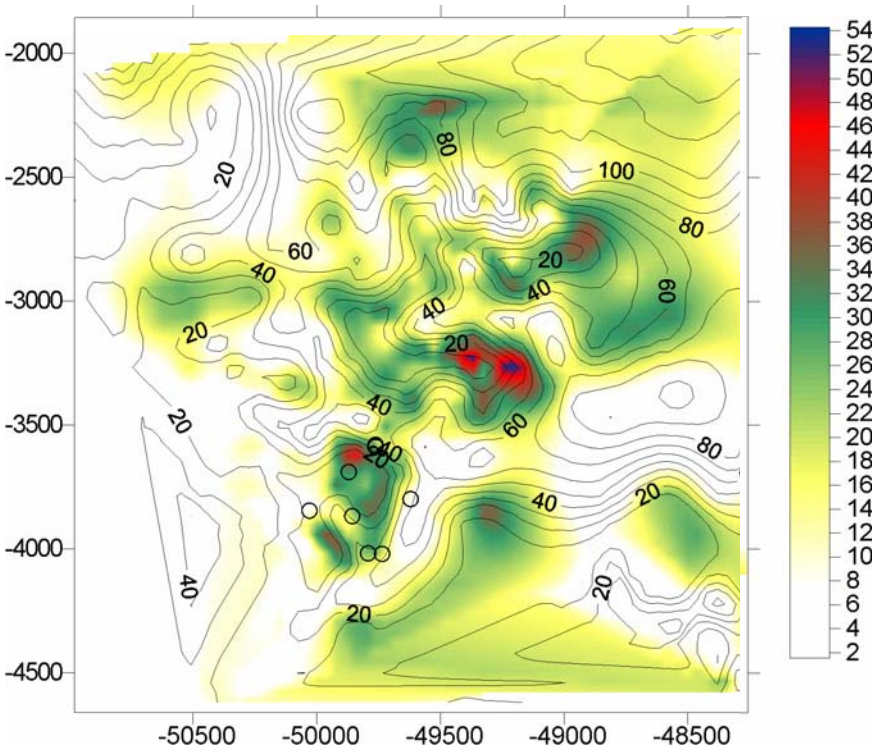

Fig. 6.5: Correlation of depth of interface pyroclastic sediments / kaolin (isolines [m below ground]) with kaolin thickness (colour-scale [m])

A second argument for the main kaolinization process after covering with volcanic ash is the strong slope of kaolin hills, which would not have been stable without a stabilizing cover. Further indication for uranium release after cover with volcanic ash is significantly less altered surface granite at Velky rybnik compared to underlying granite in NA6. In Fig. 6.6 the height and angles of slopes from the kaolin observed at the site are illustrated. It can be seen that slopes of 25 to 35° occur. By comparison with the slope stability for unconsolidated sediments, shown in Fig. 6.7, it is evident, that a slope of 30° is the limit for a sediment pile of 8.3 m. The height of kaolin “hills” at Ruprechtov site is up to app. 80 m which could not be stable at an open surface with slopes indicated above. This result again is an additional indication for hypthesis A.

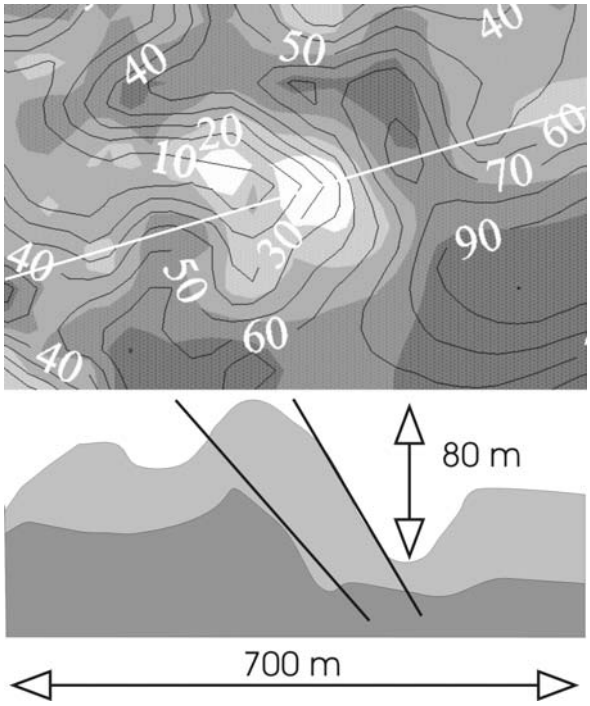

Fig. 6.6: Profile across a kaolin "hill" at Ruprechtov with marked slope for unconsolidated sediments stability of 25° – 35° (values following /KET 55/). The height of the slope is more than 5 times greater than that for the stability limit of the 30° slope for a height of 13 m (cf. Fig. 6.7).

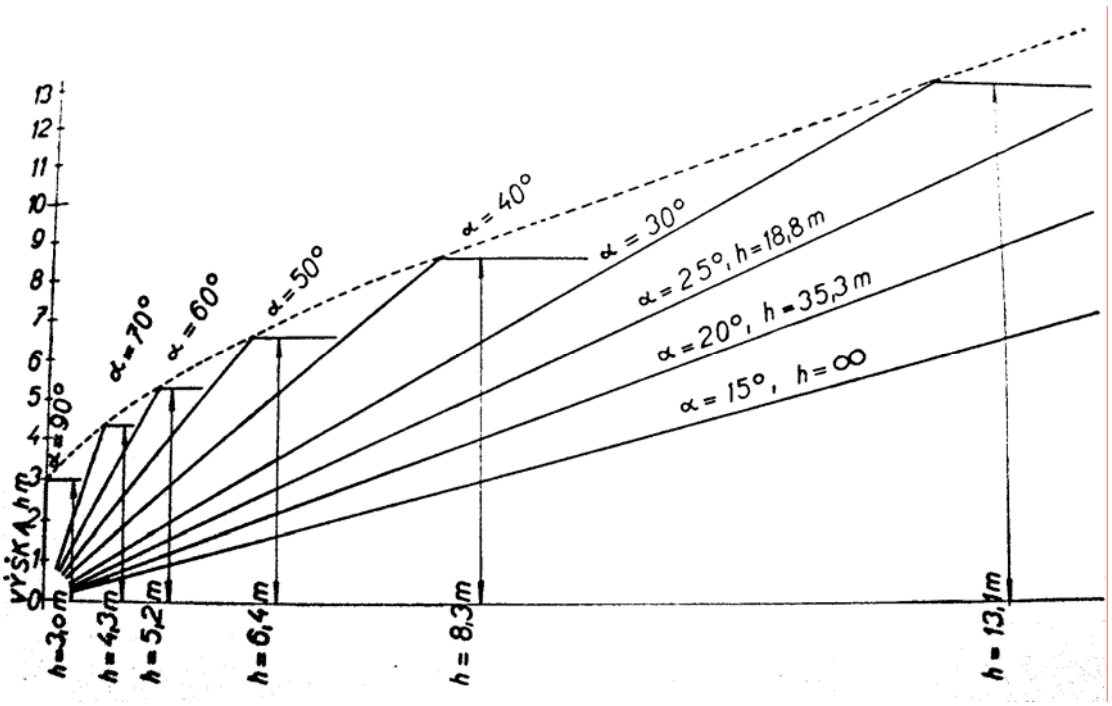

Fig. 6.7: Slope stability of unconsolidated sediments for different heights. Cohesion of the clay solid = 0,10 kg/cm^2 and angle of the inner friction phi = 15° /KET 55/

In conclusion we assume, that kaolin alteration occurred after deposition of greater thickness of volcanic ashes. This is the basis for the scenario described in the following.

6.3 Scenario for uranium mobilization and enrichment at Ruprechtov

The scenario for uranium mobilization and enrichment can be divided into five main periods. The description is simplified in a way that only the periods with main effects and processes with reference to the current project are displayed. These five periods are directly correlated to the periods of geological development of the Hroznetin part of Sokolv basin at Ruprechtov which have already been described in Chapter 3.6. The five periods are schematically shown in Fig. 6.8.

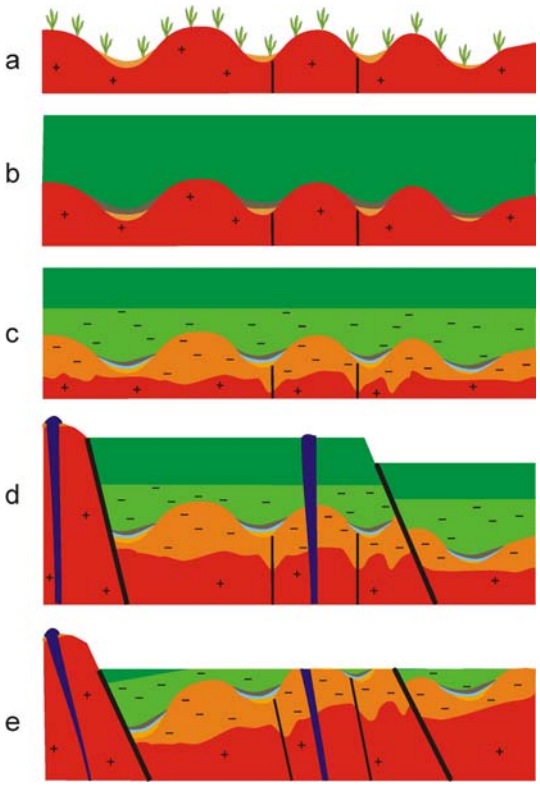

1. Input of detritic material
   (Before Lower Oligocene, > 30 My)

2. Main volcanic activity
   (Lower Oligocene to Miocene 30 – 16 My)

3. Alteration of granite and tuff
   (Lower Oligocene to Miocene 30 – 16 My)

4. Basaltic Intrusion
   (Miocene 15 – 16 My)

5. Partial erosion of pyroclastic sediments
   (Pliocene, Quaternary, < 5 My)

Fig. 6.8: Schematic presentation of the development of the Hroznetin part of Sokolov basin at Ruprechtov site in single stages. See text for explanation.

Before the Tertiary a significant fraction of uranium was already mobilized from the granites as described above. Uranium, which was released during this period has been

transported away and is no more present in the area. Therefore it is not considered in the further description.

1. Period with input of detritic material (before Lower Oligocene, >30 My)

During this period the “old” Pre-Tertiary landscape is dominated by a hill and valley structure of outcropping granite. Few older faults are present. The landscape is covered by vegetation - grass and trees and swamps dominate the valleys.

Input of coarse clastic material including detritic uranium minerals occurred by slope and/or short distance alluvial transport forming small sandy layers with limited thickness (at Ruprechtov in the range of app. 1 m) referred to the Staré Sedlo formation. As described in Chapters 5.3.1 and 5.3.2 the properties of the U-bearing mineral phases monazite-(Ce), xenotime-(Y) and zircon in the U-enriched clay-lignite layer are indistinguishable from the respective mineral phases in granite. SEM images of the mineral phases in the clay/lignite-sand layer clearly show mechanical disturbance of the monazite minerals, indicating their detrital input. However, the amount of uranium in these detritic phases amounts to max. 10 % of the whole uranium content in the clay/lignite-sand layer.

2. Period with main volcanic activity (Lower Oligocene to Miocene, 30 – 16 My)

This period was characterized by strong volcanic and also tectonic activity. The granites were covered by volcanic ashes. The former estimated thickness of the ash fall at Ruprechtov is approximately 200 m. Temperature of the groundwater and sediments was slightly elevated at that time. The volcanic ashes destroyed the plants leading to areas of organic matter at the bottom of the volcanic ash horizon. This organic matter is probably more accumulated in valley areas.

3. Period with main granite/tuff alteration (Lower Oligocene to Miocene, 30 – 16 My)

Certainly, a large amount of mantle CO_2 was released by the volcanic activity and trapped, probably together with oxygen, in the volcanic ashes deposited. It is very likely that additionally CO_2 poured out from fault zones. These processes caused CO_2-rich waters, which were able to strongly alter the volcanic material and the underlying granite, which is schematically shown in Fig. 6.9.

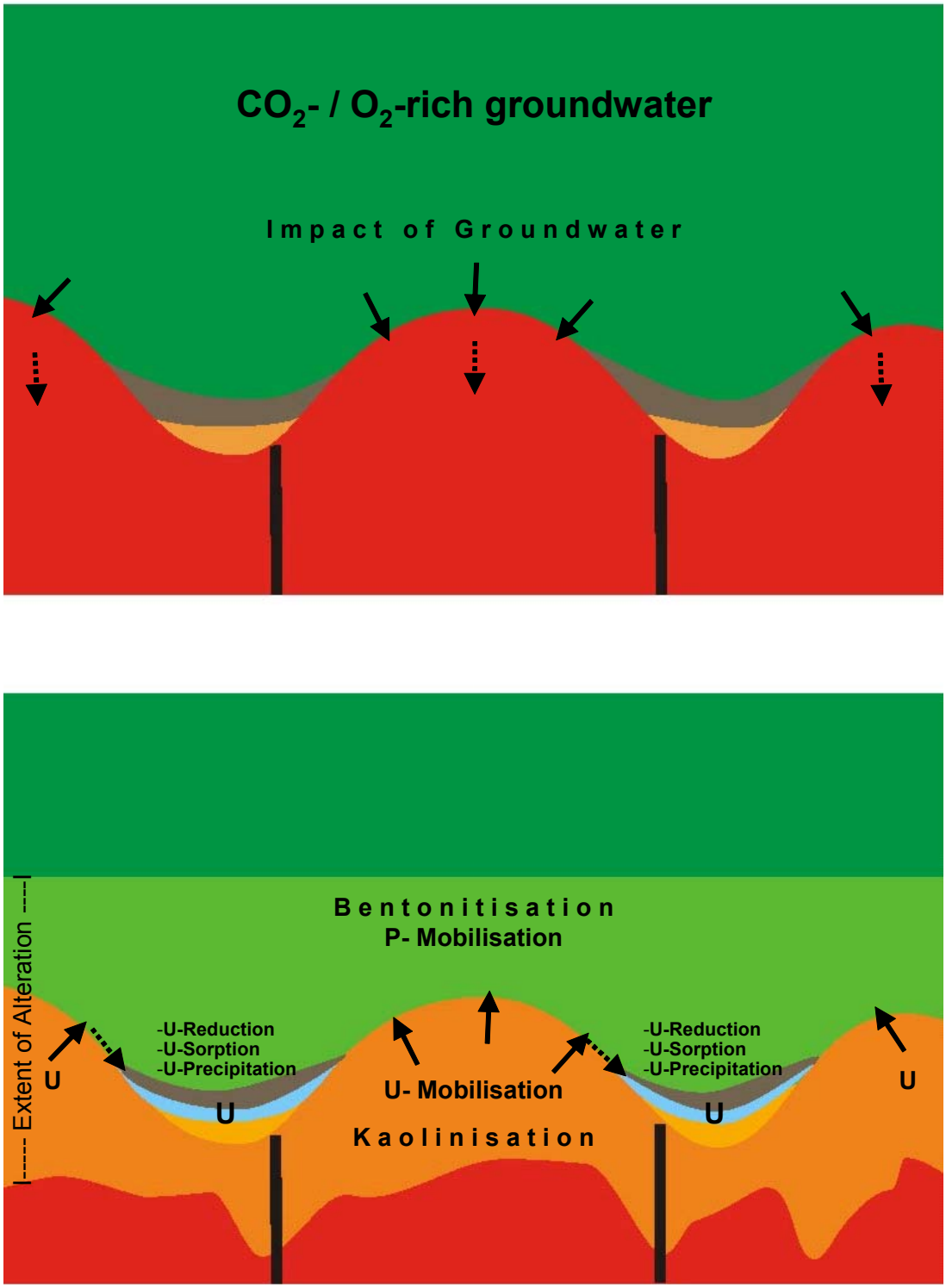

Fig. 6.9: Schematic presentation of alteration processes in granite and tuffitic material

By argillization (mainly bentonitization) of the tuffites, clay minerals like smectite were formed. In the course of this alteration processes also iron was released. Presence of carbonate rich waters represented also favourable conditions for siderite formation. The high δ^{13}C-values between 2 and 3 measured on siderite samples from RP5 and

NA6 could only be reached, if DIC was isotopically heavy at that time. This can be explained by a significant input of mantle CO_2 during the period of siderite formation. Mantle CO_2 shows ^{13}C-values of -2.7 in the Eger rift area /WEI 99/.

Alteration of the underlying granite mainly occurred by reaction of feldspars with CO_2 rich water and formation of kaolinite as described in Chapter 6.2.1. Due to this reaction kaolin is formed in the place of granites which led to slope and valley deposits. Stronger kaolinization occurs in the elevated areas leading to higher thickness of the kaolin in these areas.

The CO_2 rich water could also initiate uranium release from accessory minerals by formation of soluble UO_2 carbonate complexes. Transport through kaolin layers occurred mainly by diffusion. At the interface of kaolin and pyroclastic sediments higher hydraulic conductivity could have enhanced advective transport of uranium released from the kaolin. Uranium accumulation then occurred in lignite rich sediments by sorption on newly formed lignites and also by reduction to Uranium(IV) and precipitation of phosporous bearing minerals.

Further arguments for granite alteration during this period are the occurrence of high concentrations of titanium and phosphate in the uppermost kaolin as shown in Fig. 6.10. Phosphate and titanium originate from volcanic material. This assumption is also supported by the concentration profile of Th, which shows no elevated concentration in kaolin demonstrating that elevated titanium and phosphate concentrations are not an enrichment effect from granite alteration. The alteration of the tuffites enhanced the mobilization of Ti and P that is introduced into the top of originating kaolin. Transport of TiO_2 and PO_4 was favoured by rather porous material at that time. High phosphate concentrations also favoured formation of U / phosphate bearing minerals like ningyoite.

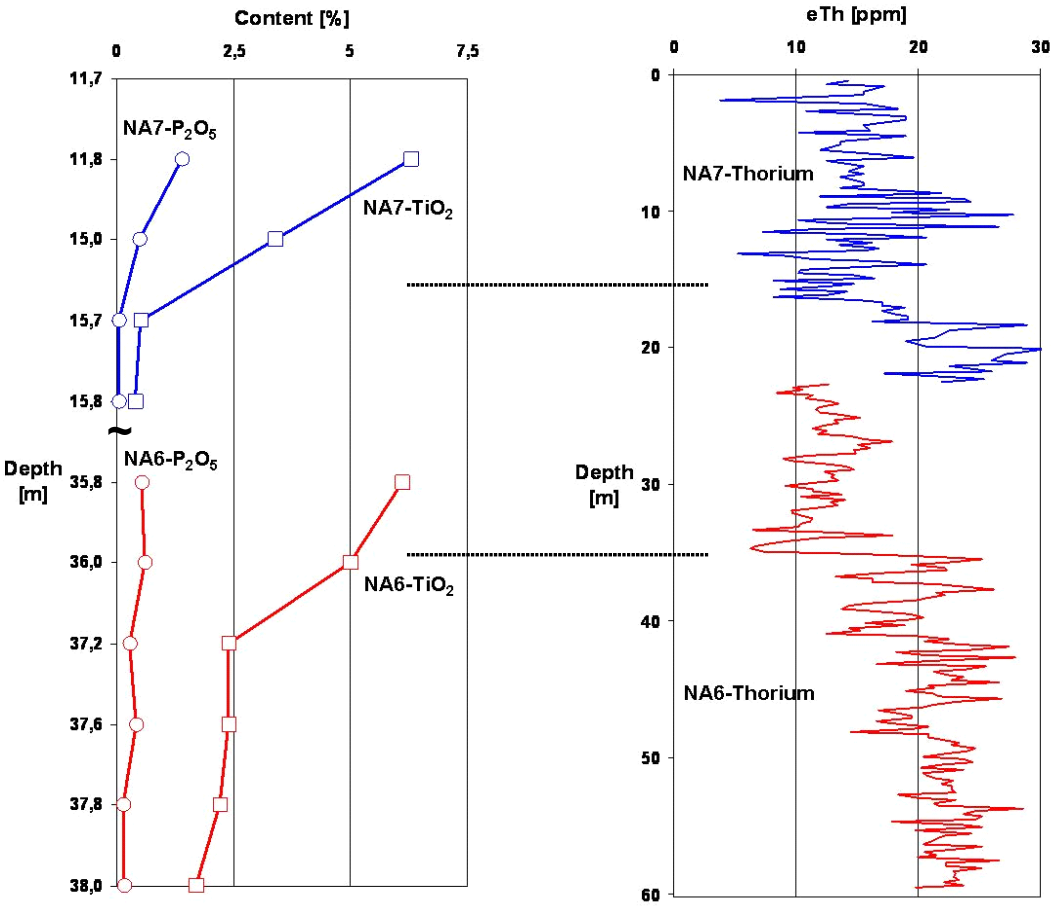

Fig. 6.10: Concentration profiles of TiO_2 and P_2O_5 (left diagram) at the transition from Tertiary sediments to underlying kaolin in boreholes NA6 (red) and NA7 (blue) [left figure not to scale ! - please note the different position of depth]. In addition (right diagram) continuous distribution of Th-concentrations in NA6 and NA7; the abrupt drops of mean Th concentrations at about 16 m (NA7), resp. 36 m (NA6) [dotted lines] mark the transition between both formations

In Fig. 6.11 uranium concentrations are plotted compared to the depth of the base of pyroclastic sediments (as a measure for the morphology of the kaolin). This figure demonstrates that high uranium concentrations are not found on top of kaolin hills but are located oftenly at the slope or in kaolin valleys itself.

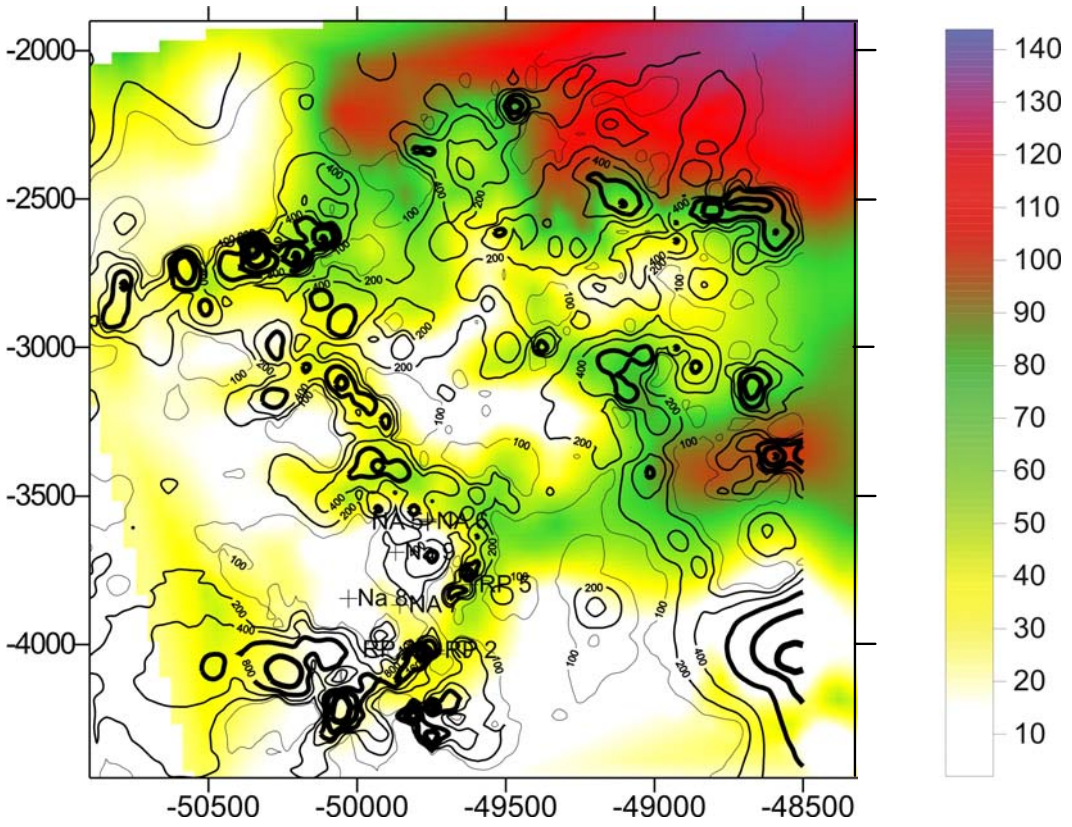

Fig. 6.11: Elevated uranium concentrations [ppm] in the clay/lignite-sand horizon denoted by isolines correlated to the depth of the base of pyroclastic sediments [m] marked by colour.

This result again supports the assumed scenario where most of today's uranium content in clay/lignite-sand horizon is released from surounding kaolin during main phase of granite alteration

4. Period with Basaltic Intrusion (Miocene, 16 - 15 My)

Basaltic intrusions into the tertiary sediments occurred at approximately 16 - 15 My ago. This assumption has been proofed by dating of three basalt samples from two different dykes at nearby Hajek site. The samples have been analysed by the K/Ar method (using milled grain fraction between 200-315 µm for analyses). The results are shown in Tab. 6.2.

The analysed age of all three samples is in range between 16 and 15 My. This tectonic period is marked by the intrusions of basalts in the form of dykes and laccolithes, which lead to contact metamorphism of the already bentonitised and kaolinised surrounding

rocks. In addition elevated temperatures could have also caused convective flow conditions boosting uranium release from deeper parts of granite.

Tab. 6.2: Results from K/Ar-dating of three basalt samples from Hajek site

sample	amount [mg]	K [%]	$^{40}Ar_{rad}$ [nl/g]	$^{40}Ar_{rad}$ [%]	**age [Ma]**
basalt 1a	256.8	0.95	0.585 ± 0.016	34	**15.78 ± 0.47**
basalt 1b	282.4	0.99	0.612 ± 0.017	32	**15.84 ± 0.45**
basalt 2	214.3	1.38	0.824 ± 0.014	57	**15.30 ± 0.30**

Today the major amount of uranium is accumulated in the clay/lignite-sand layer due to sorption processes and/or reduction from uranium (VI) to uranium (IV), prevailed in places of thin and/or absent underlying kaolin.

This result again agrees with the fact that uranium accumulations are not equally distributed, as already discussed, but show distribution pattern which is related to the morphology of kaolin layer (cf. Fig. 6.11) as well as kaolin thickness. There is a strong inverse correlation between kaolin thickness and uranium content in the sediment, which is shown in Fig. 6.12. The different colours denote different kaolin thickness. The isolines show the uranium concentrations in the sediment in the uranium enriched layer. Highest uranium concentrations are found in areas with lowest kaolin thickness (in most areas below 10 m). The combination of this figure with the detailled geological map (cf. chapter 3) in Fig. 6.13 clearly underlines this fact. In the S of investigation area the already described hill & valley structure of granit and kaolin has, in total, a higher elevation than in the N and comes close to the surface. It is clearly demonstrated that the uranium enrichment is predominantly in areas of low kaolin thickness. Orientation and structure of these areas might already indicate the effect of fault zones (see below).

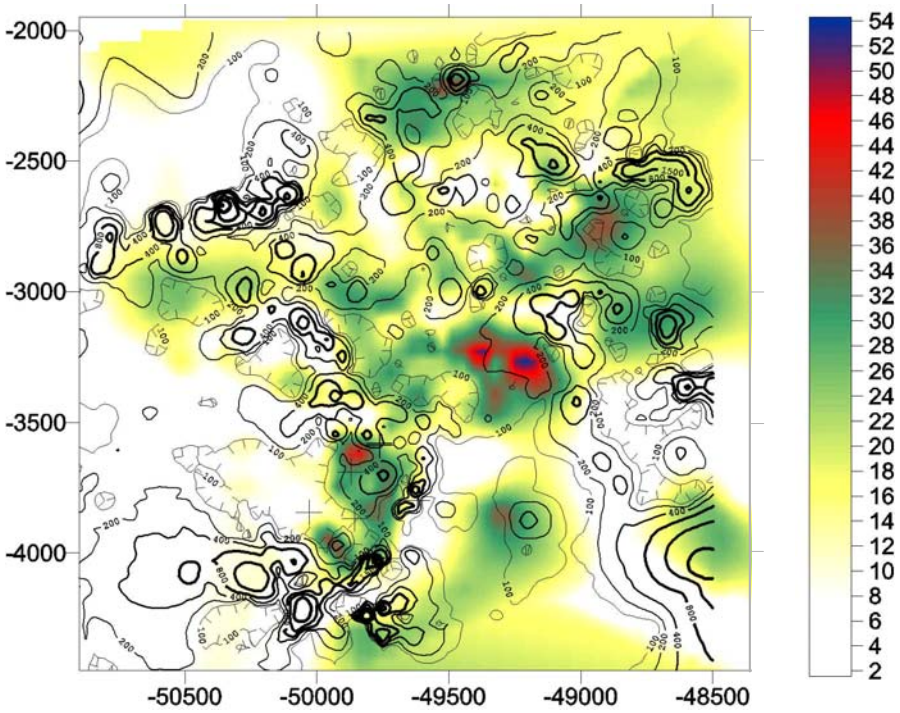

Fig. 6.12: Elevated uranium concentrations in the enriched layer denoted by isolines [ppm] correlated to kaolin thickness [m] marked by colour

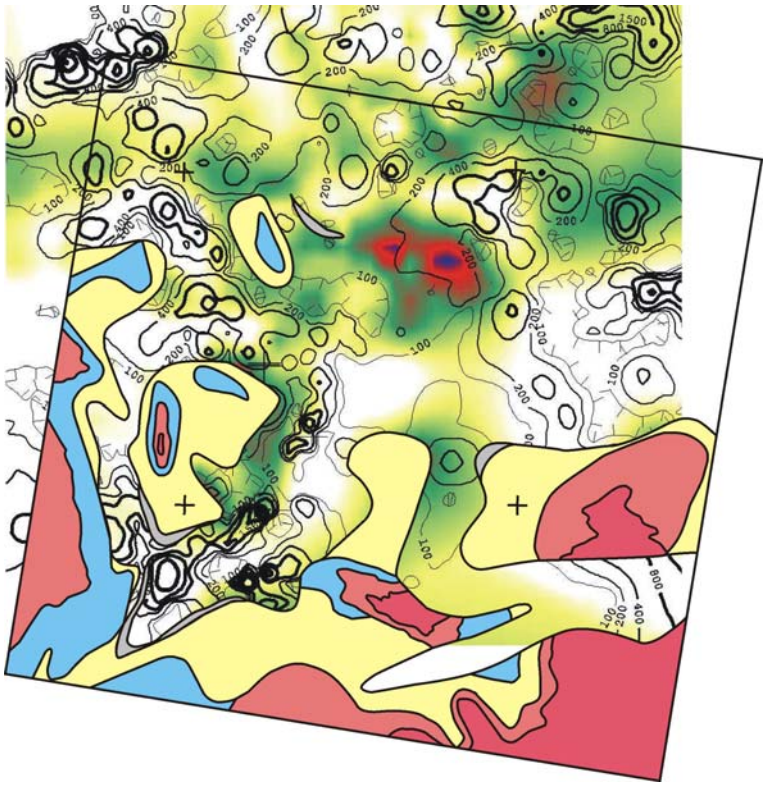

Fig. 6.13: Combination of part of Fig. 6.12 with geological map of investigation area (cf. chapter 3). Pyroclastic sediments covering wide parts of investigation area are not shown. For legend of colours and isolines see Fig. 6.12

Furthermore, uranium transport through fault zones could have played an additional role in this period, since areas with low kaolin thickness and high uranium accumulation are also correlated to regional fault zones as indicated in Fig. 6.14.

Another argument for the important role of basaltic phase in uranium migration is the fact that highest uranium concentrations are found in Hajek and Ruprechtov area, where occurrence of basaltic intrusions are by far strongest. Especially at nearby Hajek site uranium concentrations were that high that it was mined for some short period after 1960.

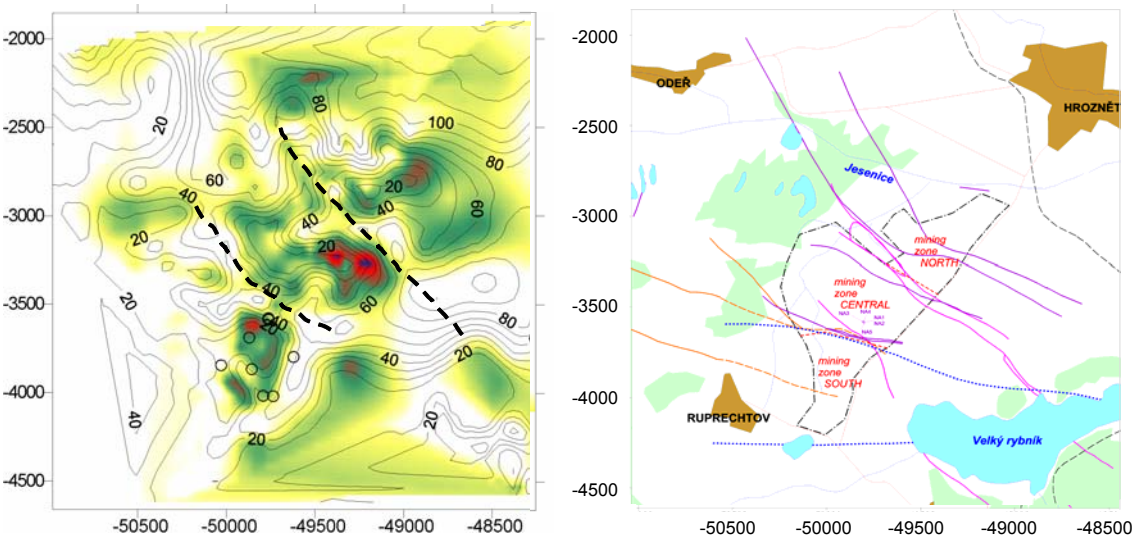

Fig. 6.14: Possible fault zones deduced from depth of interface of kaolin/Upper Tertiary and kaolin thickness (left) and fault zones described by Czech geological survey (orange and magenta lines, right)

In summary, the scenario described above is mainly based on post sedimentary uranium input. An additional argument for post sedimentary uranium input is deduced from microscopic pictures. Microprobe analysis of samples from Hajek site show that uranium enrichment in coal does not follow stratigraphical layers, which would be expected for synsedimentary processes (s. Fig. 6.15)

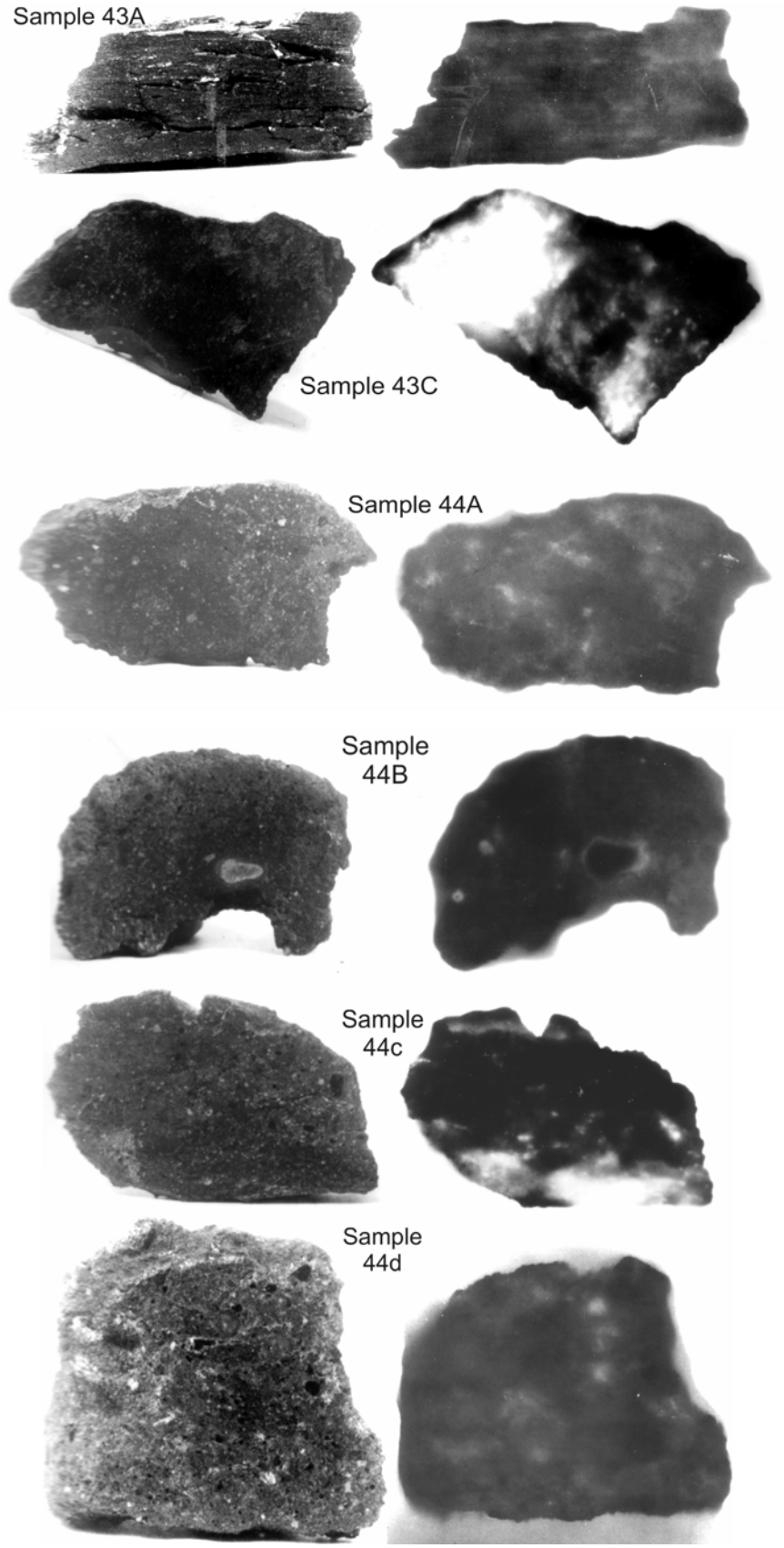

Fig. 6.15: Radiographs show uranium enrichment (light areas) in coal samples from Hajek site

5: Period with partial erosion of pyroclastic sediments (Pliocene to Quaternary, < 5My)

Very young (Pliocene?) phase that affects slope deposits of the main Erzgebirge fault occurs in the area. Important erosion removes larger parts of volcanic strata. The whole area is tilted in the normal faulting as a consequence of the crustal stretching. The deepest part of the basin (140 m) is therefore close to main Erzgebirge fault.

6.4 Possible additional enrichment processes

It is also mentioned that an enrichment with significantly lower uranium content is observed in few boreholes in spatially limited lignite seams several ten meters above the interface kaolin / pyroclastic sediments. The existence of this enrichment can be better explained by assuming a synsedimentary uranium enrichment during the time where volcanic activity had stopped and vegetation growed. Enrichment could have occurred in swampy areas on organic material, uranium was delivered from surrounding granites.

Tab. 6.3: Summarized pro and contra arguments for the scenario of uranium release and migration

pro arguments	contra arguments
Alteration of the cover ongoing with the alteration of granites. Siderite occurrence in both	Occasionally lower uranium enrichments are found around lignite seams in upper parts of the pyroclastic sediments. This can be described better by syn-sedimentary enrichment
The shaping of the rocky and hilly landscape preferentially along fractured zones	
Ti, P enrichment just in the uppermost kaolin	
Heavy (volcanic) carbon in siderites Slope of kaolin hills (up to 80 m heigth) greater then the acceptable angle of 30° for the maximum of 13 m height Systematical occurrence of thicker kaolin on the top of hills. In the case of pre Tertiary kaolinization it should be vice versa (and all the kaolin hills should be contoured by faults)	

For such scenario the major formation of secondary uranium phases should have also occurred synsedimentary. Such a synsedimentary accumulation of uranium in the clay/lignite-sand horizon could have occurred before or in the early stage of volcanic activity, since the high uranium concentrations are found in the clay/lignite-sand layers and below. There is no significant uranium enrichment above the clay/lignite layer. Weathering fluids enriched in soluble uranium complexes and compounds were derived from surrounding granitic rocks. Major part of uranium could have been sorbed by organic-rich sediments and iron compounds. In our opinion, this process is of minor importance at Ruprechtov site.

6.5 Today's situation

The uranium enrichment processes described above have occurred more than 1 My ago, i.e. the radionuclides from the uranium decay chain must be in a secular equilibrium. But, one main observation is the existence of disequilibria in the uranium decay chain in bulk samples from the clay/lignite-sand horizon. This indicates that there is/was still some uranium input in the clay/lignite-sand horizon during the last few 100 000 years.

Two possibilities of recent uranium input exist, so far:

- through water bearing horizons from surface near granite
- through fractures from underlying granite

Today's measurements of uranium concentrations show, that waters from near surface granite, as can be seen in boreholes RP1, NA10 and to a lesser extent in NA8, contain uranium concentrations, which are roughly increased by a factor of ten compared to concentrations in water from the clay/lignite-sand horizon (Fig. 4.12).

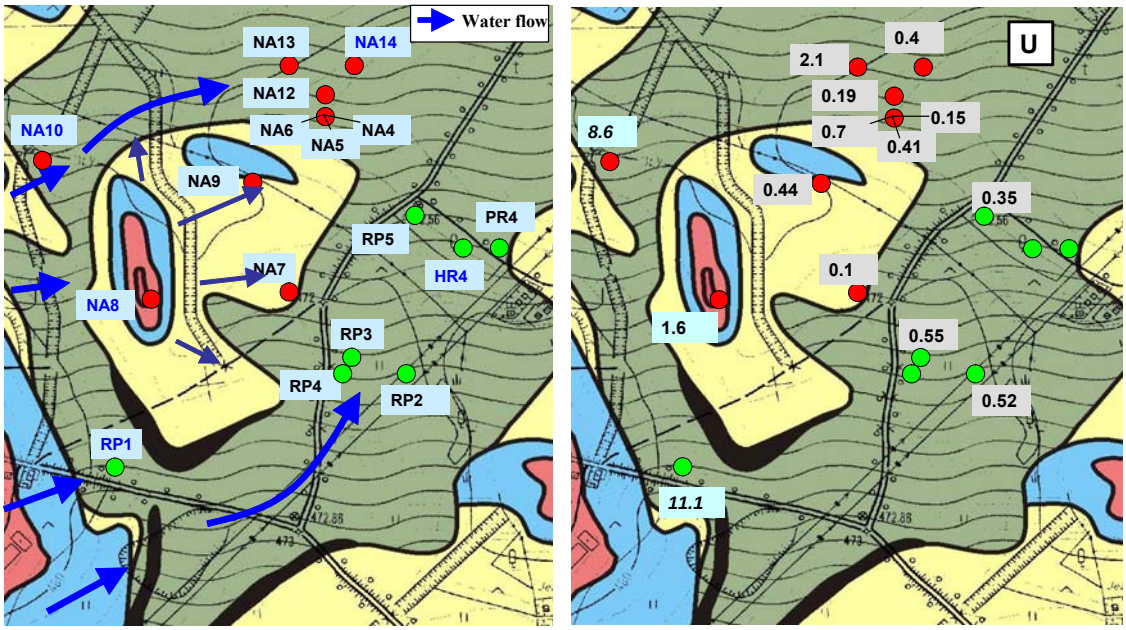

Fig. 6.16: Generally expected groundwater flow (left) and uranium concentrations (ppb) in distinct boreholes

Therefore partial uranium input from near surface granites seems to be possible. Such uranium by mobilization from surface near granite and transport through water bearing horizons in the pyroclastic sediments (esp. clay/lignite-sand layer), as supposed in the first conceptual model /NOS 02/, can hardly explain the observed distribution of uranium enrichment over a wider area (cf. Fig. 6.12). If uranium transport did occur in this way, highest uranium concentrations would be expected in the south western part of the area near to the outcropping granites. Fig 6 shows that this is not the case and even higher concentrations are found in the more eastern part, far away from any granit outcrop.

Secondly, the sedimentary investigation of the wider area also showed that the clay/lignite-sand horizon with a somewhat higher hydraulic conductivity does not spread over the whole area. Therefore such a long-scale uranium transport through clay/lignite-sand horizon seems not to be possible.

It is more likely, that uranium transport during the last 500 000 years occurred from underlying granite via pathways through kaolin into the clay/lignite-sand horizon. Such pathways are expected in areas with very low kaolin thickness and/or fault zones in granite/kaolin. In these areas highest uranium concentrations are observed.

Borehole NA14 was drilled to analyse the water from underlying granite. The filter area was established in 67.5 to 82.2 m depth in the granite. The uranium concentration in this borehole is significantly lower than those in near surface granites, which are in the range of magnitude of the values obtained in the clay/lignite horizon. Furthermore the $^{234}U/^{238}U$-ratio is significantly higher than 1. This indicates, that we already observe a mixture of water from granite and clay/lignite-sand horizons in the deep part of borehole NA14, caused by the very low kaolin thickness and/or fault zones in this area.

7 Conclusions and relevance for performance assessment

The aim of the Natural Analogue study at Ruprechtov site (CZ) was to investigate the potential mobility of uranium in tertiary argillaceous sediments under representative long-term conditions. Such sediments often build up the overburden of potential host rocks for deep geological waste repositories. The Ruprechtov site represents a tertiary basin with argillized volcano-detritic sediments, which is surrounded by granite and underlain by kaolin and granite. U-enrichment mainly occurs in distinct layers of limited thickness on top of the kaolin close to aquiferous horizons and the clay-lignite seams, the so-called clay/lignite-sand horizon.

During the current project the previous site investigation was extended from a punctual scale of about 200 m^2 to an area of about 2 km^2. After detailed characterisation of sediments including outcropping and underlying granite and kaolin as well as groundwater from clay/lignite-sand horizon and infiltration area, the site turned out to be rather complex with regard to geological development and in particular uranium mobilization / immobilization processes.

7.1 Relation to far-field processes of radioactive waste repositories

In many cases host rocks for radioactive waste disposal are covered by tertiary/quaternary sediment formations, which are considered as additional geological barriers for transport of contaminants from the repository. The structure of such an overburden is exemplary shown for the overburden of the salt dome at Gorleben in Fig. 7.1. The overburden consists of sandy-argillaceous and marly unconsolidated rocks of Tertiary and Quaternary. With regard to retardation of radionuclides as well as generation of humic colloids, areas with lignite seams of Miocene are of interest. The thickness of the overburden amounts to about 250 m.

The hydrogeological conditions at Gorleben represent a structure, which is typical for the whole northern lowland plain. It is characteristised by an upper fresh water body (< 1 g/l TDS) and a lower body with mineraalised water (> 10 g/l TDS). The groundwaters in this vertical structure can be divided in $CaSO_4$-, $CaHCO_3$- $NaHCO_3$- and NaCl-type (from top to bottom). The pH-values are in a range of 6.5 to 8, where values of lower pH are found in deeper waters and increase with decreasing depth. One specific feature of Gorleben site is the fact that, at least in some areas - especially

in depth between 50 m and 150 m - relatively high concentrations of humic acids up to 200 mg DOC / l are observed.

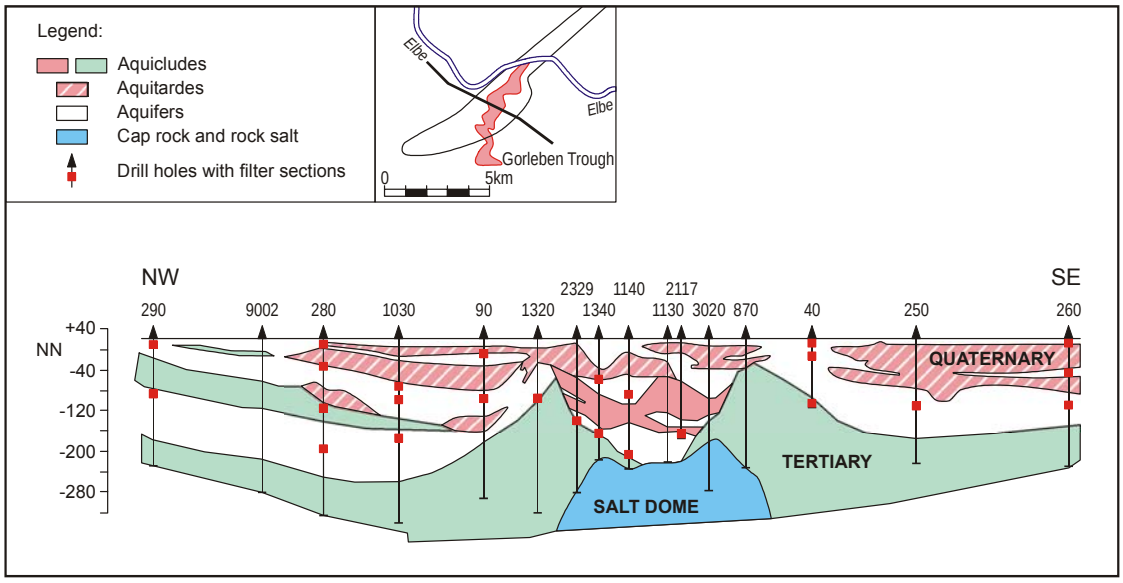

Fig. 7.1: Geological cross section across the overburden of the Gorleben salt dome

Ruprechtov site shows a number of similarities to the structure of the overburden. It consists of tertiary argillaceous sediments with high content of kaolinite in the area of interest and also areas of limited thickness with high content of organic matter (lignite). The fact that at Ruprechtov site areas with high content of uranium exist and that these areas with high U-content are oftenly found in the vicinity of water-bearing horizons enabled us to study radionuclide transport in these sediments.

Furthermore, Ruprechtov site with its typical unconsolidated clays shows similarities to plastic clays, i.e. to formations like Boom clay, which are for example considered as host rock for a deep geological repository for radioactive waste in Belgium.

7.2 Uranium transport

Based on all results that were available after first 3 exploration drillings and two drillings for detailed geochemical and groundwater analysis in the clay/lignite-horizon in a very limited area of 10 x 20 m^2 a first conceptual model considering mobilisation and migration of uranium was formulated (Fig. 7.2) /NOS 02b/. In this model, uranium was assumed to be mobilised from granite under oxidising conditions and then transported

through the water bearing layer in the vicinity of the clay/lignite-sand horizon. Reducing conditions in this lignite-rich horizon have led to reduction and subsequent precipitation and/or sorption of uranium, resulting in a roll front type of U-deposit. The aim of the study presented here was to characterise the uranium source and the hydrogeological conditions over a larger area and to simulate the uranium transport based on this conceptual model.

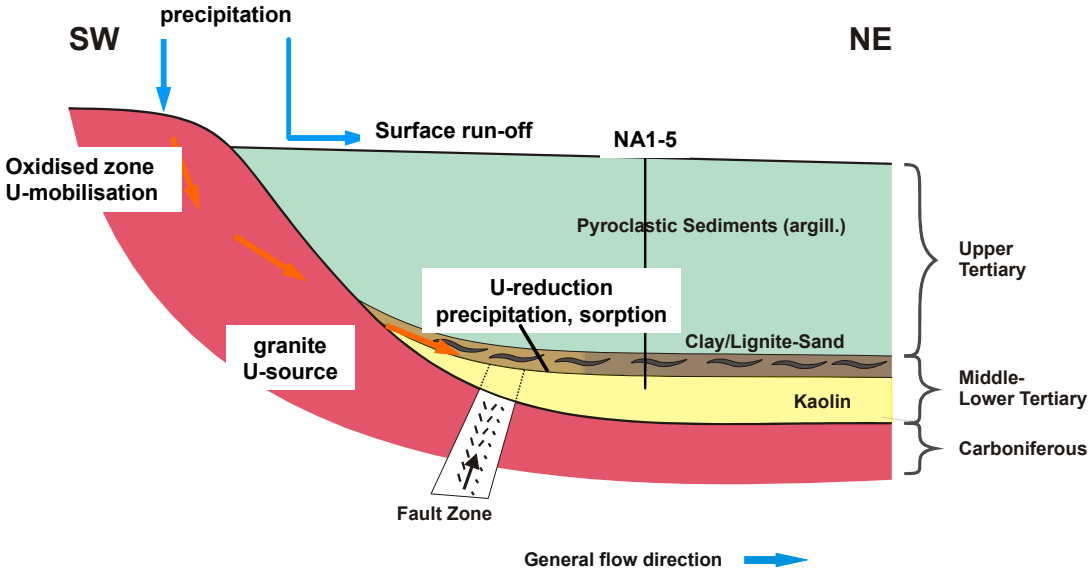

Fig. 7.2: First conceptual model for uranium mobilisation, transport and immobilisation at Ruprechtov site

After extension of the investigation area and evaluation of all informations from sediment and groundwater characterisation of all new boreholes as well as additional informations it became clear that this conceptual model can not comprehensively explain the observed uranium distribution at the site. Ruprechtov site turned out to be more complex than initially thought concerning hydrogeology and uranium enrichment processes.

The assumption of a hydraulic model consisting of one aquiferous layer of limited thickness at the interface kaoline/pyroclastic sediment is, in fact, not correct. In many but not in all boreholes the so called clay/lignite-sand horizon was coming across. But there are also some boreholes where no clay/lignite and no water bearing horizon was observed at the interface kaolin/pyroclastic sediments. This indicates that a continuous

aquifer over the whole area doesn't exist. Secondly, the interface kaolin/pyroclastic sediments is not flat but consists of a structure with hills and valleys.

Furthermore, the assumption of the Tertiary to be hydraulically separated from the hydraulic system in the underlying granite seems not to be true. There is strong evidence that both systems are interconnected in areas with rather low kaolin thickness and/or fault zones. Therefore a hydrogeological flow model would need a better characterisation of the hydrogeological properties of the granite.

Concerning uranium transport processes, it became clear that the uranium transport did not occur that straight forward as assumed. It is very likely that different processes of uranium enrichment in the clay/lignite-sand horizon occurred at the site (cf. Chapter 6 and Fig. 7.3) which can be summarised as

- Input of detritic uranium minerals
- retardation in the clay/lignite layer after
  - possibly additional syn-sedimentary enrichment in wet areas
  - U-mobilisation during granite alteration and diffusion from kaolin to the interface kaolin/pyroclastic sediment and
  - input via underlying granite through zones of low kaolin/thickness and/or fault zones

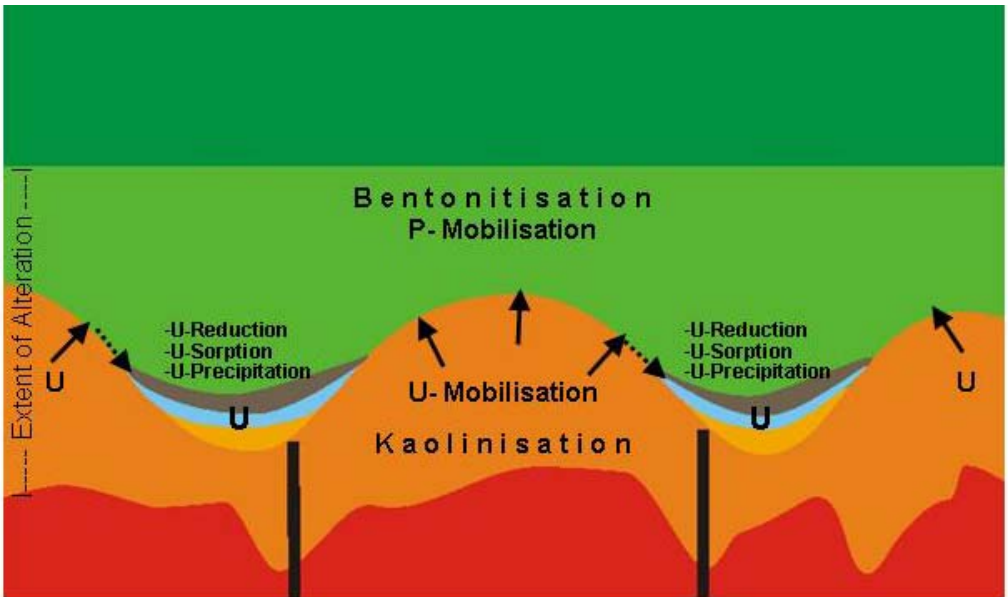

Fig. 7.3: New conceptual model for major uranium enrichment processes

The initially proposed process of uranium transport directly from outcropping granite through water bearing layers into the Tertiary might take place in some areas near to the outcropping granite (cf. discussion in Chapter 4) but does not explain the uranium enrichment over the whole area.

Because of the complexity in hydrogeology and uranium enrichment processes, it was abstained from the development of a detailed transport model for the whole site. Instead, we tried by use of a simplified model to estimate a mass balance for the process *U-mobilisation during granite alteration and diffusion from kaolin to the interface kaolin/pyroclastic sediment*, which was postulated in chapter 6 to dominate the uranium enrichment in the area. The mass balance is performed for the selected area marked by the black frame in Fig. 7.4 and is based on the following assumptions:

- Uranium is transported from the kaolinised horizon into the enriched areas of clay/lignite horizon,

- uranium loss from granite during kaolinisation was app. 12 ppm U according to the estimation in Chapter 6.1,

- the area with “kaolin hills” is about 50 % of the whole area, the kaolin hills are cylinders of 30 m height (this is estimated from Fig. 7.4, kaolin hills are marked by red frames),

- thickness of the uranium bearing layer in the clay/lignite-sand horizon is 2 m according to observations in most boreholes,

- all uranium released from the kaolin becomes fixed in the clay/lignite-sand horizon and uranium enrichment is limited to 50 % of the area.

With these assumptions the mass balance leads to an uranium content of 180 ppm in the enriched areas in the clay/lignite horizon. This value is in the order of magnitude of concentrations observed in several boreholes, but slightly lower than concentrations indicated by isolines for the uranium distribution in Fig. 7.4.

This rough estimation shows that the clay/lignite-sand horizon was/is a strong barrier for uranium. The major amount of uranium was brought into the system during Tertiary. However, some uranium enrichment was/is still going on during the last several

100 000 years, shown by disequilibria states in the uranium decay chain. There is no indication of uranium release from the already enriched layer.

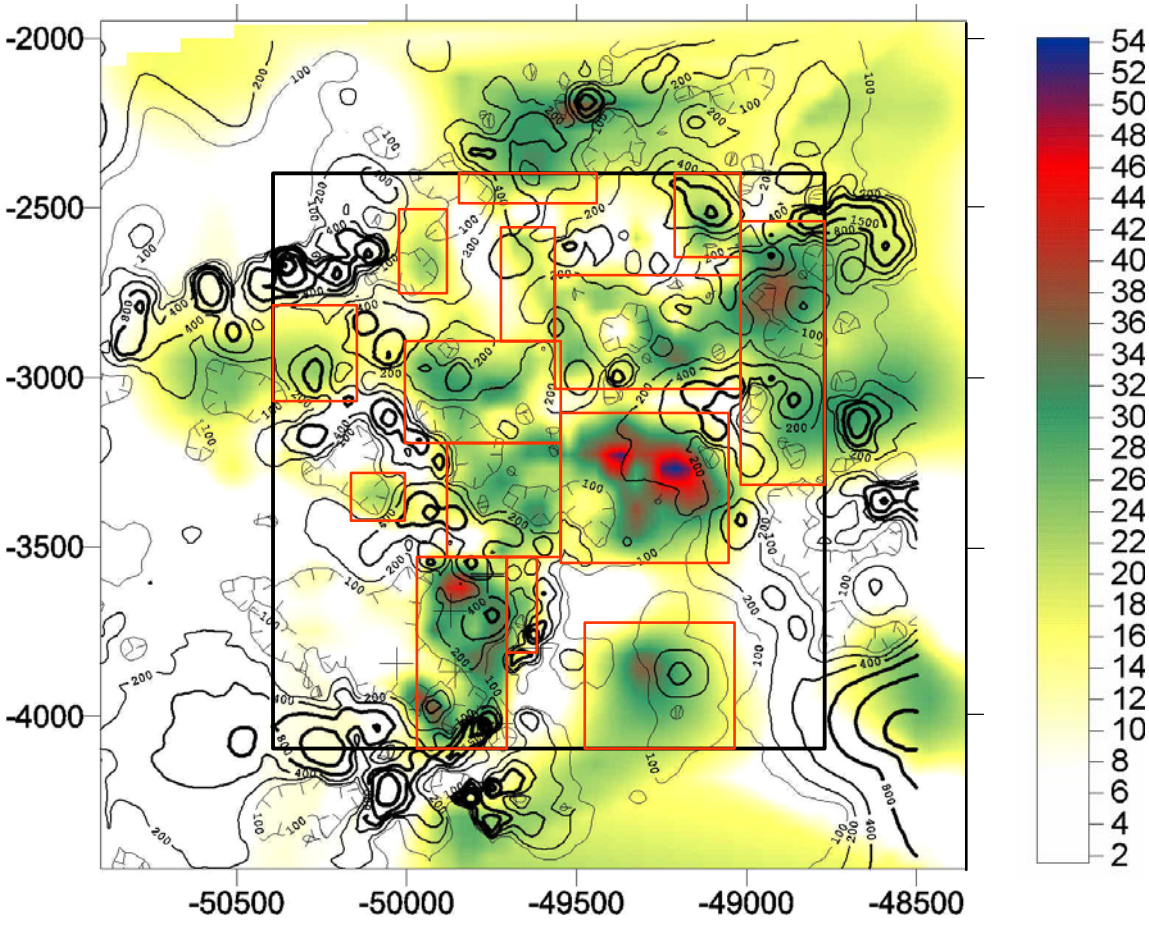

Fig. 7.4: Uranium enrichment versus kaolin depth. The black frame covers the area considered for mass balance; the red frames indicate areas with elevated kaolin thickness used for mass balance

7.3 Uranium retention

As already mentioned the uranium input into the clay/lignite-sand layer is the result of a multiphase process. Nevertheless, the major immobilisation process is the reduction of uranium and formation of secondary uranium(IV) minerals, i.e. uraninite and phosphate bearing minerals like ningyoite and rhabdophane. This process occurred in a zone of limited thickness, the so-called clay/lignite-sand horizon, which is characterised by an elevated SOC-content up to 50 % in the upper part, clay content up to 50 % in the

lower part (mainly kaolinite, lower amount of muscovite/illite and smectite) and occurrence of minerals like pyrite, siderite, and anatase / rutile.

This zone comprises a very efficient barrier for uranium. It was shown that arsenopyrites, which have formed thin covers on pyrite nodules, are implemented in the uranium reduction process. This is concluded from correlation of As(V) in areas of high uranium content, where uranium has been identified as U(IV) in poorly crystallized phosphate minerals.

First experiments for separation of U(IV) and U(VI) indicate, that a small amount of about 10-20 % of uranium exist in oxidation state VI. It has to be confirmed in analysis of further samples, if oxidation occurred during the experiment or if it is original U(VI). However, this phase shows the same $^{234}U/^{238}U$-ratio as the groundwater and therefore is thought to be accessible. It probably represents uranium sorbed to organic or clay-organic material, which is also supported by sequential extraction experiments.

7.3.1 Role of colloids

In the overburden above the Gorleben salt dome zones with lignite seams occur in tertiary and quaternary sediments. DOC concentrations up to 200 mg C / l are observed in some groundwaters at Gorleben site. Such high concentrations of organic colloids can play a role in facilitating the transport of higher valent cationic pollutants as actinides by sorption of the actinides to the colloids and colloidal transport without/or with only low sorption of the colloids, e.g. /ART 98, SCH 00, EUR 04/. Therefore it is a topic which has to be addressed by performance assessment.

The generation of colloids at Gorleben site is mainly due to microbial degradation of sedimentary organic matter /BUC 00/. This degradation process leads on one hand to generation of CO_2, which dissolves and causes additional dissolution of sedimentary carbonates. The degradation of SOC results in the release of DOC, preferentially as humic and fulvic acids.

Ruprechtov site was expected as suitable analogue for the investigation of the role of organic colloids - i.e. humic and fulvic acids - in a natural environment, since seams with high content of organic matter occur in sedimentary layers, similar to the situation at Gorleben.

However, the results up to now, show, that the DOC content of groundwater from Ruprechtov site is generally low with concentrations of only 1-10 mg C / l, although in principle the conditions for microbial activity are fulfilled. The sulphate concentration is high enough, sedimentary lignite material is available and microorganisms are present. Analysis of carbon isotopes $\delta^{13}C$ and ^{14}C in dissolved inorganic carbon do not allow to judge if microbial degradation currently takes place or not. Observed ^{13}C signatures in groundwater from clay/lignite-sand horizon can not be explained by DIC input via microbial degradation alone.

Currently, it is not completely clear why the DOC concentrations at Ruprechtov site are significantly lower than at Gorleben. Probably, differences in composition of sedimentary organic matter play a role. Therefore, detailed investigation of sedimentary organic matter from Ruprechtov site might illustrate the reason for low concentrations. Such investigations for organic matter from different European sites are on the way as part of the integrated project FUNMIG /EUR 05/.

Sorption experiments with tetravalent uranium on sediments from the clay/lignite horizon with and without humic acids showed an impact on uranium sorption at humic acid concentrations above 20 mg DOC / l. This indicates that the role of humic colloids on uranium mobility at Ruprechtov site is limited, because of the low concentrations of DOC. Thermodynamic sorption modelling of these experiments will also be part of FUNMIG.

7.3.2 Role of microbes

Analyses of microbes have been performed at samples from the clay/lignite-sand horizon. Different kinds of microbes have been detected at Ruprechtov site. Important consequences of microbial activity at Ruprechtov site were expected in two aspects

- impact on redox conditions
- impact on degradation of organic matter

Concerning the impact on redox conditions, emphasis was placed on the role of sulfate reducing bacteria. This is due to the existence of a significant amount of sulfide minerals in the clay/lignite-sand horizon; in particular pyrite nodules. Indeed, autochthonous sulfate reducing bacteria were detected in undisturbed samples derived under as far as possible sterile conditions. Experiments with groundwater/sediment

system from NA4 showed that stimulation of growth of sulphate reducing bacteria by sulphate, lactate and phosphate addition under initially oxidising conditions caused decrease of Eh-value from 400 mV to about -100 mV. Thereby initial uranium concentration of $2 \cdot 10^{-6}$ mol/l dropped to values about 10^{-8} mol/l. Composed sulfide precipitated by formation of iron sulfides. This showed the important role of sulphate reducing bacteria. Firstly, formation of sulfides can be of relevance in uranium retention processes, as shown in this study. Furthermore, they are able to maintain the reducing conditions, in a range, where uranium exist as U(VI). Finally they can contribute to the long-term stability of reducing environment by consumption of oxygen in infiltrating groundwater.

The impact of the second important role of bacteria in degradation of organic matter and release of dissolved organic material like humic and fulvic acids has already been discussed above. How far DOC generation due to degradation of sedimentary organic matter occurs is investigated in the project FUNMIG.

7.4 Conclusion

Ruprechtov site is a good example to demonstrate that tertiary argillaceous sediments can exert a strong barrier function of for uranium, when specific prerequisites are fulfilled. Major uranium transport occurred only over distances of about tens to max. some 100 m during Tertiary. Uranium was transported as U(VI) and was reduced in a lignite rich clay horizon with occurrence of pyrite and arsenopyrite minerals. It was immobilized by forming uraninite, and phosphate bearing minerals like ningyoite and rhabdophane. There is no evidence of uranium mobilisation during the last million years. But there is indication that still during the last several 100 000 years further uranium enrichment occurred in this lignite rich clay horizon. This is probably due to transport from underlying granite through zones of low kaolin thickness and/or fault zones.

The uranium concentrations in groundwater of the clay/lignite-sand horizon are low in the range of 10^{-9} mol/l although this horizon is only 25 to 65 m below the surface.

7.5 Outlook

There are still several open questions to be answered at Ruprechtov site. In the frame of the integrated project FUNMIG /EUR 05/, which is carried out from 2005 until 2008, some of these questions are addressed.

Firstly, the role of organic matter will be investigated in more detail. By characterisation of sedimentary organic matter on one hand, and by further isotope geochemical measurements like analysis of ^{34}S-isotope content in dissolved sulfate and C-14 analysis of dissolved organic matter on the other hand, the mechanism of organic matter degradation will be studied. It will be analysed, whether microbial reactions are involved today at Ruprechtov site or not.

Secondly, further studies of immobile uranium phases are on the way. The application of µ-XRF and µ-XAFS with higher spatial resolution will be performed to confirm the occurrence of thin arsenopyrite layers directly on the surface of pyrite nodules. If possible, further samples will be analysed by this method to get more confidence that this process is the major reduction process for uranium.

Further interest is also given to an easier accessible uranium phase, which makes up about 10-20 % of uranium in the enriched horizon and probably represents a uranium(VI) phase, which is sorbed to organic material. This will be investigated by optimization of the U(IV)/U(VI)-separation method and application to further samples.

All analyses of immobile uranium phases will be accompanied by further specific sequential extraction methods and specific uranium desorption (exchange) measurements with the non-naturally occurring ^{236}U tracer. Application of surface complexation models are planned to quantify the sorption process.

8 References

/ABD 05/ Abdelouas, A.; Grambow, B.; Andres, Y.; Noseck, U.: Uranium sorption/desorption and biological reduction study in argillaceous sediments. To be published.

/ABD 00/ Abdelouas, A., Lutze, W., Gong, W., Nuttall, E., Strietelmeier, B. A., Travis, B. J.: Biological reduction of uranium in groundwater and subsurface soil. The Sci. Total Environ. **250**, 21-35 (2000).

/ADL 91/ Adloff, J.P.; Roessler, K.: Recoil and Transmutation Effects in the Migration Behaviour of Actinides.- Radiochim. Acta **52/53**, 269-274 (1991).

/AND 89/ Anderson, R.F.; Fleisher, M.Q.; Lehyray, A.P.: Concentration, oxidation state and particulate flux of uranium in the Black Sea, Geochim. et Cosmochim. Acta **53**, 2215-2224 (1989).

/ART 98/ Artinger, R.; Kienzler, B.; Schüßler, W.; Kim, J.I.: Effects of humic substances on the ^{241}Am migration in a sandy aquifer: column experiments with Gorleben groundwater / sediment systems. J. Contam. Hydrol. **35**, 261-275 (1998).

/BAR 93/ Barnes, C.E.; Cochran, J.K.: Uranium geochemistry in estuarine sediments: Controls on removal and release processes. Geochim. Cosmochim. Acta **57**, 555-569 (1993).

/BEA 96/ Bea, F.: Residence of REE, Y, Th and U in granites and crustal protoliths; Implications for the chemistry of crustal melts. – J. Petrol., **37** 521-552 (1996).

/BOS 05/ Bosák, P., personal communication, 2005.

/BRA 98/ Brasser, Th. et al.: Untersuchung der Uran- / Thorium-Mobilisation als natürliches Analogon für den Radionuklidtransport im Deckgebirge eines Endlagers für radioaktive Abfälle.- GRS-A-2652, Köln, 1998.

/BRO 99/ Brown, D. A. and Sherriff, B. L.: Evaluation of the effect of microbial subsurface ecosystems on spent nuclear fuel repositories. Environmental Technology. **20**, 469-477 (1999).

/BUC 00/ Buckau, G.; Artinger, R.; Geyer, S.; Wolf, M.; Fritz, P.; Kim, J.I.: Groundwater in-situ generation of aquatic humic and fulvic acids and the mineralization of sedimentary organic carbon. Appl. Geochem. **15** (2000) 819-832.

/CHR 01/ Christensen, N. I.; Medaris, L. G.; Wang, H. F. and Jelínek, E.: Depth variation of seismic anisotropy and petrology in central European lithosphere: A tectonothermal synthesis from spinel lherzolite xenoliths.- J. Geoph. Res. – Solid Earth, **106**, B1, 645-664, 2001.

/DEN 05/ Denecke, M.; Janssens, K.; Proost, K.; Rothe, J.; Noseck, U.: Confocal micrometer-scale X-ray fluorescence and X-ray absorption fine structure studies of uranium speciation in a tertiary sediment from a waste disposal natural analogue site. Env. Sci .Technol. **39**, 2049-2058 (2005).

/DEN 96/ Denecke, M.; Friedrich H.; Reich, T.; Bernhard, G.; Kniess, T.; Rettig, D.; Zorn, T.; Nitsche, H.: Determination of relative arsenite and arsenate concentrations in aqueous mixtures by XANES. HASYLAB Annu. Rep. 751-752 (1996).

/DIS 89/ Disnar, J.R.; Sureau, J.F.: Organic matter in ore genesis: Progress and perspectives. Adv. Org. Geochem. **16**, 577-599 (1989).

/DVO 98/ Dvořák, J.: Hydrogeology and the genesis of mineral waters of the Carlsbad type in western Bohemia.- In: Annau, R., Bender, S. and Wohnlich, S. (Eds.): Hardrock Hydrogeology of the Bohemian Massif, Proc. 3rd Intern. Workshop, Windischeschenbach 1998, Münchner Geol. Hefte, **B8**, 63-69, 1998.

/DUF 02/ Duff, M.C.; Coughlin, J.U.; Hunter, D.B.: Uranium co-precipitation with iron oxide minerals. Geochim. et Cosmochim. Acta, **66** (20) 3533-3547 (2002).

/DUL 01/ Dulski, P.: Reference materials for geochemical studies: New analytical data by ICP-MS and critical discussion of reference values. – Geostandards Newsletter, **25**, p. 87–125 (2001).

/ERV 96/ Ervanne, H.; Suksi, J.: Comparison of Ion-Exchange and Coprecipitation Methods in Determining Uranium Oxidation States in Solid Phases. Radiochem. **38** (4), p. 306-309 (1996).

/EUR 05/ European Commission: Fundamental processes of radionuclide migration (FUNMIG). FP 516 514, EC-project within the 6th frame programme, (2004-2007)

/EUR 04/ European Commission: Humic substances in performance assessment of nuclear waste disposal: actinide and iodine migration in the far-field (HUPA). FIKW-CT-2001-00128. EC-Project within the 5th frame programme, (2001-2004).

/FOE 05/ Förster, H. J.: Persönliche Mitteilung Februar 2005.

/FOE 01/ Förster, H.-J.: The radioactive accessory-mineral assemblage of the Podlesí granite-pegmatite system, western Krušné hory, Czech Republic: Implications to intrusion age and magmatic/hydro-thermal fluid-rock interaction. In: K. Breiter (ed.): *Int. Workshop "Phosphorus- and fluorine-rich fractionated granites",* Podlesi, Oct. 16–19, Czech Republic, Abstracts and Excursion Guide, Czech Geological Survey, Prague, p. 14–15 (2001).

/FOE 99/ Förster, H.-J. (1999): The chemical composition of uraninite in Variscan granites of the Erzgebirge, Germany. – Mineral. Mag. **63**, No. 417, p. 239–252.

/FOE 98a/ Förster, H.-J.: The chemical composition of REE–Y–Th–U-rich accessory minerals from peraluminous granites of the Erzgebirge–Fichtelgebirge region, Germany. Part I: The monazite-(Ce) – brabantite solid solution series. – Amer. Mineral. **83**, No. 3–4, p. 259–272 (1998).

/FOE 98b/ Förster, H.-J.: The chemical composition of REE–Y–Th–U-rich accessory minerals from peraluminous granites of the Erzgebirge–Fichtelgebirge region, Germany. Part II: Xenotime. – Amer. Mineral. **83**, No. 11–12, p. 1302–1315 (1998).

/FRE 00/ Fredrickson, J.K.; Zachara, J.M.; Kennedy, D.W.; Duff, M.C.; Gorby, Y.A.; Li, S.W.; Krupka, K.M.: Reduction of U(VI) in goethite (a-FeOOH) suspensions by a dissimilatory metal-reducing bacterium. Geochim. et Cosmochim. Acta, **64** (18) 3085-3098 (2000).

/HAU 05/ Hauser, W.; Geckeis, R.; Götz, R.; Fuß, M.: Colloid detection in Natural Groundwater from Ruprechtov by Laser-induced Breakdown Detection. To be published.

/HUM 02/ Hummel,W. Berner, U., Curti, E., Thoenen, T. and Pearson, F.J.: Nagra/PSI Chemical Thermodynamic Data Base Version 01/01. (Nagra/PSI TDB 01/01) NAPSI_290502.DAT LAST MOD. 26-AUG-2002.

/JAN 04/ Janssens, K.; Proost, K.; Falkenberg G.: Confocal microscopic X-ray fluorescence at the HASYLAB Microfocus beamline: Characteristics and possibilities, Spectrochimica Acta B, ***59***, 1637-1645 (2004).

/KET 55/ Kettner R.: *General geologgy*, IV, Geological influence of gravity on the Earth´s surface, slope movements of the soil. - Nakl. ČSAV, 364 s. Praha (1955).

/KLI 91/ Klinkhammer, G.P.; Palmer, M.R.: Uranium in the oceans: Where it goes and why. Geochim. et Cosmochim. Acta, **53** 1799-1806 (1991).

/KOM 94/ Komínek, J.; Chrt, J. and Landa, O.: Uranium mineralization in the western Krušné hory Mts. (Erzgebirge) and the Slavkovský les region, Czech Republic.- In: v. Gehlen, K. and Klemm, D.D. (Eds.): Mineral deposits of the Erzgebirge/ Krušné hory (Germany/ Czech Republic, Monograph Series on Mineral deposits, No. 31, pp.209-230, Gebrüder Bornträger, Berlin – Stuttgart, 1994.

/KRO 67/ Kronberg, P: Photogeologie – Eine Einführung in die geologische Luftbildauswertung.- Clausthaler Tektonische Hefte, **6**, 235 S., Clausthal-Zellerfeld 1967.

/LIG 99/ Liger,E.; Charlet, L.; Van Cappellen, P.: Surface catalyses of uranium(VI) reduction by iron(II). Geochim. et Cosmochim. Acta, **63** (19/20) 2939-2955 (1999).

/LOV 91/ Loveley, D.R.; Phillips, E.J.P.; Gorby, Y.A.; Landa, E.R.: Microbial reduction of uranium. Nature **350**, 413–416 (1991).

/LOV 92/ Lovely, D.R.; Phillips, E.J.P.: Reduction of Uranium by Desulfovibrio desulfuricans. Appl. Environ. Microbiol. **58**(3), 850-856 (1992).

/LOV 93/ Loveley, D.R.; Roden, E.J.; Phillips, E.J.P.; Woodward, J.C.: Enzymatic iron and uranium by sulfate reducing bacteria. Mar. Geol. **113**, 41-53 (1993).

/MCK 93/ McKee, B.A.; Todd, J.F.: Uranium behaviour in a permanent anoxic fjord: Microbial Control? Limnol. Oceanogr. **38**, 408-414 (1993).

/NAK 84/ Nakashima, S.; Disnar, J.R.; Perruchot, A.; Trichet, J.: Experimental study of mechanisms of fixation and reduction of uranium by sedimentary organic matter under diagenetic or hydrothermal conditions. Geochim. Cosmochim. Acta **48**, 2321-2329.

/NER 95/ Del Nero, M.; Salah, S.; Miura, T., Clément, A., Gauthier-Lafaye, F.: Sorption/Desorption Processes of Uranium in Clayey Samples of the Bangombé Natural Reactor Zone, Gabon. Radiochim. Acta, **87,** 135-149 (1999).

/NOS 04/ Noseck, U.; Brasser, Th.; Raijlich, P.; Hercik, M.; Laciok, A.: Mobility of uranium in tertiary argillaceous sediments – a natural analogue study. Radiochim. Acta **92**, 797-801 (2004).

/NOS 02a/ Noseck,U.; Brasser, Th.; Pohl, W.: Tertiäre Sedimente als Barriere für die U/Th-Migration im Fernfeld von Endlagern. Gesellschaft für Anlagen- und Reaktorsicherheit (GRS) mbH, GRS-176, Braunschweig, März 2002.

/NOS 02b/ Noseck, U.; Brasser, Th.; Laciok, A.; Hercik, M.; Woller, F.: Uranium migration in argillaceous sediments as analogue for transport processes in the far field of repositories (Ruprechtov site, Czech Republic). In: *Uranium in the Aquatic Chemistry* (B. Merkel et al., eds.) Springer, Berlin, Heidelberg 2002

/OSM 83/ Osmond, J.K.; Cowart, J.B.; Ivanovich, M.: Uranium Isotopic Disequilibrium in Ground Water as an Indicator of Anomalies.- Int. J. Appl. Radiat. Isot. **34**/1, 283-308 (1983).

/PAS 93/ Pasava, J.; Sulovsky, P.; Kovalova, M.: Geochemistry and mineralogy of Proterozoic metal rich black shales from the Bohemian massif, Czech Republic, with a description of possible new molybdenium, selenide and telluride phases. Can. Mineral. **31**, 745-754 (1993).

/POS 87/ Posey-Dowty, J.; Axtmann, E.; Crerar, D.; Borcsik, M.; Ronk, A.; Woods, W.: Dissolution rates of uraninites and uranium roll front ores. Econ. Geol. **82**, 184-194 (1987).

/POS 84/ Postgate J. R.: The sulfate-reducing bacteria. Cambridge University Press, Cambridge, 1984.

/PRO 95/ Prodehl, C., Mueller, S. and Haak, V.: The European Cenozoic rift system.- In: Olsen, K.H. (Ed.): Continental rifts: evolution, structure, tectonics.- Development in Geotectonics, 25, 133-212, Elsevier, Amsterdam, 1995.

/RAJ 05/ Rajlich, P., peronal communication, 2005.

/RHE 96/ Rhede, D.; Förster, H.-J.; Teufel, S.: Th-U-Pb Dating of Accessory minerals by electron microprobe. J. Conf. Abst. **1** (1996).

/SCH 00/ Schüßler, W.; Artinger, R.; Kienzler, B.; Kim, J.I.: Conceptual modelling of the humic colloid borne americieum(III) migration by a kinetic approach. Environ. Sci. Technol. **34**, 2608-2611 (2000).

/SCH 87/ Schwyn B. and Neilands J.B.: Universal Chemical Assay for the Detection and Determination of Siderophores - Analytical Biochemistry (1987).

/STU 92/ Stumm, W.; Sulzberger, B.: The cycling of iron in natural environments: Considerations based on laboratory studies of heterogeneous redox processes. Geochim. Cosmochim. Acta **56**, 3233-3257 (1992).

/SVO 66/ Svoboda, J. et al.: Regional Geology of Czechoslovakia, Part I: The Bohemian Massif.- Geol. Survey of Czechoslovakia, Prague, 1966.

/ULR 02/ Ulrych, J.; Cajz, V.; Adamovič, J.; and Bosák, P. (Eds.): Hibsch 2002 Symposium – Excursion Guide and Abstracts.- 3-8 June 2002, Czech Geological Survey, Prague, 2002.

/WAB 91/ Waber, N.: Mineralogy, petrology and geochemistry of the Pocos de Caldas analogy study site, Minas Gerais, Brazil II: Morro de Ferro. SKB Technical report 90-12, Stockholm Schweden (1991).

/WEH 91/ Wehrli, B.: Redox reactions of metal ions at mineral surfaces. In “Aquatic chemical kinetics. Ed. W. Stumm, 311-336, Wiley-Verlag.

/WEI 99/ Weinlich, F.H.; Bräuer, K.; Kämpf, H.; Strauch, G.; Tesar, J.: An active subcontinental mantle volatile system in the western Eger rift. Central Europe: Gas flux, isotopic (He, C, N) and compositional fingerprints. Geochim. Cosmochim. Acta **63**, 3653-3671 (1999).

/WER 94/ Wersin, P.; Hochella, M.F.; Persson, P.; Redden, G.; Leckie, J.O. Harris, D.W.: Interaction between aqueous uranium (VI) and sulfide minerals: Spectroscopic evidence for sorption and reduction. Geochim. et Cosmochim. Acta, **58** (13) 2829-2843 (1994)

Figures

Tables

Gesellschaft für Anlagen- und Reaktorsicherheit (GRS) mbH

Schwertnergasse 1
50667 Köln
Telefon +49 221 2068-0
Telefax +49 221 2068-888

Forschungsinstitute
85748 Garching b. München
Telefon +49 89 32004-0
Telefax +49 89 32004-300

Kurfürstendamm 200
10719 Berlin
Telefon +49 30 88589-0
Telefax +49 30 88589-111

Theodor-Heuss-Straße 4
38122 Braunschweig
Telefon +49 531 8012-0
Telefax +49 531 8012-200

www.grs.de

ISBN 3-931995-88-7